TECHNISCHE UNIVERSITÄT
BERGAKADEMIE FREIBERG
Die Ressourcenuniversität. Seit 1765.

Density functional study of the electronic and magnetic properties of selected transition metal complexes

By the Faculty of Chemistry and Physics
of the Technische Universität Freiberg

approved

Thesis

to attain the academic degree of

doctor rerum naturalium
(Dr. rer. nat.)

submitted by **Dipl. Nat. Claudia Martin** née Loose
born on the 28th May, 1983 in Frankenberg

Assessor: Prof. Dr. Jens Kortus
Prof. Dr. Eliseo Ruiz

Date of the Award: 29th November, 2013

Versicherung

Hiermit versichere ich, dass ich die vorliegende Arbeit ohne unzulässige Hilfe Dritter und ohne Benutzung anderer als der angegebenen Hilfsmittel angefertigt habe; die aus fremden Quellen direkt oder indirekt übernommenen Gedanken sind als solche kenntlich gemacht. Die Hilfe eines Promotionsberaters habe ich nicht in Anspruch genommen. Weitere Personen haben von mir keine geldwerten Leistungen für Arbeiten erhalten, die nicht als solche kenntlich gemacht worden sind. Die Arbeit wurde bisher weder im Inland noch im Ausland in gleicher oder ähnlicher Form einer anderen Prüfungsbehörde vorgelegt.

February 3, 2014 Dipl. Nat. Claudia Martin

Declaration

I hereby declare that I completed this work without any improper help from a third party and without using any aids other than those cited. All ideas derived directly or indirectly from other sources are identified as such. I did not seek the help of a professional doctorate-consultant. Only those persons identified as having done so received any financial payment from me for any work done for me. This thesis has not previously been published in the same or a similar form in Germany or abroad.

February 3, 2014 Dipl. Nat. Claudia Martin

To my daughters

-

you teach me all there is to know

Contents

1 Introduction

There is a wide range of applications for magnetic materials nowadays. They are present in motors, generators, sensors, used for data storage and signal transfer. However, all these applications require bulk materials in more or less large quantities whereas the trend goes to smaller and smaller devices, especially in the field of data storage. In order to keep pace with these developments it is necessary to reduce the amount of space used to store one bit of information steadily. This naturally leads to a miniaturization. According to Moore's Law[144] the number of transistors per integrated circuit doubles every 18 month. This statement is still valid for the transistor density and can be extended to several other properties such as size, cost, speed of components and the storage density. But there are physical limits to the downsizing and miniaturization. Especially for the storage density which is up to now based nearly exclusively on magnetic recording (except for solid-state drives). Below a critical size of the magnetic domains the superparamagnetic limit is approached. Beneath this critical size thermal excitations can flip the orientation of the magnetic moment resulting in data loss.

Given the current rate of minimization it is unavoidable to reach the superparamagnetic limit within the next few years. Hence, new concepts for data storage are needed. One promising approach is the use of single-molecule magnets (SMMs)[103]. Single molecule magnets are characterized by a large ground state S and a large easy axis magnetic anisotropy D. A widely known representative of single molecule magnets is Mn_{12}-acetat which was already known since 1980[123]. However, it took 11 more years until the magnetic properties of the complex were studied. As shown by Sessoli and co-workers[185] there exists a magnetic hysteresis which is due to a energy barrier between the bistable ground states of the molecule. This results in a slowing of the relaxation (months at 2K) of the spins and hence in the experimentally observed hysteresis. In contrast to usual magnets the hysteresis is not due to long range order effects but a unique feature of the molecule itself. Therefore, each of these magnetic molecules is in principle capable to store one bit of information.

Since we deal now with molecules which are much smaller than the bulk material usually used for storage purposes, we have to take into account quantum mechanics to characterize the SMMs. In order to apply SMMs to high-density information

storage it is necessary to understand the mechanisms that lead to the desired single molecule magnet properties: a high spin ground state as well as an easy axis for the magnetic anisotropy. Given that both criteria are fulfilled the energy barrier U between the bistable ground states $|\pm S>$ is given by $U = S^2|D|$ as explained in more detail in section 2.4.4. For a possible application in the field of data storage an as large as possible barrier U is desired. Accordingly a simultaneous optimization of both quantities (S and D) would be preferred.

A high spin ground state can be realized by an overall ferromagnetic coupling of the magnetic centers. As shown in section 2.4.2 there are several possibilities to realize a ferromagnetic coupling and the underlying mechanisms are rather well understood. The well-known Goodenough-Kanamori rules[75, 76, 104] relate the strength and type (i.e. ferromagnetic or antiferromagnetic) of the coupling to the overlap of the involved magnetic orbitals. A more quantitative approach to the explanation and prediction of the magnetic coupling within weakly coupled transition metal systems is given within the Hay-Thibeault-Hoffmann model[90]. However, no such easily applicable rules to predict the magnetic anisotropy exist. As shown in section 2.4.4 there are attempts to relate the strength and sign of the magnetic anisotropy to structural parameters as well as the single-ion anisotropies of the given system (see for example[19, 191]). Ruiz and co-worker[200] on the other hand suggested that "the zero-field splitting parameter" which is closely related to the magnetic anisotropy D "depends mostly on the ground state rather than on structural details". It has also been shown clearly that there is a connection between the ligands surrounding the metal center and the strength of the magnetic anisotropy[18, 19, 77]. Despite all these interesting approaches there is up to now no way to predict the magnetic anisotropy in a steady way. Therefore, it is consequently not possible to optimize the energy barrier U in a reliable way as there is no certain control of one of the two parameters involved. Moreover, as already indicated by Ruiz et al.[200] and stated more clearly by Neese and coworkers[150] ("the hidden dependence of the zero-field splitting parameter D to the spin quantum number implies that maximizing the total S through construction of polynuclear entities may not be needed to make better single-molecule magnets.") it is well possible that a simultaneous optimization of the magnetic anisotropy and the total ground state spin S of a given system is not possible at all.

The present work will address this issue of a dual optimization of the magnetic anisotropy D and the ground state S in more detail. All results are based on density functional theory (DFT)[93, 111] within the generalized gradient approximation (GGA) using mainly the PBE[168] functional. It is well known that ground state properties such as the total energy[170], charge densities or structural energy differences[84–86, 174, 232] are described quite accurate within DFT. However, there are some problems when it comes to the description of excited states, orbital energies, strongly correlated systems[14, 15], long range interactions (for example hydrogen bonds or Van der Waals forces), localized d- and f-electrons and band gaps in semiconductors and insulators[167, 208]. The problem of the localized d-electrons is well known and leads usually to an overestimation of the calculated exchange coupling with respect to experimental results[83, 114]. However, this is a systematic error and trends in the exchange coupling are usually well reproduced. The same applies to the band gap problem. Within DFT calculations the band gap is usually calculated too small in comparison to experiment or high level quantum mechanical methods. Despite all these problems DFT provides a fast and parameter-free first principle method for the computation of material properties such as electronic structure, total magnetic moments, exchange coupling constants and magnetic anisotropy energies. A short overview of the basics of density functional theory can be found in section 2.3, whereas the mechanism and basic principles for the magnetic interactions are described in more detail in section 2.4. Chapter 3 finally gives a short introduction on the software packages used for the calculations, visualization and analysis done in the present work.

Within chapter 4.1 various Robson-type hexamine-dithiophenolate macrocycles are studied with respect to their electronic and magnetic properties (exchange coupling and magnetic anisotropy). After a detailed discussion of the influence of different exchange correlation functionals on the computation of the magnetic anisotropy we will focus on the electronic and magnetic description of various third row transition metal complexes of the general structure $[M^{II}_2(L^6)(OAc)]^+$ (L=polyamine-dithiophenolate ligand ($C_{38}H_{64}N_6S_2$)). We will see that only Ni-dimers show the desired ferromagnetic coupling of the transition metal centers. Consequently, a detailed discussion of the electronic and magnetic properties of various bridged Robson-type hexamine-dithiophenolate macrocycles follows. It can be shown that trends in the magnetic

coupling can be explained in terms of the Goodenough-Kanamori rules[75, 76, 104] and within the Hay-Thibeault-Hoffmann[90] model whereas trends in the magnetic anisotropy can be related to geometric distortions and the gap between the highest occupied molecular orbital (HOMO) and the lowest unoccupied molecular orbital (LUMO). Furthermore, we will see that the size and charge of the third bridging ligand does not influence the magnetic coupling. However, weak ligands should be preferred as they open new ferromagnetic pathways across the third bridging ligand that enhance the ferromagnetic coupling. Another interesting finding is that a strong ferromagnetic coupling is related to a small magnetic anisotropy and vice versa.

In chapter 4.2 we will focus on the question whether or not it is possible to combine a large spin ground state S and a high magnetic anisotropy. As already discussed would be preferred in order to build single molecule magnets with a large barrier of magnetization U which is given by $U = S^2|D|$ (see also section 2.4.4). In order to get comparable results we restricted ourselves to octahedral coordinated, azido-bridged copper(II), nickel(II) and manganese(II) dimers. We would of course expect the highest barrier for the manganese complexes as those show the largest total spin ($S = 5$). Surprisingly, this is not the case. Instead, the largest barrier U is observed for the copper(II) ($S = 1$) complexes. Upon the discussion of these – at first glance unexpected – findings we will see that a high spin ground state S does not necessarily result in a large barrier. This is mainly due to the fact that the magnetic anisotropy can be related to the free ion single electron spin-orbit coupling parameter ζ (which increases from manganese to copper).

Finall, we will focus our studies on a family of polynuclear Mn_6 complexes. Here we will rule out the influence of the free ion single electron spin-orbit coupling parameter ζ as we focus only on Mn^{3+} ions. Instead, we will discuss the influence of the ligand and the ground state of a given molecule on the magnetic anisotropy. Our results reveal that the influence of the different ligands is rather small compared to the impact of the ground state. The differences in the barrier U for one given ground state S among the different complexes under investigation is much smaller than the difference in the barrier U for various ground states S of a given complex. This indicates that it is not possible to maximize the magnetic anisotropy D and the ground state S of a given system together.

2 Theoretical background

2.1 Classical and quantum mechanical Hamiltonian

As known from classical physics the total energy of any system is given by the sum over the kinetic energy T and the potential energy U:

$$\begin{aligned} E &= T + U \\ &= \frac{\vec{p}^{\,2}}{2m} + U(\vec{r}) \end{aligned} \tag{2.1}$$

This is also a common expression for the Hamilton $H(\vec{r}, \vec{p})$ in classical mechanics. Due to the correspondence principle[33] it is possible to obtain the respective quantum mechanical expression by replacing the classical quantities with the respective quantum mechanical operators:

$$\begin{aligned} E &\rightarrow \hat{E} = i\hbar\frac{\partial}{\partial t} \\ p &\rightarrow \hat{p} = -\frac{\hbar}{i}\nabla \\ \vec{r} &\rightarrow \hat{r} = \vec{r} \\ U &\rightarrow \hat{U} = \text{Coulomb interaction} \\ H(\vec{r}, \vec{p}) &\rightarrow \hat{H}(\hat{r}, \hat{p}). \end{aligned} \tag{2.2}$$

Therefore the classical Hamiltonian can be rewritten in the following form:

$$\begin{aligned} \hat{E} &= \hat{T} + \hat{U} \\ i\hbar\frac{\partial}{\partial t} &= -\frac{\hbar^2}{2m}\triangle + \hat{U}(\vec{r}). \end{aligned} \tag{2.3}$$

The application of the quantum mechanical Hamiltonian to the unknown wave function Ψ yields the fully time dependent Schrödinger Equation

$$\hat{H}\Psi = \hat{E}\Psi \tag{2.4}$$

2.2 Transition to electronic structure theory

The solution of the above described time dependent Schrödinger Equation is rather complex and for many applications it is not necessary to deal with an explicit time

dependence. Therefore it is possible to replace the energy operator $\hat{E}$ by the energy eigenvalue E for the time independent case.

$$\hat{H}\Psi = E\Psi \tag{2.5}$$

This is called the stationary Schrödinger equation[206, 207], which is appropriate to describe stable, stationary states with a fixed energy E. Despite these simplification the stationary Schrödinger equation is still very difficult to solve for many electron systems. For example the Hamiltonian for electrons and nuclei interacting through the coulomb potential is given by:

$$\hat{H} = \hat{T} + \hat{U}. \tag{2.6}$$

Here we get for the kinetic energy operator $\hat{T}$

$$\hat{T} = -\frac{\hbar^2}{2m}\sum_{i}^{N}\nabla_i^2 - \frac{\hbar^2}{2M}\sum_{K}^{M}\nabla_K^2 \tag{2.7}$$

describing the kinetic energy of the electrons i and the nuclei K. The operator $\hat{U}$ on the other hand is given by the coulomb interaction:

$$\hat{U} = -\frac{e^2}{4\pi\varepsilon_0}\sum_{i}^{N}\sum_{K}^{M}\frac{Z_K}{|\vec{R}_K - \vec{r_j}|} + \frac{e^2}{8\pi\varepsilon_0}\sum_{L\neq K}^{M}\frac{Z_K Z_L}{|\vec{R}_K - \vec{R_L}|} + \frac{e^2}{8\pi\varepsilon_0}\sum_{j\neq i}^{N}\frac{1}{|\vec{r}_i - \vec{r_j}|}. \tag{2.8}$$

including an attractive interaction is given between electrons and nuclei as well as the nucleus-nucleus and electron-electron repulsion.

A further simplification of the Schrödinger Equation is given within the so-called Born-Oppenheimer approximation[34]. It is based on the fact that the nuclei are much heavier ($\sim$ 1836 times) than the electrons. Thus, the movement of the electrons is very fast compared to the movement of the nuclei. Hence, in the system of nuclei and electrons the electrons are always in their ground state with respect to the instantaneous position of the nuclei. In other words it is possible to think about the electrons moving in a lattice defined by the nuclei. Thus, it is possible to separate the motion of the electrons from the nuclei. Consequently the presumption that coulomb interaction $\hat{U}$ depends only parametrically on the nucleus coordinates $\vec{R}_K$ is made:

$$\hat{U} = \hat{U}(\hat{r}_j; \vec{R}_K) \tag{2.9}$$

This assumption fails only in rare cases[60] and is therefore used widely nowadays. Within this approximation the kinetic energy operator $\hat{T}$ given in equation (2.7) reduces to:

$$\hat{T} = -\frac{\hbar^2}{2m}\sum_i^N \nabla_i^2 \tag{2.10}$$

since we can presume that

$$\frac{\hbar^2}{2M}\sum_K^M \nabla_K^2 = 0 \tag{2.11}$$

due to the assumption that the electrons move in a lattice defined by the nuclei. In this case the nuclei are at the nodes of the lattice and therefore they have no kinetic energy. Due to the same assumption it is possible to disregard the nucleus-nucleus repulsion. Therefore $\hat{U}$ reduces to:

$$\hat{U} = -\frac{e^2}{4\pi\varepsilon_0}\sum_i^N\sum_K^M \frac{Z_K}{|\vec{R}_K - \vec{r_j}|} + \frac{e^2}{8\pi\varepsilon_0}\sum_{j\neq i}^N \frac{1}{|\vec{r_i} - \vec{r_j}|}. \tag{2.12}$$

Within this approach we now define that the electrons move in the external field V_{ext} created by the positions of the nuclei. Therefore, the Schrödinger Equation can be now described in terms of $\hat{T}, \hat{U}$ (electron-electron repulsion) and $\hat{V_{\text{ext}}}$

$$\begin{aligned} \hat{H} &= \hat{T} + \hat{U} + \hat{V_{ext}} \\ &= -\frac{\hbar^2}{2m}\sum_i^N \nabla_i^2 + \frac{e^2}{8\pi\varepsilon_0}\sum_i^N\sum_{j\neq i}^N \frac{1}{|\vec{r_i} - \vec{r_j}|} - \frac{e^2}{4\pi\varepsilon_0}\sum_i^N\sum_K^M \frac{Z_K}{|\vec{R}_K - \vec{r_j}|}. \end{aligned} \tag{2.13}$$

It should be noted that in principle every observable O is given by the eigenvalue problem:

$$O[\Psi] = < \Psi|\hat{H}|\Psi > \tag{2.14}$$

This includes of course the energy E. According to the Rayleigh-Ritz principle[193] it is now possible to minimize the eigenvalue problem:

$$E_0 = \min_{\Psi\to\Psi_0} < \Psi|\hat{H}|\Psi > \tag{2.15}$$

in an iterative way. All wave functions yield an energy that is larger or in the case of Ψ_0 equal to the ground state energy E_0.

However, the problem is still not solvable which is mainly due to the electron-electron interaction $\hat{U}$. Note that $\hat{U}$ is a two-particle operator, hence the many-body effects have to be considered. These are namely exchange and correlation. Especially correlation (i.e. the instantaneous reaction of a given electronic system to a change at one localized position) is very hard to describe accurately. The core of the problem is that the whole system is more than the sum of its parts[13].
As already discussed above, every feature of a system is given by the exact solution of the Schrödinger Equation

$$\hat{T}\Psi + \hat{U}\Psi + \hat{V}_{ext}\Psi = i\hbar\frac{\partial}{\partial t}\Psi, \tag{2.16}$$

which is given in the stationary state and within the Born-Oppenheimer approximation by equation (2.13). But there is one fundamental drawback: An exact solution of the Schrödinger Equation is only possible for very simple cases. And even then the solution includes a many-body wave function $\Psi(\vec{r}_1, \vec{r}_2, ..., \vec{r}_N)$ containing $3N$ spatial coordinates. Since the number of electrons N increases very fast for real systems it is necessary to introduce approximations.
An straightforward approach to solve equation 2.13 is given in the Hartee-Fock theory[70, 87]. It is a variational method based on the Rayleigh-Ritz principle using a single Slater determinant to describe the many body wave function Ψ of a given system. By construction the method includes the exchange energy of the system. However, the correlation is completely missing[3]. This is to be expected as $\hat{U}$ is a two-particle operator. Therefore Ψ can not be described by a single Slater determinant. In other words, within the mean field approximation the instantaneous reaction of a given electronic system to a change at one localized position is approximated by a single averaged effect. This reduces the many-body problem to an one-body problem where correlation is missing by construction. However, correlation effects are extremely important, especially in chemistry. For example the flourine molecule F_2 would not be stable without taking correlation[187] into account. There are several post-Hartree-Fock methods that try to account for this weakness for example:

- the configuration interaction (CI) method[209],
- the multiconfiguration approach (MCHF/MCSCF)[69],

- coupled-cluster (CC) theories[96] all of which expand the true multi-electron wave function in terms of a linear combination of Slater determinants.
- the generator coordinate approach (GC)[81, 92], where the total Hamiltonian is diagonalized in a basis defined by mean-field wave functions. These wave functions are generated by a constraint on a collective variable, like the quadrupole moment of a nucleus.
- variational quantum Monte-Carlo[45, 137], where the Hartee-Fock wave function is modified by a correlation function ("Jastrow" factor) that is a function of multiple electrons.
- the many-body perturbation theory (MBPT), for example Møller-Plesset perturbation theory[143] which treats correlation as a perturbation of the Fock operator.
- the random phase approximation (RPA)[31, 32, 176] which has been developed to describe collective excitations that are a coherent superposition of single particle excitations.
- density functional theory (DFT) which treats exchange and correlation energies in an approximate way.

Out of the above mentioned methods DFT provides a fast and reliable method for the computation of ground state properties. Therefore, the next section will give a more detailed description of density functional theory.

2.3 Density Functional Theory

As the name "density functional theory" already suggests we will now try to replace the many-body wave function $\Psi(\vec{r}_1, \vec{r}_2, ..., \vec{r}_N)$ by a wave function that depends only on the density $n(\vec{r})$. This results in a tremendous reduction of the problem as we now consider a function of 3 instead of $3N$ spatial coordinates. Furthermore, suitable expressions for $\hat{T}$, $\hat{U}$ and $\hat{V_{ext}}$ are needed in order to keep the problem solvable. This is rather straightforward for the external potential $v(\vec{r})$:

$$V_{ext}[n] = \int n(\vec{r})v(\vec{r})\vec{r}, \tag{2.17}$$

and a bit more sophisticated for the potential and kinetic energy.

2.3.1 Thomas-Fermi model

The very first approximation to the potential and kinetic energy was proposed in 1927 by Thomas and Fermi[68, 216]. They suggested the use of a local system of non-interacting electrons instead of the complicated system of interacting electrons. In order to do that it is necessary to connect the electron density $n(\vec{r})$ and the kinetic energy T. The starting point is the kinetic energy T of the free electron gas given by the average of the kinetic energy of all electrons N within the system:

$$T = \frac{3}{5} N E_f \tag{2.18}$$

The Fermi energy E_f is given by the dispersion relation

$$E_f = \frac{\hbar^2}{2m} k_f^2 \tag{2.19}$$

including the mass m of an electron and the radius of the Fermi sphere k_f. Now it is possible to define the kinetic energy density $t[n(\vec{r})]$ as the kinetic energy T per volume V in terms of the density $n = \frac{N}{V} = \frac{1}{3\pi^2} k_f^3$:

$$t[n(\vec{r})] = \frac{3}{5} (3\pi)^{\frac{2}{3}} \frac{\hbar^2}{2m} n^{\frac{5}{3}}(\vec{r}) \tag{2.20}$$

Therefore, the kinetic energy T becomes a functional of the electron density $n(\vec{r})$ of the free electron gas:

$$T[n(\vec{r})] = \frac{3}{5} (3\pi)^{\frac{2}{3}} \frac{\hbar^2}{2m} \int n^{\frac{5}{3}}(\vec{r}) d^3r \tag{2.21}$$

Furthermore, the pair density of the electrons $n_2(\vec{r_i}, \vec{r_j})$ within the term for the potential energy $\hat{U}$ is replaced by the product of the single densities $n(\vec{r_i})$ and $n(\vec{r_j})$:

$$U[n(\vec{r})] = \frac{e^2}{8\pi\varepsilon_0} \int \int \frac{n(\vec{r_i}) n(\vec{r_j})}{|\vec{r_i} - \vec{r_j}|} d\vec{r_i} d\vec{r_j}, \tag{2.22}$$

which reduces the many-body problem to a single-particle problem. This results of course in a neglect of the exchange and correlation effects because these are many-body effects.

The Thomas-Fermi model was the first approach to solve the Schrödinger equation within the framework of a density $n(\vec{r})$. However, due to the crude approximation of the kinetic energy T and the neglect of exchange and correlation effects it often fails. The shell structure of atoms is not reproduced, atoms are smaller and more charged than in reality and molecular binding is not described[28].

2.3.2 Hohenberg-Kohn theorem

Another approach was proposed in 1964 by Hohenberg and Kohn[93]. First of all they proved that the initial idea - namely the treatment of a quantum mechanical problem in terms of the density $n(\vec{r})$ - is appropriate given that $\int n(\vec{r})d\vec{r} = N$. It turns out that the electron density is indeed a suitable variable that contains all information about a system in its ground state. They proved the ground state density $n_0(\vec{r})$ to be an unique functional of the external potential. To state this more clearly: it is not possible that two different external potentials $v_1(\vec{r})$ and $v_2(\vec{r})$ exist that yield the same ground state density $n_0(\vec{r})$.
Since all other parts of the Hamiltonian given in equation (2.13) are universal it can be concluded that the whole Hamiltonian is fully determined by the ground state density $n_0(\vec{r})$. Consequently, the ground state wave function is also a functional uniquely determined by the ground state density

$$\Psi(\vec{r}_1, \vec{r}_2, ..., \vec{r}_N) = \Psi[n(\vec{r})]. \tag{2.23}$$

This leads directly to the conclusion that every observable O (i.e. every expectation value $\langle\Psi|\hat{O}|\Psi\rangle$) is a functional of the ground state density. For example the ground state energy E_0 is given by:

$$E_0 = E_0[n(\vec{r})], \tag{2.24}$$

Furthermore they showed that there is a variational principle in terms of the density

$$E[n(\vec{r})] \geq E_0[n_0(\vec{r})] \tag{2.25}$$

where we get $E[n] = E_0[n]$ for degenerate ground states. Therefore it is not possible to find an initial density that leads to an energy smaller than the ground state energy E_0.

Finally, Levi[120] proved that it is possible to obtain the energy functional $E[n(\vec{r})]$ as a minimum of all wave functions resulting to the electron density $n(\vec{r})$. Hence

$$E[n(\vec{r})] = \min_{n \to n_0} \langle \Psi | \hat{T} + \hat{U} + \hat{V}_{ext} | \Psi \rangle \geq E_0, \tag{2.26}$$

The evaluation of this term gives:

$$E[n(\vec{r})] = F[n(\vec{r})] + \int n(\vec{r}) v(\vec{r}) d\vec{r} \tag{2.27}$$

including the universal functional (i.e. independent of V_{ext})

$$F[n(\vec{r})] = \min_{\Psi \to n} \langle \Psi | \hat{T} + \hat{U} | \Psi \rangle. \tag{2.28}$$

It is straightforward that the application of the ground state wave functions to equation (2.26) results in the computation of the ground state energy E_0

$$E[n_0(\vec{r})] = \langle \Psi_0 | \hat{T} + \hat{U} + \hat{V}_{ext} | \Psi_0 \rangle = E_0. \tag{2.29}$$

Given all these information it is possible to create a minimization algorithm in order to obtain the ground state energy:

$$E_0 = \min_n E[n(\vec{r})] \tag{2.30}$$

Within this algorithm minimization is carried out via all the electron densities originating from antisymmetric wave functions of all the electrons N. Therefore it is possible to evaluate the ground state density $n_0(\vec{r})$. Provided the functional $F[n(\vec{r})]$ is known it is also feasible to obtain the ground state energy E_0. Since we do not know the functional $F[n(\vec{r})]$, it is necessary to find suitable approximations.

2.3.3 Kohn-Sham equations

At this point the Kohn-Sham[111] equations can be applied order to transform DFT into a practical useful tool. They introduced a virtual auxiliary system consisting of non-interacting electrons that generates the same density as any given system of interacting particles. These electrons create an effective potential v_{eff}. Applying the

Hohenberg-Kohn theorem ensures that the density equals the potential. Assuming ($U \equiv 0$) equation (2.27) changes for a system of non-interacting electrons:

$$E_s[n(\vec{r})] = T_s[n(\vec{r})] + \int n(\vec{r}) v_{\text{eff}}(\vec{r}) d\vec{r} \tag{2.31}$$

including the kinetic energy T_s and the energy E_s of the system of non-interacting electrons. Equation (2.30) therefore leads directly to the Euler-Lagrange equation:

$$\frac{\partial}{\partial n(\vec{r})}\{E_s[n(\vec{r})] + \mu[N - \int n(\vec{r}) d\vec{r}]\} = \frac{\partial T_s[n(\vec{r})]}{\partial n(\vec{r})} + v_{\text{eff}}(\vec{r}) - \mu = 0. \tag{2.32}$$

The Lagrange parameter μ is introduced in order to ensure the conservation of the number of electrons N within a given system and corresponds to the electrochemical potential. For $T = 0$ it equals the Fermi energy E_F. Since it is possible to express the functional $T_s[n(\vec{r})]$ of non-interacting electrons using the single particle wave functions $\varphi_i(\vec{r})$

$$T_s[n(\vec{r})] = \sum_i^{\text{occ}} \int \varphi_i^*(\vec{r}) \left(-\frac{\hbar^2}{2m} \nabla^2 \right) \varphi_i(\vec{r}) d\vec{r}, \tag{2.33}$$

it is manageable to obtain the ground state energy given that the effective potential is known. Within this framework the density $n(\vec{r})$ of the interacting system can be obtained by summation over all occupied orbitals:

$$n(\vec{r}) = \sum_i^{\text{occ}} |\varphi_i(\vec{r})|^2. \tag{2.34}$$

Variation of $E[n(\vec{r})]$ with respect to the one particle wave function results in:

$$\left[-\frac{\hbar^2}{2m} \nabla^2 + v_{\text{eff}}(\vec{r}) - \mu \right] \varphi_i(\vec{r}) = \epsilon_i \varphi_i(\vec{r}). \tag{2.35}$$

In order to maintain $(\varphi_i, \varphi_i) = 1$ the Kohn-Sham eigenvalue ϵ_i is introduced. However, this algorithm depends on a suitable choice of v_{eff}. Therefore, Kohn and Sham reformulated equation (2.27)

$$E[n(\vec{r})] = T_s[n(\vec{r})] + \int n(\vec{r}) v_{\text{ext}}(\vec{r}) d\vec{r} + \frac{e^2}{8\pi\varepsilon_0} \int \frac{n(\vec{r_i}) n(\vec{r_j})}{|\vec{r_i} - \vec{r_j}|} d\vec{r_i} d\vec{r_j} + E_{\text{xc}}[n(\vec{r})] \tag{2.36}$$

They included the so called exchange-correlation energy $E_{xc}[n(\vec{r})]$:

$$E_{xc}[n(\vec{r})] = F[n(\vec{r})] - T_s[n(\vec{r})] - \frac{e^2}{8\pi\varepsilon_0} \int \frac{n(\vec{r_i}) n(\vec{r_j})}{|\vec{r_i} - \vec{r_j}|} d\vec{r_i} d\vec{r_j}\,'. \tag{2.37}$$

Applying the variational principle results in

$$\frac{\partial T_s[n(\vec{r})]}{\partial n(\vec{r})} + v_{\text{ext}}(\vec{r}) + \frac{e^2}{8\pi\varepsilon_0}\int \frac{n(\vec{r_j})}{|\vec{r_i} - \vec{r_j}|} d\vec{r_j} + \frac{\partial E_{\text{xc}}[n(\vec{r})]}{\partial n(\vec{r})} - \mu = 0. \tag{2.38}$$

In order to get an analytical expression for the effective potential v_{eff} it is necessary to compare equation (2.31) and (2.38). Hence the effective potential can be written as:

$$v_{\text{eff}}(\vec{r}) = v(\vec{r}) + \frac{e^2}{8\pi\varepsilon_0}\int \frac{n(\vec{r_j})}{|\vec{r_i} - \vec{r_j}|} d\vec{r_j} + v_{\text{xc}}[n(\vec{r})](\vec{r}) \tag{2.39}$$

including the exchange-correlation potential $v_{\text{xc}}[n(\vec{r})](\vec{r})$

$$v_{xc}[n(\vec{r})](\vec{r}) = \frac{\partial E_{\text{xc}}[n(\vec{r})]}{\partial n(\vec{r})}. \tag{2.40}$$

Note that the Kohn-Sham wave function is a single Slater determinant since the particles in the Kohn-Sham system are non-interacting. All interactions of the many-body system are covered by the exchange-correlation potential.
As shown in Figure 2.1 the self consistent solution of equations (2.39), (2.35) and (2.34) finally yields the ground state electron density.
A typical self consistent field (SCF) cycle would start with the guess of an initial density $n_1(\vec{r})$. Using this initial density it is possible to calculate the effective potential v_{eff}. Now it is feasible to solve the Kohn-Sham equations which yield the single particle wave functions $\varphi_i(\vec{r})$. Based on equation (2.34) we get now a new density $n_2(\vec{r})$. Now we compare both densities $n_1(\vec{r})$ and $n_2(\vec{r})$ and if the difference between those two is smaller than the chosen convergence criterion ϵ the SCF cycle is converged and we can extract the desired properties. Otherwise the new density $n_2(\vec{r})$ is plugged in again into the cycle. This will continue until the convergence criterion is met.

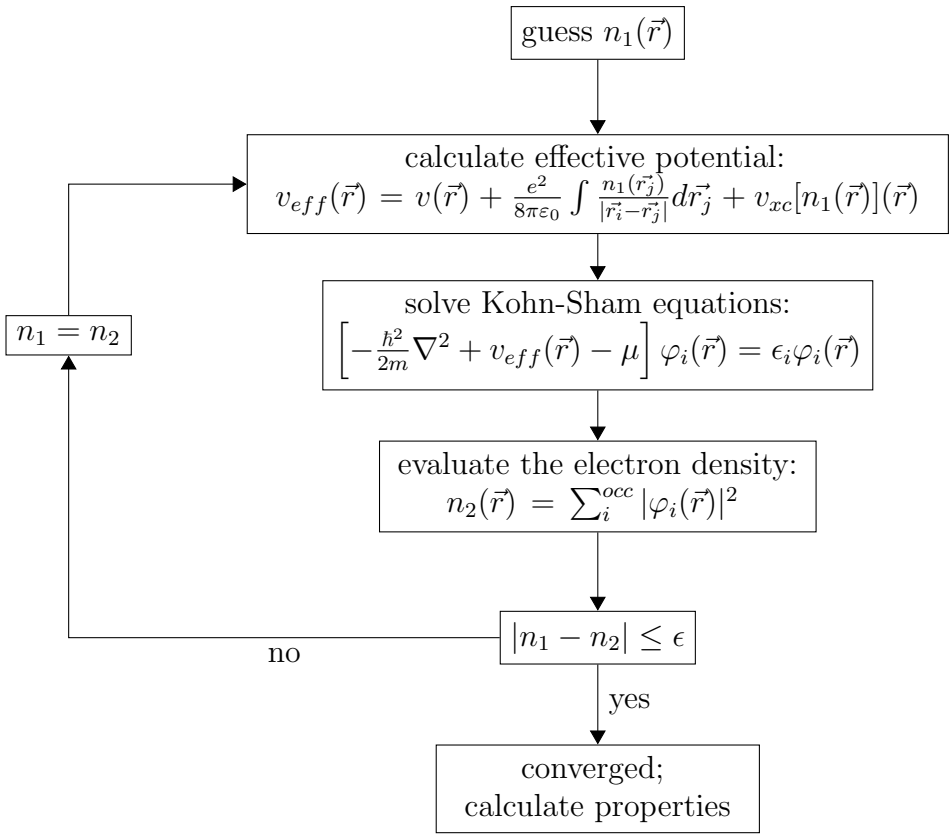

Figure 2.1: Flowchart of the iteration scheme used within density functional calculations. The convergence criterion ϵ is chosen depending on the actual problem.

2.3.4 Approximations of the exchange-correlation functional

The algorithm shown in Figure 2.1 is capable to compute the ground state density $n_0(\vec{r})$. Yet the functional $E_{xc}[n(\vec{r})]$ is still unknown. Up to now the exact form of the exchange-correlation functional is not known (except for the free electron gas) and therefore approximations are needed. The most simple approach is the local density approximation (LDA)[111]. Within the LDA it is assumed that the local density at given point $\vec{r}$ can be treated as an uniform electron gas. Therefore, the exchange-correlation energy is treated locally.

$$E_{\mathrm{xc}}^{\mathrm{LDA}}[n(\vec{r})] = \int \epsilon_{\mathrm{xc}}^{\mathrm{LDA}} n(\vec{r}) d\vec{r}, \tag{2.41}$$

including the $\epsilon_{\mathrm{xc}}^{\mathrm{LDA}} n(\vec{r})$ per-volume exchange-correlation energy of the uniform electron gas. The exchange part $\epsilon_x n(\vec{r})$ is exactly known from quantum mechanics[40]

$$\epsilon_x n(\vec{r}) = -\frac{3}{4} e^2 (\frac{3}{\pi})^{\frac{1}{3}} n^{\frac{4}{3}}. \tag{2.42}$$

It is simply the exchange energy per particle in each spatial point taken from a uniform electron gas with a density equal to the density at that point. Unfortunately no exact formulation of the correlation energy ϵ_c is known and further approximations are needed. Originally the approximation of Wigner[223, 224] was used. All modern correlation energies such as VWN[222], PZ[173] and PW[172] go back to the parametrizations of Ceperley and Alder[46] who did very accurate Quantum Monte Carlo calculations. LDA functionals are still widely used nowadays. However, there are some shortcomings. As long as systems with slowly varying electron density are considered, LDA gives reasonable good results. In the case of the homogeneous electron gas it is even the correct solution. But LDA may fail for systems with strongly inhomogeneous electron density distribution. An other problem is the overbinding which often leads to a shortening of bonds by about 1-2 %. Despite all these drawbacks geometries are usually predicted with this accuracy[66].
In order to overcome these issues another approximation - including not only the electron density distribution but also its gradient - can be used. These functionals are called generalized gradient approximation (GGA)

$$E_{\mathrm{xc}}^{\mathrm{GGA}}[n(\vec{r})] = \int f(n, \nabla n) n(\vec{r}) d\vec{r}. \tag{2.43}$$

In contrast to LDA the function $f(n, \nabla n) n(\vec{r})$ for GGA is not unique. A number of approaches exists to solve this problem. Well known is for example the GGA functional proposed by Perdew and Wang (PW91)[169] or the functional suggested by Perdew, Burke and Enzerhof (PBE)[168], but there are several more functionals known (see for example Neese[149] and references therein for a more detailed overview). Using GGA functionals instead of the LDA approximation results in more accurate total energies[170] and atomization energies[24, 170, 183]. GGA functionals are also more precise in the calculation of energy barriers as well as structural energy differences[84–86, 174, 232]. Furthermore the overbinding of the LDA functional is corrected. However it is over corrected by about 1-2 % giving rise to longer bonds

than observed in nature. Yet there are still certain system that can not be described accurately using the above mentioned approaches and further improvement was necessary. One example are meta-GGAs, which include orbital dependent quantities such as the kinetic energy density[214]. For further reading see for example[28, 118].
Another approach to enhance the accuracy are hybrid functionals introduced by Becke[25, 26, 212]. These functionals include a certain portion of exact Hartree-Fock exchange into the functional and are also referred to as hyper-GGA's. A very prominent example is the so-called B3LYP hybrid functional with the following definition:

$$E_{\mathrm{xc}}^{\mathrm{B3LYP}} = E_{\mathrm{xc}}^{\mathrm{LDA}} + a_0(E_x^{\mathrm{HF}} - E_x^{\mathrm{LDA}}) + a_x(E_x^{\mathrm{GGA}} - E_x^{\mathrm{LDA}}) + a_c(E_c^{\mathrm{GGA}} - E_c^{\mathrm{LDA}}) \quad (2.44)$$

The three empirical parameters a_0, a_x and a_c are determined via fitting of the predicted values of a set of atomization energies, ionization potentials, proton affinities, and total atomic energies[25]. The best fit was obtained with $a_0 = 0.20$, $a_x = 0.72$ and $a_c = 0.81$. Within the definition of the B3LYP potential the Becke 88 exchange functional (E_x^{GGA})[23] and the correlation functional of Lee,Yang and Parr (E_c^{GGA})[119] are used (hence the name B3LYP=Becke, three parameters, Lee, Yang and Parr) as well as the LDA exchange and correlation potential and the Hartree-Fock exchange E_x^{HF} which is given by:

$$E_x^{\mathrm{HF}} = \frac{1}{2}\sum_{i,j}\int\int \varphi_i^*(r_1)\varphi_j^*(r_1)\frac{1}{r_{12}}\varphi_i(r_2)\varphi_j(r_2)dr_1dr_2. \quad (2.45)$$

The use of hybrid functionals usually improves molecular properties such as atomization energies, bond lengths and vibration frequencies compared to the results obtained by LDA or GGA calculations. However it is important to remember that these hybrid functionals mix different approaches (Hartree-Fock vs. DFT). There are also recent studies that suggest that B3LYP becomes increasingly erroneous for larger systems[82].
It is also possible to include the spin in the LDA and GGA functionals. Concerning the LDA functional this process is quite straightforward and results in a so-called local-spin density approximation LSDA.

$$E_{\mathrm{xc}}^{\mathrm{LSDA}}[n(\vec{r})] = \int f(n_\uparrow, n_\downarrow)n(\vec{r})d\vec{r} \quad (2.46)$$

Applying this ansatz to GGA leads therefore consequently to:

$$E_{\mathrm{xc}}^{\mathrm{GGA}}[n(\vec{r})] = \int f(n_{\uparrow}, n_{\downarrow}, \nabla n_{\uparrow}, \nabla n_{\downarrow}) n(\vec{r})) d\vec{r} \tag{2.47}$$

However the local approach is not always sufficient. In order to improve the situation non-local density functionals came recently into focus such as the average density approximation (AVA) where the density at a given point $\vec{r}$ is influenced by the density everywhere else. For further reading see for example[131].
A very nice overview of various approximations for the exchange-correlation functional is for example given by Perdew et al.[171] or by Kümmel and Kronik[118].

2.3.5 Self-interaction

The above described approximations of the exchange-correlation functional have been successfully applied to many problems over the years. However, it is important to mention that there are still problems using these functionals. The most important one is the *self-interaction*. Due to the construction of the potentials an electron in an occupied orbital interacts with all N electrons of the system instead of $N-1$. In other words there is an interaction of the electron with itself. The self-interaction leads to a delocalization of orbitals due to a reduced binding energy. This is especially important for localized states such as d- and f-shells. There are several approaches to solve the problem. One is the so-called self-interaction correction (SIC) proposed by Perdew and Zunger[173] which subtracts orbital-wise the contribution the exchange-correlation functional would make if there was only one electron in the system. The use of SIC results in an improvement of the total energy, more accurate binding, more precise electron densities and an overall improvement of the long range behaviors of potential and density (see Perdew et al.[171] and references therein). However, the SIC does not always work properly[58, 79, 80, 128, 178, 201] and it is sometimes argued that the self-interaction actually simulates longe-range correlation effects (see Neese[149] and references therein).

2.3.6 Basis sets

After introducing the theoretical basics of density functional theory and some of its problems this section will focus on the actual computation of the electronic density.

Usually the wave functions Ψ are expanded in terms of basis functions ϕ_j:

$$\Psi = \sum_{i=1}^{\infty} c_j \phi_j, \tag{2.48}$$

including suitable constants c_j. There are two commonly applied classes of functions ϕ: non-localized basis functions like plane waves (PWs) on the one hand and localized atomic-like orbitals (AOs) on the other hand. Plane wave basis sets are typically applied in combination with pseudopotentials for the computation of systems with periodic boundary conditions[41] and are given by.

$$\phi_j = e^{i\vec{k_j}\vec{r}} \tag{2.49}$$

The advantage of PW basis sets is the easy computational handling and the good convergence of the calculated properties with respect to the basis-set size. However, there is one big drawback. In order to describe localized states accurately many basis functions are needed and the basis sets may get very large. This results in high computational costs. Therefore, localized atomic-like orbitals are the better choice to describe the wave functions of single molecules. There exist several types of AOs. Commonly used are augmented plane waves (APW)[225] (these are actually a mix of plane waves and localized atomic-like orbitals), linearized muffin-tin orbitals[11], Slater-type orbitals (STOs)[210] and Gaussian-type orbitals (GTOs), introduced by Boyc[35]. The general form of STOs and GTOs is described by:

$$\phi = Y * R \tag{2.50}$$

The angular part Y of the wave function is in both cases the same and are given by spacial harmonics. The main difference between STOs and GTOs is the different distance dependency in the radial part R of the wave function. Slater-type orbitals have the general form

$$R(r) = Ar^{n-1}e^{-\alpha r}. \tag{2.51}$$

and show an e^{-r} dependency in the radial part of the wave function. The constant A is simply a scaling factor, n is the main quantum number and α is a constant that determines the radius of the orbit. Gaussian-type orbitals on the other hand show a e^{-r^2} dependency:

$$R(r) = Ar^{2n-2-l}e^{-\alpha r^2} \tag{2.52}$$

Additionally to the main quantum number n the angular quantum number l is included. Slater-type orbitals are basically preferable, because they describe the properties of the atomic wave functions more accurately than Gaussian-type orbitals. This is due to the fact that the STOs have an advanced shape near to and far away from the nucleus. Therefore more GTOs than STOs are necessary in order to achieve a certain convergence. However, it is computationally not easy to use Slater-type orbitals. This is why usually Gaussian-type orbital are used to compute the basis functions since the computational handling of GTOs is much easier. The so-called "Gaussian Product Theorem" guarantees that the product of two gaussians is always a gaussian. Therefore, it is possible to reduce the product of two gaussians at different centers of a molecule (i.e. a multi-center integral) to one gaussian with a shifted center (i.e. an one-center integral). This results in a general speedup of the calculation by a factor of 4-5 compared to STOs. Hence the use of gaussian type orbitals results in less computational cost compared to the use of slater type orbitals despite the fact that more GTOs than STOs are needed to describe the system.
It is also possible to combine the good properties of gaussian type orbitals and slater type orbtials by a linear combination of GTOs in order to resemble the shape of one STO. These basis functions are called contracted gaussian type orbitals (CGTOs).

$$\phi^{CGTO} = \sum_{j=1}^{\infty} d_j \phi_j^{GTO} \tag{2.53}$$

Nowadays many DFT codes use contracted gaussian type orbitals to describe the wave functions.

2.4 Magnetic interactions - theoretical aspects

After a short introduction to density functional theory this work shall now deal with a detailed discussion of the magnetic interactions. Beginning with the Spin Hamilton formalism we will than elaborate on different possible exchange mechanisms.

2.4.1 Spin Hamilton formalism

The spin Hamiltonian is a model Hamiltonian containing only spin operators. Model Hamiltonians are used whenever a system is too complex to evaluate the appropriate Hamiltonian. Therefore, approximations and simplifications are introduced in order to describe the system. In the case of the spin Hamiltonian all orbital coordinates are integrated out keeping only the spin. Furthermore, it is supposed that the spins are independent of each other[73]. With respect to all these restrictions the Heisenberg(-Dirac)[64, 91] spin Hamiltonian can be written as:

$$H = -2\sum_{i>j} J_{ij}\hat{S}^i \cdot \hat{S}^j. \tag{2.54}$$

Within this framework $\hat{S}^{i,j}$ are spin operators acting on the i^{th} and j^{th} magnetic center. The matrix element of the interaction between spin i and j is represented by the magnetic exchange coupling parameter J_{ij}. This parameter yields the sign (ferromagnetic or antiferromagnetic coupling) and strength of the magnetic coupling. As shown nicely by Calzado and co-workers[37–39] J_{ij} arises from the quantum mechanical requirement of antisymmetry. This leads to an mixing of the spin-part and the space-part of the many-body wave function in such a way that electrostatic interactions in real space can impose requirements on the spin state[175]. With respect to these considerations the interaction can be understood as a competition of the exchange interaction (favoring $J_{ij} > 0$ = alignment of $\hat{S}^i$ and $\hat{S}^j$) and correlation effects (favoring $J_{ij} < 0$ = anti-alignment of $\hat{S}^i$ and $\hat{S}^j$). Note that each pair $\hat{S}^i, \hat{S}^j$ is considered once (no double counting). Since only the relative orientation of the spins with respect to each other is relevant, this representation of the model Hamiltonian covers just isotropic media. This assumption enables the use of symmetry operations of the system, which may results in a significant reduction of the problem (depending on the symmetry present).

In order to include anisotropy the alignment of the spins must be taken into account.

$$H = -2\sum_{i>j} J_{ij}[S_z^i S_z^j + \gamma(S_x^i S_x^j + S_y^i S_y^j)]. \tag{2.55}$$

At this point it is important to notice that there exist some slight differences in the definition of the Heisenberg Hamiltonian. It is also possible to include the negative algebraic sign and/or the pre-factor 2 in the coupling constant J. Within this definition positive J values always indicate ferromagnetic coupling. Respectively, $J < 0$ states antiferromagnetic coupling.

By taking a closer look at the Heisenberg Hamiltonian it can be seen that there is another parameter involved. Changing the value of γ leads to the occurrence of different models. In the case of $\gamma = 0$ the Ising model can be obtained. The Heisenberg model corresponds to $\gamma = 1$ and $\gamma \gg 1$ results in two-dimensional interaction.

In order to explain the differences between the Ising model and the Heisenberg model the easiest system, two interacting spins $S_1 = S_2 = \frac{1}{2}$, will be discussed in detail. The Ising model yields the following spin Hamiltonian:

$$H = -2J_{12}S_z^1 S_z^2 \tag{2.56}$$

The eigenvalues of S_z are known as $S_z\Psi = \pm\frac{1}{2}\Psi$ (assuming $\hbar = 1$). This results in the spin Hamiltonian H

$$H = \begin{pmatrix} -\frac{J}{2} & 0 & 0 & 0 \\ 0 & \frac{J}{2} & 0 & 0 \\ 0 & 0 & \frac{J}{2} & 0 \\ 0 & 0 & 0 & -\frac{J}{2} \end{pmatrix} \tag{2.57}$$

with respect to the basis $\Psi = (\uparrow\uparrow, \uparrow\downarrow, \downarrow\uparrow, \downarrow\downarrow)$. The energy eigenvalues of the matrix are given by $E_{1,2} = \pm\frac{J}{2}$. Therefore, an energy difference of J between the ferromagnetic and the antiferromagnetic state of the system is calculated. For a detailed treatment see Appendix A.

For the Heisenberg model it is assumed that the spin operator $\vec{S}$ contains components in the z direction as well as in the x and y direction resulting in:

$$H = -2J_{12}(S_x^1 S_x^2 + S_y^1 S_y^2 + S_z^1 S_z^2). \tag{2.58}$$

Since S_z commutes with $\vec{S}^2$ but not with S_x or S_y it is necessary to rewrite the Hamiltonian. For this purpose the generation and annihilation operator S_+ and S_- are defined.

$$S_+ = S_x + iS_y \tag{2.59}$$
$$S_- = S_x - iS_y. \tag{2.60}$$

The effect of these operators on a given state can be described by

$$S_\pm|S, S_z\rangle = \sqrt{S(S+1) - S_z(S_z \pm 1)}|S, S_z \pm 1\rangle \tag{2.61}$$

The anticommutator of the generation operator and the annihilation operator yields

$$S_+^1 S_-^2 + S_-^1 S_+^2 = 2S_x^1 S_x^2 + 2S_y^1 S_y^2. \tag{2.62}$$

Rearrangement of equation (2.62) and insertion into equation (2.58) results in

$$H = -2J_{12}(\frac{S_+^- S_-^2 + S_-^1 S_+^2}{2} + S_z^1 S_z^2). \tag{2.63}$$

Solving this Hamiltonian returns the interaction matrix

$$H = \begin{pmatrix} -\frac{J}{2} & 0 & 0 & 0 \\ 0 & \frac{J}{2} & -J & 0 \\ 0 & -J & \frac{J}{2} & 0 \\ 0 & 0 & 0 & -\frac{J}{2} \end{pmatrix} \tag{2.64}$$

with respect to the basis $\Psi = (\uparrow\uparrow, \uparrow\downarrow, \downarrow\uparrow, \downarrow\downarrow)$. Unlike the interaction matrix given by the Ising model non-diagonal entries appear. The computation of the energy eigenvalues shows a singlet state with $E_1 = \frac{3}{2}J$ ($S = 0$, antiferromagnetic) and a triplet state ($S = 1$, ferromagnetic) including $E_2 = E_3 = E_4 = -\frac{J}{2}$. The energy difference between the ferromagnetic and antiferromagnetic solution amounts to $2J$. In conjunction with the eigenvectors the following eigenstates can be found:

$$\psi = \frac{|\downarrow\uparrow\rangle - |\uparrow\downarrow\rangle}{\sqrt{2}} \quad \rightarrow m_s = 0 \qquad s = 0$$

$$\left.\begin{aligned} \psi &= |\downarrow\downarrow\rangle && \rightarrow m_s = -1 \\ \psi &= \frac{|\uparrow\downarrow\rangle + |\downarrow\uparrow\rangle}{\sqrt{2}} && \rightarrow m_s = 0 \\ \psi &= |\uparrow\uparrow\rangle && \rightarrow m_s = 1 \end{aligned}\right\} s = 1$$

Even in this simple case the Ising model and the Hamilton model return different solutions for the same problem. The advantage of the Ising model is its simplicity. On the other hand it fails to describe the correct splitting of the levels. Therefore the Heisenberg model will be used in all further considerations.

2.4.2 Exchange mechanism

Taking only a look at the spin Hamiltonian yields a priori no information about the mechanism of coupling (ferromagnetic or antiferromagnetic). In order to specify the exchange coupling in more detail different models can be applied.

a) direct exchange

The most intuitive model is the **direct exchange**. Whenever two magnetic particles are close together they have a sufficient overlap of their wave functions. This results in a strong coupling of short range which is rapidly decreasing as soon as the particles are separated. Taking a closer look at a simplified model (two magnetic particles with one electron each) shows that two different cases of direct exchange exist. In the first case both particles are close together as shown in Figure 2.2. Here it is favorable for the electrons to be in between the two particles in order

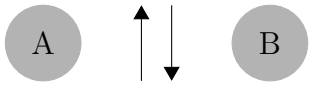

Figure 2.2: Two magnetic particles with one electron each, short distance

to minimize the coulomb interaction. The two electrons are reqiured to be at the same place in space and time. This is only possible if they are antiferromagnetically aligned. Otherwise Paulis exclusion principle would be violated.
The situation changes if the magnetic particles are far apart from each other as shown in Figure 2.3. Now the electrons spend most of their time far away from each other in order to minimize the electron repulsion. This results in a parallel alignment of the electron spin, i.e. ferromagnetic coupling is observed.
As shown in the example above the nature of the observed coupling is governed by the interplay of the atomic distance and the coulomb interaction/electron repulsion.

Figure 2.3: Two magnetic particles with one electron each, large distance

Direct exchange occurs typically in metals. It is also infrequently observed in organic molecules containing transition metal centers where it is called spin polarization.

b) indirect exchange

As already mentioned direct exchange is rarely observed in organic molecules containing transition metal centers. Within these class of molecules the magnetic exchange is often mediated by a non-magnetic bridging atom. Therefore, this kind of exchange coupling is called indirect exchange or **superexchange**.

The superexchange mechanism was first described by Anderson[12]. The observed

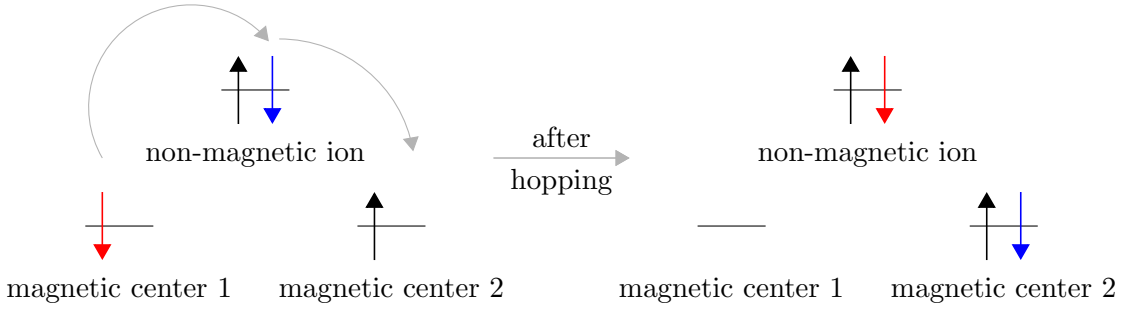

Figure 2.4: Superexchange expected for a d^9 occupation of the magnetic orbitals. Note that the non-magnetic p-orbitals are energetically lower than the d-orbitals of the magnetic center. They are drawn above them for reasons of clarity.

coupling is usually antiferromagnetic. Superexchange only occurs if the involved transition metal ions exhibit a partial empty d-shell. As soon as the d-shell is fully occupied, no magnetism is observed. Assuming a d^9 occupation of the involved d-orbitals at the transition metal ions superexchange as shown in Figure 2.4 is expected. In order to observe a superexchange it is vital that the magnetic orbitals (i.e. the d-orbitals of the transition metals) and the p-orbitals of the non-magnetic bridging ion are energetically close together. It is also important that the distance

between the metal ion and the bridging ion is not too large to get significant overlap of the involved orbitals. Given that all these requirements are met one electron of the filled p-orbital can hop to a half-filled d-orbital of magnetic center 2, provided it exhibits the right spin state. Now the p-orbital is half-filled. In order to minimize the energy the electron from metal center 1 hops over. The whole process only takes place if the spin states at the magnetic centers are different from each other. Otherwise Paulis exclusion principle would be violated. Therefore, this kind of superexchange coupling is always antiferromagnetic. The superexchange is energetically favored, because the electrons of the d-shell are strongly delocalized across the molecular orbitals. However, the situation may change for different occupations

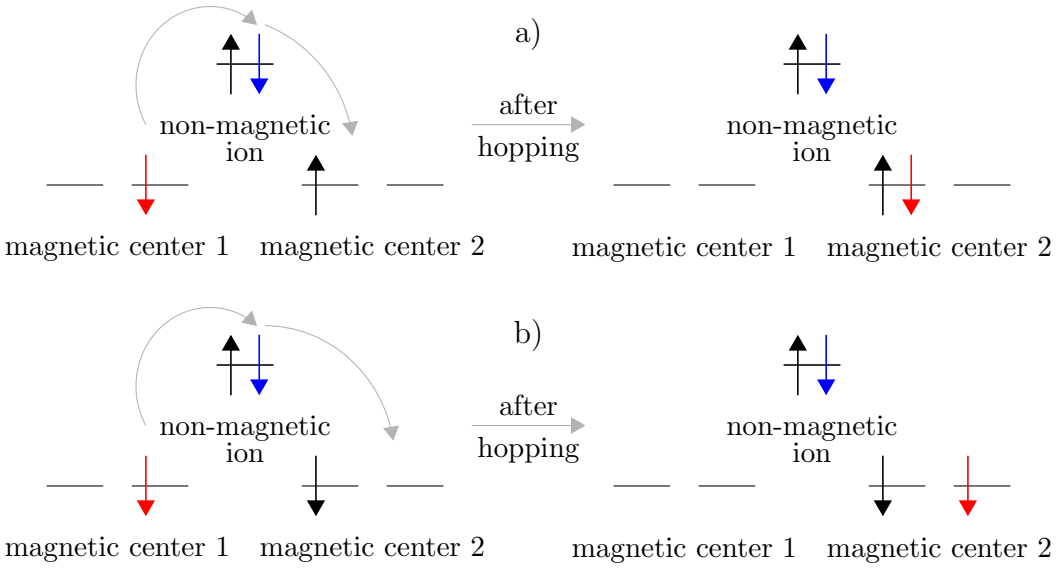

Figure 2.5: Superexchange expected for a d^1 - d^8 occupation of the magnetic orbitals; 2.5a) antiferromagnetic coupling; 2.5b) ferromagnetic coupling. Note that the non-magnetic p-orbitals are energetically lower than the d-orbitals of the magnetic center. They are drawn above them for reasons of clarity.

of the d-shell. In the case of d^1-d^8 occupation antiferromagnetic exchange is possible if the two electrons at the magnetic centers possess different spin states. The process of antiferromagnetic exchange coupling is similar to the already discussed process in the d^9 case and shown in Figure 2.5a. Given that both electrons exhibit the same spin state it is now also possible to observe ferromagnetic coupling due

to the existence of other empty, low lying d-orbitals. As shown in Figure 2.5b the electron of the magnetic center 1 can hop via the non-magnetic ion to another empty d-orbital located at the magnetic center 2. In the ideal case this empty d-orbital is degenerated in comparison to the already half-filled one at the magnetic center 2. However, this is usually not true because of the local crystal field which induces a level splitting of the d-orbitals. The ferromagnetic exchange can nevertheless occur as long as the energy difference between the two d-orbitals is small. Besides

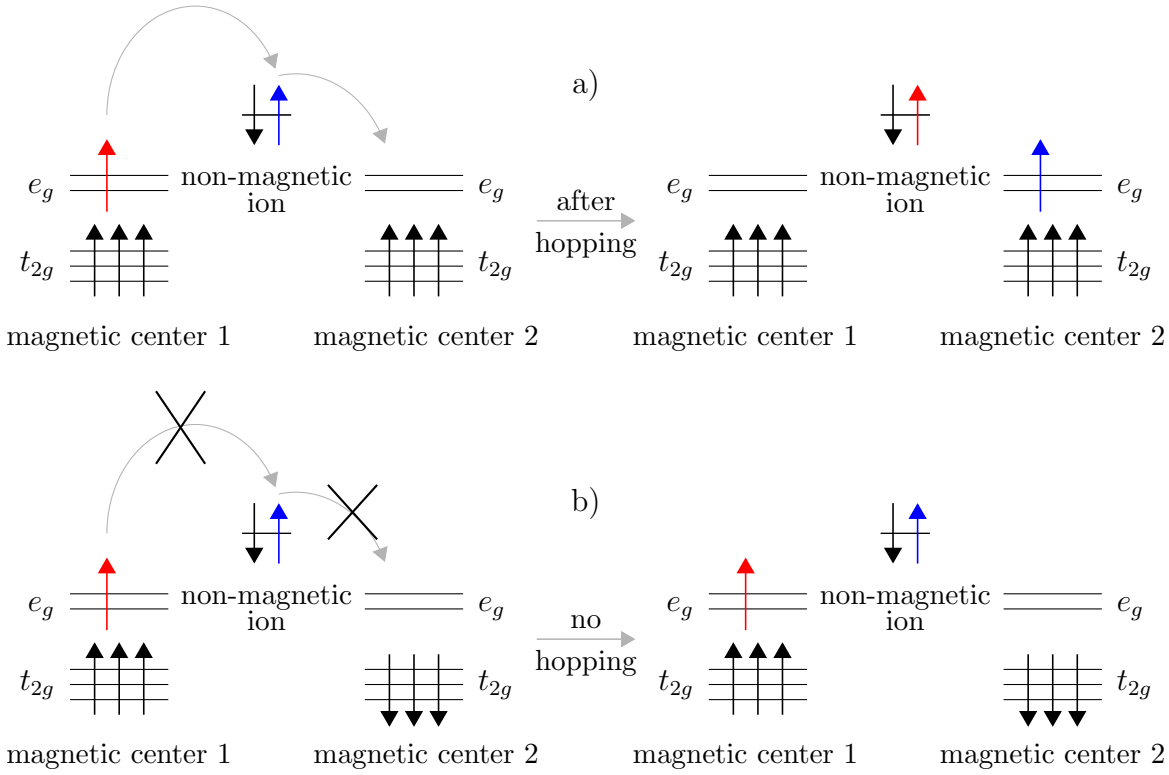

Figure 2.6: Ferromagnetic double-exchange mechanism in an octahedral crystal field; 2.6a) ferromagnetic coupling allowed; 2.6b) no coupling possible due to Paulis exclusion principle. Note that the non-magnetic p-orbitals are energetically lower than the d-orbitals of the magnetic center. They are drawn above them for reasons of clarity.

the already discussed cases it is also possible that the two magnetic centers show a mixed valence (i.e. different oxidation states or different species at magnetic center

one and two). The resulting exchange is called **double-exchange**. The double-exchange mechanism is very similar to the superexchange and was first proposed by Zener[230]. As shown in Figure 2.6a double-exchange can only occur if the electrons at both magnetic centers are parallel aligned. Otherwise the transition is forbidden due to Paulis exclusion principle (see Figure 2.6b). Given that all the involved spins are parallel aligned an electron of the p-orbital at the non-magnetic bridging ion can hop to an unoccupied e_g-orbital at the magnetic center 2. Now an electron of the e_g-orbital at the magnetic center 1 can hop to the half-filled p-orbital in order to minimize the total energy of the system. Again the ferromagnetic coupling is favored because of the energy gain due to the strong delocalization of the e_g-electron across molecular orbitals.

All of the above discussed exchange mechanisms are based on transitions between identical orbitals. But the coupling is not limited to these cases. As shown by Hotzelmann et al.[94] it is also possible to get coupling between different orbitals and/or excited states. This leads to the occurrence of many possible exchange pathways. Depending on the overlap of the involved orbitals there can be ferromagnetic and antiferromagnetic coupling within one exchange pathway. The sum over all these exchange pathways marks the resulting exchange interaction. This kind of exchange mechanism is called **crossed interaction**.

Another possible exchange interaction is the so-called **Dzyaloshinsky-Moriya interaction**. Here the coupling occurs via exited states introduced by the spin-orbit coupling. The Dzyaloshinsky-Moriya interaction gives rise to a weak ferromagnetic coupling.

It is possible to generalize the discussed exchange mechanisms since all of them depend strongly on the overlap of the involved orbitals. Therefore the exchange coupling can be described by the application of the **Goodenough-Kanamori rules**[75, 76, 104]:

1. If the magnetic orbitals of two ions have a reasonably large overlap integral, the resulting exchange is antiferromagnetic.

2. If the orbitals are expected to be in contact but have no overlap integral, the interaction is ferromagnetic.

3. A magnetic orbital overlapping an empty one leads to ferromagnetic exchange.

All the discussed exchange mechanisms can be noticed in magnetic molecules. However the mapping of the involved orbitals is not always straightforward, since a degeneracy of levels can no longer be observed. Within the molecular orbitals a huge splitting of levels occurs resulting in a large number of possible exchange pathways. So in order to understand the experimentally observed coupling it is very useful to compute the energy levels of the magnetic molecules for example by means of DFT.

2.4.3 Hay-Thibeault-Hoffmann model

The Hay-Thibeault-Hoffmann (HTH) model is a quantitative model to explain the exchange coupling of weakly interacting metal centers. The original paper[90] deals with d^9 transition metal complexes as well as the general d^n-case. For reasons of simplicity only the d^9-case will be considered here in more detail. In the d^9-case the unpaired electron occupies a d-orbital at the transition metal center. Without strong metal-metal bonds (i.e. no direct overlap of the d-orbitals) the interaction diagram of the two half-filled d-orbitals located at the transition metal centers A and B can be described as shown in Figure 2.7a. The resulting molecular orbitals

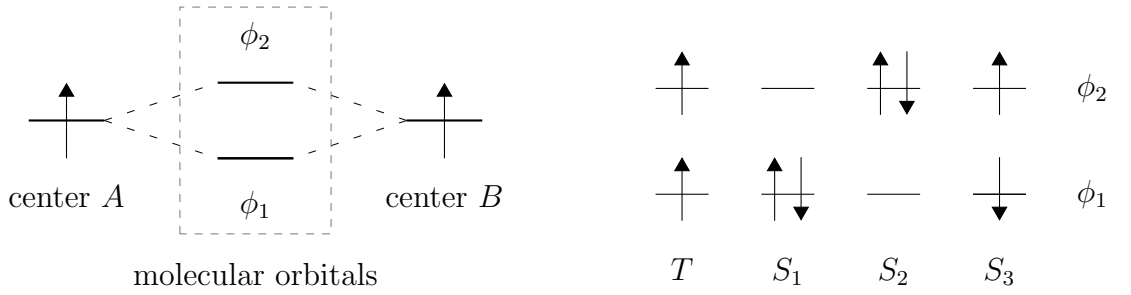

(a) molecular orbital scheme

(b) possible many-electron configurations

Figure 2.7: 2.7a) Interaction diagram of the two half-filled d-orbitals for two d^9 transition metal centers A and B; 2.7b) Possible many-electron configurations of the d^9 HTH model with respect to the molecular orbitals ϕ_1 and ϕ_2; T : triplet state, S_i: different singlet states.

ϕ_1 and ϕ_2 are linear combinations of the half-filled d-orbitals:

$$\begin{aligned} \phi_1 &\sim d^A + d^B \\ \phi_2 &\sim d^A - d^B \end{aligned} \tag{2.65}$$

The possible many-electron configurations arising from these orbitals are shown in Figure 2.7b. The different possible states with respect to the different spins α and β can be derived as shown in equation 2.66

$$\begin{aligned} T &: |\phi_1\alpha\phi_2\alpha| \\ S_1 &: |\phi_1\alpha\phi_1\beta| \\ S_2 &: |\phi_2\alpha\phi_2\beta| \\ S_3 &: \frac{1}{\sqrt{2}}(|\phi_1\alpha\phi_2\beta| - |\phi_1\beta\phi_2\alpha|) \end{aligned} \tag{2.66}$$

The lowest singlet state of the system ψ_S will be an approximately equal mixture of S_1 and S_2

$$\psi_S = \lambda_1\phi_1 + \lambda_2\phi_2. \tag{2.67}$$

Note that $|\lambda_1|$ equals $|\lambda_2|$ in the case of non-interacting metal atoms. The singlet state S_3 corresponds to an excited state of much higher energy and is therefore neglected in the further discussion.
Diagonalization of the 2×2 matrix involving S_1 and S_2 yields the energies of the singlet (E_S) and triplet (E_T) state:

$$\begin{aligned} E_T &= h_1 + h_2 + J_{12} - K_{12} \\ E_S &= h_1 + h_2 + \frac{1}{2}(J_{11} - J_{22}) - \frac{1}{2}[(2h_1 + J_{11} - 2h_2 - J_{22})^2 + 4K_{12}^2]^{\frac{1}{2}} \end{aligned} \tag{2.68}$$

with

$$\begin{aligned} h_i &= \int \phi_i^*(1)\hat{h}(1)\phi_i(1)dr_1 \\ J_{ij} &= \int \phi_i^*(1)\phi_j^*(2)\frac{1}{r_{12}}\phi_i(1)\phi_j(2)dr_1dr_2 \\ K_{ij} &= \int \phi_i^*(1)\phi_j^*(2)\frac{1}{r_{12}}\phi_j(1)\phi_i(2)dr_1dr_2 \end{aligned} \tag{2.69}$$

$\hat{h}$ represents the core operator consisting of the kinetic energy, nuclear attraction and all electron repulsion terms. Therefore, the singlet-triplet splitting becomes

$$\begin{aligned} E_T - E_S &= -2J \\ &= J_{12} - K_{12} - \frac{1}{2}(J_{11} + J_{22}) + \\ &\quad \frac{1}{2}[(2h_1 + J_{11} - 2h_2 - J_{22})^2 + 4K_{12}^2 + 4K_{12}^2]^{\frac{1}{2}}. \end{aligned} \tag{2.70}$$

To simplify the above equation the orthogonal localized molecular orbitals (LMO's) ϕ_a and ϕ_b are introduced as follows:

$$\begin{aligned} \phi_a &= \frac{1}{\sqrt{2}}(\phi_1 + \phi_2) \\ \phi_b &= \frac{1}{\sqrt{2}}(\phi_1 - \phi_2) \\ 0 &= < \phi_a | \phi_b > . \end{aligned} \tag{2.71}$$

As shown in Figure 2.8 ϕ_a contains both metal and ligand character but will be essentially a d-orbital located on metal A and ϕ_b will be the mirror image located at metal center B. In terms of these orbitals the following identities arise:

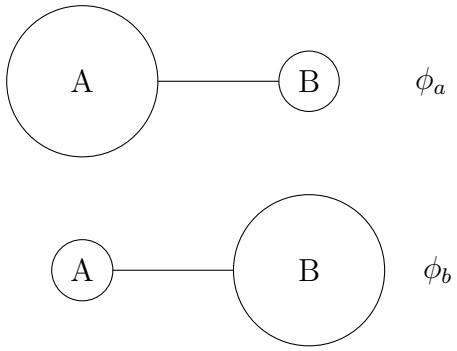

Figure 2.8: Orthogonal localized orbitals ϕ_a and ϕ_b of the HTH model

$$\begin{aligned} J_{11} &= \frac{1}{2}(J_{aa} + J_{ab}) + K_{ab} + 2 < aa|ab > \\ J_{22} &= \frac{1}{2}(J_{aa} + J_{ab}) + K_{ab} - 2 < aa|ab > \\ J_{12} &= \frac{1}{2}(J_{aa} + J_{ab}) - K_{ab} \\ K_{12} &= \frac{1}{2}(J_{aa} - J_{ab}) \end{aligned} \tag{2.72}$$

with the dominant one-center and two-center coulomb repulsion integrals J_{aa} and J_{ab}, respectively. Given that the splitting between h_1 and h_2 is small compared to K_{12} ($\sim 2.5eV$) equation (2.70) becomes:

$$E_T - E_S = J_{12} - \frac{1}{2}(J_{11} + J_{22}) + \frac{(h_1 - h_2)^2}{2K_{12}} \tag{2.73}$$

Finally, a relation between h_1 and h_2 and the orbital energies ϵ_1 and ϵ_2 is needed. As shown above, neither S_1 nor S_2 is an adequate description of the singlet state, therefore the Hartree-Fock operator for the triplet state orbitals is considered.

$$\begin{aligned} \epsilon_1 &= h_1 + J_{12} - K_{12} \\ \epsilon_2 &= h_2 + J_{12} - K_{12} \end{aligned} \tag{2.74}$$

and hence

$$h_1 - h_2 = \epsilon_1 - \epsilon_2. \tag{2.75}$$

Consequently, this yields

$$\begin{aligned} E_T - E_S &= J_{12} - \frac{1}{2}(J_{11} + J_{22}) + \frac{(\epsilon_1 - \epsilon_2)^2}{2K_{12}} \\ &= -K_{ab} + \frac{(\epsilon_1 - \epsilon_2)^2}{J_{aa} - J_{ab}}. \end{aligned} \tag{2.76}$$

For the degenerated case $\epsilon_1 = \epsilon_2$, the triplet state is the ground state, while a significant splitting between the molecular orbitals ϕ_1 and ϕ_2 yields a singlet ground state. The denominator $J_{aa} - J_{ab}$ usually is a fairly slow varying quantity as a function of distortions or substituent effects. The same considerations apply to K_{ab} which is usually small. Thus. the difference of the orbital energies $\epsilon_1 - \epsilon_2$ becomes a measure of the singlet-triplet splitting.

As already mentioned it is possible to expand the HTH model to the general d^n case with m unpaired electrons. The general ferromagnetic (J_{FM}) and antiferromagnetic (J_{AFM}) contributions can be written:

$$\begin{aligned} J_{FM} &= \frac{1}{m^2} \sum_{i \in A} \sum_{j \in B} K_{ij} \\ J_{AFM} &= -\frac{1}{m^2} \sum_{i=1}^{m} \frac{\frac{1}{2}(\epsilon_{2i} - \epsilon_{2i-1})^2}{J_{ai,ai} - J_{ai,bi}}. \end{aligned} \tag{2.77}$$

Note that the second sum is over distinct pairs of molecular orbitals. In the specific case of two high spin d^8 monomers the singlet-triplet splitting is therefore proportional to the splitting of the orbital energies.

$$E_T - E_S \sim (\epsilon_1 - \epsilon_2)^2 + (\epsilon_3 - \epsilon_4)^2 \tag{2.78}$$

2.4.4 Magnetic anisotropy D

Taking a closer look at the interaction of a system containing unpaired electrons with an applied external field it becomes obvious that the whole system can be described as a quasiparticle with spin S in an energy window well below electronic excitations[220]. Thus, the following phenomenological spin Hamiltonian can be applied:

$$\hat{H} = \sum_{\alpha,\beta} D_{\alpha,\beta} \hat{S}_\alpha \hat{S}_\beta - g_e \mu_B \sum_\alpha B_\alpha \hat{S}_\alpha, \tag{2.79}$$

considering the zero-field-splitting (ZFS) and the Zeeman interaction. Here α and β run over the cartesian coordinates x, y, z; g_e is the electron g value; μ_B is the Bohr magneton and $\vec{B} = (B_x, B_y, B_z)$ is the external magnetic field which is assumed to be homogeneous. The field strength B is given by $B = |\vec{B}|$. The ZFS tensor D is finally given by $D_{\alpha,\beta}$.

The easiest situation is given by $D = B = 0$. Then we get $2S + 1$ degenerate eigenfunctions of $\hat{H}$. In the case of $D = 0$ and $B \neq 0$ the energy of the ground state is given by the Zeeman interaction $-g_e \mu_B BS$ thus depending only on the field strength but not on the field direction. Consequently non of the $2S + 1$ energy levels are changed. For $D \neq 0$ and $B = 0$ on the other hand the $2S + 1$ degeneracy is lifted without an applied magnetic field ($B = 0$!). Hence the name zero-field splitting parameter. As a consequence of $D \neq 0$ the ground state energy depends on the direction of the magnetic field for $B \neq 0$. This directional dependence is called magnetic anisotropy. Note that neither the ZFS nor the Zeeman term alone can bring forth magnetic anisotropy. Only the interaction between both terms leads to magnetic anisotropy. However, the magnetic anisotropy and the ZFS are closely related and differ only by a constant as explained nicely by van Wüllen[220].

As shown in Figure 2.9 there are basically two different cases for the magnetic anisotropy. For an **easy plane system** ($D > 0$) the magnetization is aligned

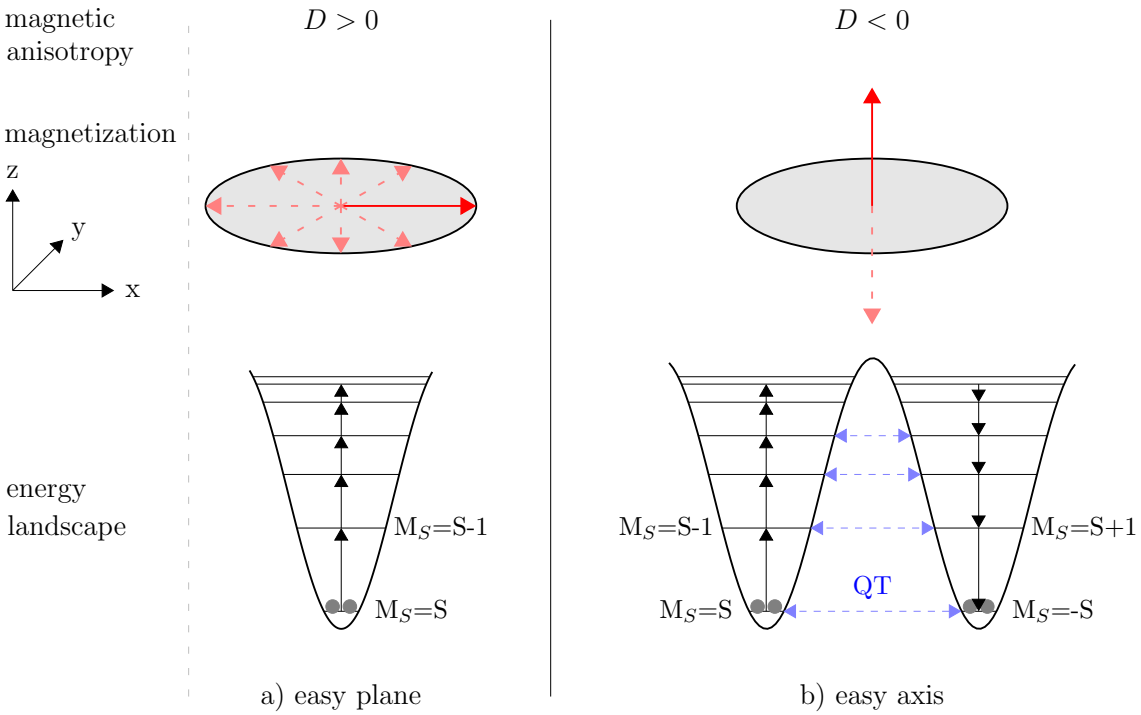

Figure 2.9: Magnetic anisotropy of a ferromagnetic system; a) magnetization aligned in a plane; b) orientation of magnetization along an axis

within a plane as shown in Figure 2.9a. The magnetization can rotate freely within this plane and the energy landscape exhibits only one ground state, hence there is no difference between the spin state $+S$ and $-S$. States that are higher in energy (for example spin state M_S=S-1) can be populated for instance via thermal excitation (black arrows in Figure 2.9a. For an **easy axis system** ($D < 0$) the situation is somewhat more complex. Here we observe an alignment of the magnetization along a distinguished axis as shown in Figure 2.9a. This gives rise to a bistable ground state where $+S$ and $-S$ states are each in a potential well separated by a significant energy barrier. Without a magnetic field the two wells are equally populated as shown in the energy landscape of Figure 2.9b. Applying a magnetic field to this system will result in the selective population of one of the wells emptying the other one. For example, we could end up with a fully populated $+S$ state and an empty $-S$ state (or the other way around depending on the applied magnetic field). After the removal of the magnetic field all states are trapped at $+S$. This

state is very stable at sufficient low temperatures resulting in the experimentally observed hysteresis. More precisely without the application of an external field the state is stable for temperatures below a given blocking temperature. A measure of the blocking temperature is the barrier U which is given by $U = S^2|D|$ for integer spin ($U = (S^2 - \frac{1}{4})|D|$ for molecules with half integer spin[72]). For energies above the barrier U the equilibrium is re-established through a series of steps by thermal excitation indicated by the black arrows in Figure 2.9b. Another interesting feature that can be observed during the relaxation of the system is quantum tunneling (QT). Whenever the energy levels of the right and the left potential well are aligned, it is possible for the electrons to tunnel through the barrier as indicated by the dashed blue arrows in Figure 2.9b. Note that the tunneling does not necessarily occur between the same spin states as indicated in the Figure. Only the alignment of the energetic levels is important. The quantum tunneling can also be observed experimentally as is leads to steps in the hysteresis[71, 161, 215].

Today many magnetic molecules are known, some of them exhibiting SMM behavior, others not. Although the well understood Goodenough-Kanamori rules[75, 76, 104] predict the magnetic exchange coupling of the metal centers within a magnetic molecule there is still a lack of such easy to understand and easy to apply rules for the magnetic anisotropy. However, there have been several attempts to gain some insight into the topic. For example it was shown by Collison et al.[51] that "the relative orientations of the local and cluster magnetic axes can lead to a cluster ZFS opposite in sign to the single ion, even when this is the only significant contribution. This implies that SMM research need not to be restricted to the use of metal ions that give rise to negative ZFSs.". Goswani and Misra[77] relate an increasing magnetic anisotropy to a decreasing HOMO-LUMO gap and showed the influence of π-donor and π-acceptor ligands on the magnetic anisotropy. Ribas-Arino et al.[192] studied "the variation of the D value as a function of several geometrical parameters". It is also know from calculations[191] as well as experimental results[72] "that the sources of the anisotropy of a molecular cluster [...] are twofold: the single-ion anisotropies and the geometry of the whole structure"[191]. Cirera et al.[50] also confirmed the influence of the local geometry on the strength and the sign of the magnetic anisotropy for octahedral coordinated complexes. Maurice et al.[134] did a systematic study of the magnetic anisotropy as a function of symmetry lowering in a model monatomic

Mn^{III} complex. Starting point is the octahedral conformation and the symmetry is lowered successive. They showed that axial distortion has nearly no influence on the magnetic anisotropy whereas rhombic distortion leads to a slight decrease of the magnetic anisotropy and a noticeable increase of the biaxial anisotropy E. Angular distortions on the other hand increase the magnetic anisotropy and introduce a small biaxial anisotropy. On the other hand Ruiz and coworkers[200] demonstrated that "the zero-field splitting parameter depends mostly on the ground state rather than on structural details". A similar conclusion is reached by Neese and coworkers[150] who stated that "the hidden dependence of the zero-field splitting parameter D to the spin quantum number implies that maximizing the total S through construction of polynuclear entities may not be needed to make better single-molecule magnets." Of course, there are several more studies available in literature. The references cited here shall just provide the interested reader with an informative basis about the topic and show that there is still no consensus about simple and intuitive rules for the prediction of the sign and size of the magnetic anisotropy of a given system.
While a number of experimental techniques (like electron spin resonance/electron paramagnetic resonance (ESR/EPR) measurements or superconducting quantum interference device (SQUID) measurements) exist to obtain the magnetic anisotropy, it is far from trivial to compute it. A detailed discussion of this topic can be found in section 2.5.3.

2.5 Magnetic interactions - computational aspects

2.5.1 Computation of the exchange coupling constant J

In order to obtain the exchange coupling constant J a ferromagnetic (FM) and an antiferromagnetic (AFM) solution for the coupling of spins was computed. The solution with the lowest energy is the stable one. Therefore, it can immediately be seen whether the electrons of the transition metal will couple in a ferromagnetic or antiferromagnetic way. However, to get information about the strength of the coupling (i.e. the coupling constant J) some further considerations are needed. As discussed in section 2.4.1 the Heisenberg Hamiltonian will be used in order to obtain

the exchange coupling constant J:

$$H = -2J\hat{S}_1 \cdot \hat{S}_2. \tag{2.80}$$

Possible solutions for the Hamiltonian are a ferromagnetic solution (H_{FM}) and an antiferromagnetic solution (H_{AFM}) of the given dimer. Since we get two different energies for the two solutions, the energy difference ΔE can be defined as:

$$\begin{aligned} \Delta E &= E_{FM} - E_{AFM} \\ &= -2J[(\hat{S}_1 \cdot \hat{S}_2)_{FM} - (\hat{S}_1 \cdot \hat{S}_2)_{AFM}]. \end{aligned} \tag{2.81}$$

Therefore, the exchange coupling constant J is given by:

$$J = \frac{-\Delta E}{2[(\hat{S}_1 \cdot \hat{S}_2)_{FM} - (\hat{S}_1 \cdot \hat{S}_2)_{AFM}]}. \tag{2.82}$$

Ferromagnetic coupling is obtained for $J > 0$ and $J < 0$ relates to antiferromagnetic coupling of the spins.
However, it is not possible to evaluate $\hat{S}_1 \cdot \hat{S}_2$ directly since the eigenvalues of this expression are unknown. Therefore, the total spin $\hat{S}_t$ is introduced:

$$\hat{S}_t = \hat{S}_1 + \hat{S}_2. \tag{2.83}$$

This is sufficient as we assumed in section 2.4.1 that the spins are independent of each other. The square of the total spin $\hat{S}_t$ yields:

$$\begin{aligned} \hat{S}_t^2 &= (\hat{S}_1 + \hat{S}_2)^2 \\ &= \hat{S}_1^2 + 2\hat{S}_1 \cdot \hat{S}_2 + \hat{S}_2^2. \end{aligned} \tag{2.84}$$

Hence $\hat{S}_1 \cdot \hat{S}_2$ is given by:

$$\hat{S}_1 \cdot \hat{S}_2 = \frac{\hat{S}_t^2 - \hat{S}_1^2 - \hat{S}_2^2}{2}. \tag{2.85}$$

The eigenvalues of $\hat{S}^2$ are well known:

$$\hat{S}^2 \rightarrow S(S+1) \tag{2.86}$$

In the case of a Ni^{+2} dimer $S_1 = S_2 = 1$. The ferromagnetic solution results in a total spin $S_t = 2$ and therefore $\hat{S}_1 \cdot \hat{S}_2 = 1$. For the antiferromagnetic solution the total spin equals $S_t = 0$ resulting in $\hat{S}_1 \cdot \hat{S}_2 = -2$. Consequently, J is given by

$$\begin{aligned} J &= -\frac{\Delta E}{6} \\ &= -\frac{\Delta E}{S_t(S_t+1)}. \end{aligned} \tag{2.87}$$

Depending on the spin of the transition metal ions different expressions for the coupling constant J are possible as shown in Table 2.1

Table 2.1: Spin dependence of the denominator $S_t(S_t+1)$ of $J = \frac{-\Delta E}{S_t(S_t+1)}$, given $\hat{S}_1 = \hat{S}_2$

S_1	$\frac{1}{2}$	1	$\frac{3}{2}$	2	$\frac{5}{2}$
$S_t(S_t+1)$	2	6	12	20	30

2.5.2 Broken symmetry approach

In the last section we discussed how to relate the energies obtained by DFT calculation to the magnetic exchange coupling J. But it is important to note that especially the computation of the antiferromagnetic solution of a given system is not straightforward. As shown in section 2.4.1 the solution of two interacting spins $S_1 = S_2 = \frac{1}{2}$ yields the following eigenstate of the antiferromagnetic solution:

$$\psi = \frac{|\downarrow\uparrow\rangle - |\uparrow\downarrow\rangle}{\sqrt{2}} \tag{2.88}$$

The exact wavefunction ψ consist of two states $|\downarrow\uparrow\rangle$ and $|\uparrow\downarrow\rangle$, i.e. the wave function is an linear combination of the states shown in Figure 2.10. The solution of the DFT calculation corresponds only to one of these two states. This is due to the fact that the Kohn-Sham orbitals are build upon a single-determinant reference wave function. (Only the high spin states for $m_s = \pm 1$ have a single determinant solution within DFT calculations, see also section 2.4.1). Therefore, the energy difference between the high spin and the low spin state can not be obtained directly

Figure 2.10: The two states of the antiferromagnetic solution $\psi = \frac{|\downarrow\uparrow\rangle - |\uparrow\downarrow\rangle}{\sqrt{2}}$.

from density functional calculations. A solution for this problem for the magnetic coupling was proposed by Noodleman[155, 159]. Their work goes back to the approach of Bagus et al.[20] and Ziegler et al.[231]. Within the broken symmetry (BS) approach the Kohn-Sham wave functions are calculated for a single-determinant reference function.

$$\sigma^1_{BS} = \frac{|a\bar{b}|}{\sqrt{2}} \qquad \text{or} \qquad \sigma^2_{BS} = \frac{|\bar{a}b|}{\sqrt{2}} \tag{2.89}$$

Apparently these wave functions are no eigenfunctions of the total spin operator. However, a suitable singlet function can be obtained as a linear combination of the two BS determinants:

$$\psi_{S=0} = \frac{\sigma^1_{BS} - \sigma^2_{BS}}{\sqrt{2 - 2 < \sigma^1_{BS} | \sigma^2_{BS} >}}. \tag{2.90}$$

As shown elsewhere[36, 155] the coupling constant J depends then on the energy difference ΔE divided by the overlap integral $< \sigma^1_{BS} | \sigma^2_{BS} >$.

Note that these functions σ^1_{BS} and σ^2_{BS} usually break the spin symmetry. For example, in the case of a Ni^{+2} dimer the antiferromagnetic DFT calculation would correspond to a case where all unpaired spin up electrons are localized at one center and all spin down electrons are localized at the other center. This would of course result in an overall magnetization of $S = 0$. But in contrast to the exact wave function $\psi = \frac{|\downarrow\uparrow\rangle - |\uparrow\downarrow\rangle}{\sqrt{2}}$ we deal now with a single-determinant wave function (either $\psi = |\downarrow\uparrow\rangle$ or $\psi = |\uparrow\downarrow\rangle$). Furthermore, it should be noted that the Kohn-Sham wave functions obtained within the broken symmetry approach are not orthogonal to each other. This is due to the fact that spin densities from different metal centers overlap in the broken symmetry approach. This results in spin-contamination of the broken symmetry solution. The amount of spin-contamination can vary over a large range depending and depends crucially on the given system and DFT functional used. As shown elsewhere[194, 196] the influence of the DFT functional is mainly due

to the self-interaction error[179] (for further reading about the self-interaction error and DFT see for example[57, 78]). Due to these problems there is an ongoing discussion in literature[4, 196, 199] how to relate the energy difference ΔE with the coupling constant J. There is the "spin-projected" mapping

$$J = -\frac{\Delta E}{2S_1 S_2} \tag{2.91}$$

which goes back to the original proposal of Noodleman[155].
Another route is taken within the "non-projected" approach[196, 198]. Here the coupling constant J is given by by the energy difference of the high spin state and the singlet[155] (not the broken symmetry solution!):

$$J = -\frac{\Delta E}{2S_1 S_2 + S_2}; \qquad S_1 \geq S_2. \tag{2.92}$$

This yields for $S_1 = S_2$ and $S_t = S_1 + S_2$:

$$J = -\frac{\Delta E}{S_t(S_t + 1)}; \tag{2.93}$$

which is the approach that will be used in the present work. Yet another approach is the "approximate spin-projected" mapping[154, 211, 227]:

$$J = -\frac{\Delta E}{< \hat{S}^2 >_{HS} - < \hat{S}^2 >_{BS}}. \tag{2.94}$$

There is no agreement on which of the three mappings should be used. The spin-projected mapping is valid in the weakly interacting limit. Here the overlap of the magnetic orbitals in the broken symmetry solution approaches zero. The non-projected mapping is valid in the opposite case of strong interaction ($< \sigma^1_{BS} | \sigma^2_{BS} > \sim 1$). The approximate spin-projected mapping on the other hand interpolates between the two limits and includes both of them as special cases[149]. A nice review about the three different mapping methods given by Phillips and Peralta[175] and Neese[149]. Regardless of the actual mapping the sign of the exchange coupling constant J is usually well reproduced. Trends of the magnetic exchange are also in good agreement with experimental data. However, the value of J obtained by DFT-PBE calculations is usually too large. This is due to a general failure of DFT since the standard DFT functionals do not localize the d-states strong enough[83, 114]. For further reading on the broken symmetry approach see for example[17, 36, 149, 155–159].

2.5.3 Computation of the magnetic anisotropy D

In order to characterize the magnetic properties of a given system it is not always enough to know the sign and strength of the magnetic coupling constant J. As already mentioned in section 2.4.4 it is also interesting to have a closer look at the magnetic anisotropy which can be described by the zero-field splitting parameter D[50, 98]. Considering the phenomenological spin Hamiltonian introduced in section 2.4.4 (equation (2.79)) there are two limiting cases $g\mu_B B \ll |D|$ (weak-field limit) and $g\mu_B B \gg |D|$ (strong-field limit) that are analytically solvable within first order perturbation theory. In the weak-field limit $g\mu_B B \ll |D|$ the ground state is degenerate for $D < 0$ and $E = 0$. This degeneracy is lifted by a weak magnetic field. As shown elsewhere[219] the magnetic anisotropy does not depend on the zero-field splitting D for this limiting case. In the strong-field limit $g\mu_B B \gg |D|$ the spins are aligned parallel to the applied magnetic field due to the Zeeman term. For the limiting case of $D = 0$ the ground state energy can be calculated easily to be the Zeeman energy $E_0 = -g\mu_B B$ which is independent of the direction of the magnetic field. As $g\mu_B B \gg |D|$ is assumed in the strong-field limit it is now possible to treat the zero-field splitting as a perturbation to the ground state. The main microscopic contribution to the ZFS and hence to the magnetic anisotropy come from spin-orbit coupling[42] (besides dipole spin-spin interactions). The spin-orbit contribution to the magnetic anisotropy can be discussed in different frameworks for example in the many electron theory[29, 98, 99], an approach which shall be discussed in more detail in the present work or within the framework of linear response theory[148, 151, 152]. A detailed comparison of both methods is given by Schmitt et al[205].
As already mentioned, the ZFS parameter can be considered as a perturbation within the strong-field limit. Furthermore, the giant spin approach ($S \gg D$) is valid. Hence it is possible to calculate the ZFS parameter within second-order perturbation theory as a second-order correction to the total energy[165]. This correction Δ_2 can be expressed as:

$$\Delta_2 = \sum_{\sigma\sigma'} \sum_{ij} M_{ij}^{\sigma\sigma'} S_i^{\sigma\sigma'} S_j^{\sigma'\sigma} \tag{2.95}$$

where σ denotes different spin degrees of freedom and i,j are coordinate labels x, y, z. Within this framework $S_i^{\sigma\sigma'}$ is defined as

$$S_i^{\sigma\sigma'} = \langle \chi^{\sigma} \mid S_i \mid \chi^{\sigma'} \rangle \tag{2.96}$$

where χ^{σ} and $\chi^{\sigma'}$ are a set of spinors. These spinors are constructed from a unitary transformation of the S_z eigenstates. The matrix element $M_{ij}^{\sigma\sigma'}$ is given by:

$$M_{ij}^{\sigma\sigma'} = -\sum_{kl} \frac{\langle \varphi_{l\sigma} \mid \hat{V}_i \mid \varphi_{k\sigma'} \rangle \langle \varphi_{k\sigma'} \mid \hat{V}_j \mid \varphi_{l\sigma} \rangle}{\epsilon_{l\sigma} - \epsilon_{k\sigma'}} \tag{2.97}$$

with the occupied and unoccupied states $\varphi_{l\sigma}$ and $\varphi_{k\sigma'}$ and the respective energies $\epsilon_{l\sigma}$ and $\epsilon_{k\sigma'}$. The operator $\hat{V}$ is spin-orbit related. In the absence of a magnetic field the second order perturbation energy can be rewritten in terms of the anisotropy tensor D_{ij}:

$$\Delta_2 = \sum_{ij} D_{ij} \langle S_i \rangle \langle S_j \rangle. \tag{2.98}$$

For a diagonal form of the D tensor the following expression is obtained:

$$\sum_{\sigma\sigma'} \sum_{ij} M_{ij}^{\sigma\sigma'} S_i^{\sigma\sigma'} S_j^{\sigma'\sigma} = D_{xx} S_x^2 + D_{yy} S_y^2 + D_{zz} S_z^2 \tag{2.99}$$

with the components

$$\begin{aligned} D_{xx} &= -\frac{1}{3} D + E \\ D_{yy} &= -\frac{1}{3} D - E \\ D_{zz} &= \frac{2}{3} D. \end{aligned} \tag{2.100}$$

All other elements are zero. Choosing the orientation in a way that $|D_{zz}|$ is the largest diagonal element implies $0 \leq \mid \frac{E}{D} \mid \leq \frac{1}{3}$. From the components of the tensor the usual D parameter commonly employed in the spin Hamiltonian can be extracted:

$$D = D_{zz} - \frac{1}{2}(D_{xx} + D_{yy}) \tag{2.101}$$

Note that it is appropriate to order the terms of equation 2.99 according to the spin associated with the respective orbitals. This relates directly to four sets of

contributions to the values of D which will be called *spin channels* in the following. Diagonalization of the anisotropy tensor yields the eigenvalues D_{xx}, D_{yy} and D_{zz} and consequently the Δ_2 can be written as:

$$\begin{aligned}\Delta_2 = \quad & \tfrac{1}{3} \quad (D_{xx} + D_{yy} + D_{zz})S(S+1) \\ & + \quad \frac{1}{3}\left[D_{zz} - \frac{1}{2}(D_{xx} + D_{yy})\right][3S^2 - S(S+1)] \\ & + \quad \frac{1}{2}(D_{xx} - D_{yy})(S_x^2 - S_y^2) \end{aligned} \tag{2.102}$$

Parametrization of D_{xx}, D_{yy} and D_{zz} with the magnetic anisotropy D and the biaxial anisotropy E results in the following simplified expression:

$$H_{ZFS} = D[S_z^2 - \frac{1}{3}S(S+1)] + E[S_x^2 - S_y^2] \tag{2.103}$$

The biaxial anisotropy E is usually very small compared to D. It is zero in the case of uniaxial systems. Within the used sofware package NRLMOL (see section 3.1.1) another Hamiltonian is used, namely:

$$H_{ZFS} = \gamma_1 S_x^2 + \gamma_2 S_y^2 + \gamma_3 S_z^2 + \gamma_0(S_x^2 + S_y^2 + S_z^2), \tag{2.104}$$

with the constant γ_0. Equating the coefficients of (2.103) and (2.104) yields:

$$\begin{aligned}\gamma_0 &= -\frac{1}{2}(\gamma_1 + \gamma_2) \\ E &= \frac{1}{2}(\gamma_1 - \gamma_2) \\ D &= -\frac{1}{2}(\gamma_1 + \gamma_2) + \gamma_3 \end{aligned} \tag{2.105}$$

Within this framework $D > 0$ correspond to an **easy plane system** and $D < 0$ to an **easy axis system**. For the biaxial anisotropy $E > 0$ the spins in the xy plane will try to avoid the x axis which is then called the **hard axis**. Respectively, the y axis is called intermediate axis. Of course, this is reversed for $E < 0$. There are several examples in literature showing that this approach works well[29, 115, 116, 148, 151, 160, 162, 165, 181, 191, 192, 200, 229]. However, one should be careful about the results. As pointed out by Wüllen[219] basically an axial magnetic anisotropy energy (MAE) is calculated which is divided by S^2 in order to obtain the ZFS parameter (i.e. the magnetic anisotropy). However, this is only valid if the spin is

treated classically. Treating the spin quantum mechanically gives rise to a factor of $\frac{1}{S(S-\frac{1}{2})}$ instead of $\frac{1}{S^2}$ as proposed by Pederson et al[98]. Hence we get:

$$D_{\mathrm{NRLMOL}} = \frac{MAE}{S^2} \tag{2.106}$$

$$D_{\mathrm{vW}} = \frac{MAE}{S(S-0.5)}. \tag{2.107}$$

Obviously, the difference is rather small for systems with a large ferromagnetic ground state, however it is substantial for small spins. For a $S = 1$ system for example there is a difference of 50% between the two different approaches. This results in a factor of two that D_{NRLMOL} is off compared to experimental data for $S = 1$ systems as shown for example by Reviakine et al[188]. Note that the magnetic anisotropy energy itself is calculated correctly. The only problem is the evaluation of D therefrom (wrong pre-factor applied!). For the approach of Neese[148, 151, 152] on the other hand there have been reported several errors[188]. Fixing those yields comparable results for the ZFS parameter within the Pederson-Khanna approach, the Neese approach and the approach of Schmitt et al[205]. Overall the Pederson-Khanna approach is preferable for the computation of the ZFS parameter[205].
However, there still remain problems. Very often a considerable underestimation of the D parameter is observed within the calculations[50] which is basically due to an intrinsic inaccuracy of the GGA functionals[152]. Using hybrid functionals does also not improve the situation significantly[152, 168, 188].
As already mentioned there are spin-orbit and spin-spin contributions to the ZFS parameter, however only spin-orbit interaction is included in the approach of Pederson and Khanna. This is sufficient since the spin-orbit interaction becomes the dominant contribution to the ZFS tensor already for systems containing second-row-elements, a trend which is resumed when going down the periodic table[188]. Note that the perturbative approach might also fail for heavier atoms as the spin-orbit coupling is usually large there and can no longer be treated as a perturbation of the total energy. However, it works well for third-row transition metals which will be dealt with in the present work.

3 Computational details

3.1 DFT-codes

3.1.1 NRLMOL

Most of the density functional theory calculations have been carried out using the Naval Research Laboratory Molecular Orbital Library (NRLMOL) program package, which is an all-electron implementation of DFT. NRLMOL combines large Gaussian orbital basis sets as shown in Table (3.1), numerically precise variational integration and an analytic solution of Poissons equation to accurately determine the self-consistent potentials, secular matrix, total energies and Hellmann-Feymann-Pulay forces[98, 163, 164, 166, 180].

Table 3.1: Basis set information: shown are the Gaussian-type orbitals (GTO's), contracted Gaussian-type orbitals (CGTO's) respectivly for the s, p and d orbitals and the largest and smallest exponent ($\alpha_{max}/\alpha_{min}$) of the Gaussian-type orbitals (see also (2.52))

	GTO's	CGTO's			exponents	
		s	p	d	α_{max}	α_{min}
Br	21	7	6	4	$0.79 * 10^{7}$	$0.78 * 10^{-1}$
Ni	20	7	5	4	$0.44 * 10^{7}$	$0.51 * 10^{-1}$
S	17	6	5	3	$0.67 * 10^{6}$	$0.71 * 10^{-1}$
Cl	17	6	5	3	$0.76 * 10^{6}$	$0.85 * 10^{-1}$
F	14	5	4	3	$0.12 * 10^{6}$	$0.12 * 10^{0}$
Ne	14	5	4	3	$0.15 * 10^{6}$	$0.14 * 10^{0}$
O	13	5	4	3	$0.61 * 10^{5}$	$0.10 * 10^{0}$
N	13	5	4	3	$0.51 * 10^{5}$	$0.94 * 10^{-1}$
B	12	5	4	3	$0.17 * 10^{5}$	$0.54 * 10^{-1}$
C	12	5	4	3	$0.22 * 10^{5}$	$0.77 * 10^{-1}$
H	6	4	3	1	$0.77 * 10^{2}$	$0.74 * 10^{-1}$

Starting from the experimental X-ray structure an isolated single molecule was gen-

erated which has been used for the calculation. All calculations are done using the PBE exchange correlation functional[168].

3.1.2 ORCA

In order to compare the results obtained from the NRLMOL calculations additional calculations using ORCA[146, 147] have been carried out for selected molecules. ORCA offers many features to the interested user[1]. Within the present work the broken symmetry approach is used for the calculation of the exchange coupling constants J. All calculations are done using revision 2.80 of the program package and Ahlrichs triple ζ valence basis set[204] as well as either the PBE exchange correlation functional[168] or B3LYP.

3.2 Visualization

3.2.1 XCrysDen

In order to understand certain features in more detail it is necessary to visualize not only the structure of a given complex but also certain ground state properties such as wave functions. For this purpose XCrysDen[112, 113] is used within this work.
XCrysDen is released under GNU General Public License and is able to read the very common and easy to work with structure data format *.xyz. It also includes very intuitive to use measurement tools for distances, angles and dihedral angels. Furthermore, is is possible to keep track of geometry optimization and can visualize wave functions. All wave function plots presented in the present work are done using an isovalue of $0.3\sqrt{e/a_0^3}$ unless stated otherwise. There is also an extensive toolbox for the treatment of periodic structures available.

3.2.2 Jmol

Another tool for visualization used within the present work is Jmol[2]. Jmol is a free, open source, java-based molecule viewer. It can be used for example for the visualization of vibrations, surfaces and orbitals. A huge advantage of Jmol is the support for RasMol/Chime scripting language which makes it highly adaptable and easy to use.

3.3 The SHAPE package

SHAPE[9, 10, 43, 44, 49] is a program package for the calculation of continuous shape measures of polygonal and polyhedral molecular fragments based on an algorithm proposed by Pinsky and Avnir[177].

The amount of symmetry in a given structure is given as a function of a normalized root-mean deviation from the closest structure with the desired symmetry group G. Assuming a structure composed of N vertices whose coordinates are given by $Q_k, k = 1, 2, 3, ..., N$ the search for the nearest reference structure defined by the vertex coordinates $P_k, k = 1, 2, 3, ..., N$ can be described by:

$$S = \min \frac{\sum_{k=1}^{N} |Q_k - P_k|^2}{\sum_{k=1}^{N} |Q_k - Q_0|^2} * 100 \tag{3.1}$$

The coordinate vector of the center of mass of the investigated structure Q_0 is introduced in order to avoid size effects

$$Q_0 = \frac{1}{N} \sum_{k=1}^{N} Q_k \tag{3.2}$$

Note that S ranges between 0 and 1 by definition. Since nearly all symmetry-related studies focus on small distortions the $0 - 1$ range is expanded by a factor of 100. Therefore the bounds are $100 \leq S \leq 0$, with $S(G) = 0$ if a structure has the desired symmetry. The symmetry measurement increases as it departs from the given symmetry group. Note that all $S(G)$ values are on the same scale and hence comparable - regardless of the G.

4 Results and discussion

4.1 The Robson-type hexamine-dithiophenolate macrocycles $[M_2^{\mathrm{II}}(\mathrm{L}^6)(\mathrm{L}')]^{\mathrm{n}+}$

The series of robson-type polyamine-dithiopenolate macrocycles offers an interesting possibility to elucidate the influence of different bridging ions and metal centers on the magnetic properties[126], since the main framework of the complex remains relatively unchanged by these changes. A schematic representation of the structure is shown in Figure 4.1. Note that there are two different structural motifs, type A

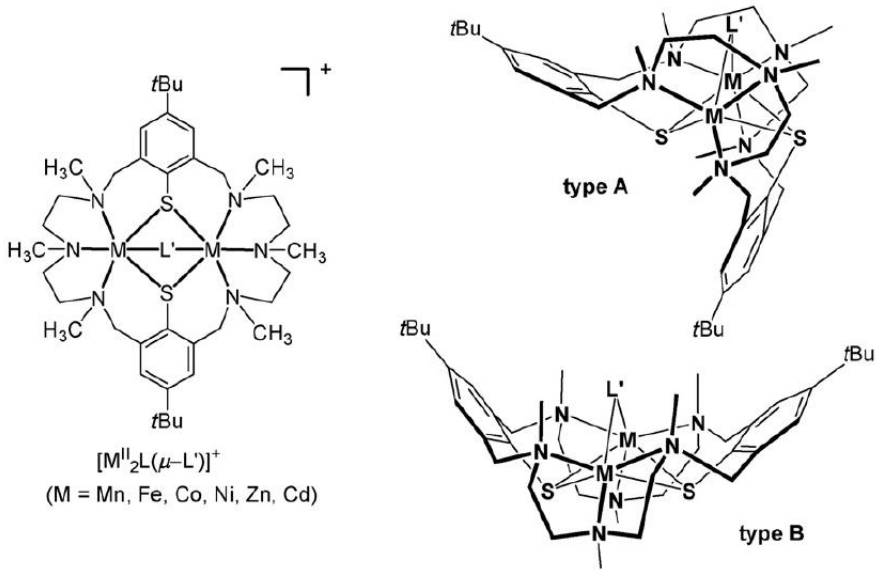

Figure 4.1: Schematic sketch of the Robson-type polyamine-dithiophenolate macrocycles, L^6=polyamine-dithiophenolate ligand ($C_{38}H_{64}N_6S_2$), L'=coligand, M=metal center, taken from[126], Fig. 8

and type B. Each metal center is in an octahedral environment, independent of the structure motif. The present work deals only with structures of type B, since a larger number of experimentally accessible compounds exists for this structure motif. The structure information of the molecules is obtained from the experimental X-ray structure. First of all, we will test the influence of various program packages (namely NRLMOL, GAUSSIAN and ORCA) and exchange correlation functionals

(PBE, B3LYP) on the calculation of the magnetic exchange coupling. Afterwards, we will discuss the influence of different transition metal centers M (M = Ni, Mn, Fe, Co) on the electronic structure and the magnetic coupling of a complex of type $[M_2^{II}(L^6)(OAc)]^+$. As only the Ni-complexes show ferromagnetic coupling we will then focus on the description of the electronic structure and magnetic properties (exchange coupling, magnetic anisotropy) of various $[Ni_2^{II}(L^6)(L')]^{n+}$ complexes. Here we can switch the magnetic coupling with respect to the third bridging ligand L'. Trends in the magnetic coupling can be e plained in terms of the Goodenough-Kanamori rules and within the Hay-Thibeault-Hoffmann model whereas trends in the magnetic anisotropy can be related to geometric distortions and the HOMO-LUMO gap. Furthermore, we will see that the size and charge of the third bridging ligand does not influence the magnetic coupling. However, weak ligands should be preferred as those open new ferromagnetic pathways across L' that enhance the ferromagnetic coupling.

4.1.1 The influence of different exchange correlation functionals and program packages on the computation of the exchange coupling J

In order to verify our results testing of different exchange-correlation functionals (namely PBE and B3LYP) using different program packages (NRLMOL, GAUSSIAN 03 and ORCA) was done:

- NRLMOL → PBE
- GAUSSIAN 03 → B3LYP
- ORCA → PBE, B3LYP.

An overview over the different calculations done for selected co-ligands L' is given in Table 4.1. It can be immediately seen that all the calculations shown in Table 4.1 reproduce the experimentally observed coupling. The PBE and B3LYP calculations yield nearly identical results respectively. The remaining small discrepancies are due to the use of different basis sets.
For the PBE calculations the known overestimation (approximately a factor of four) of the exchange coupling constant is observed. Only for L'=BH_4^- a surprising agreement between the experimental and calculated coupling constant is observed. The

Table 4.1: Magnetic exchange coupling constants J for selected third bridging ligands L'. The coupling constants are calculated using the PBE exchange-correlation as implemented in NRLMOL (J_{nrl}) and ORCA (J_{orca}) and the B3LYP hybrid functional as implemented in GAUSSIAN 03 (J_{gau}) and ORCA. The results for the calculation using GAUSSIAN 03 are taken from[125]. For comparison experimental data (J_{exp}) are shown as well.

complex	L'	PBE		B3LYP		J_{exp}	Refs.
		J_{nrl} [cm^{-1}]	J_{orca} [cm^{-1}]	J_{gau} [cm^{-1}]	J_{orca} [cm^{-1}]	[cm^{-1}]	
21	N_3^-	-173	-184	-73	-78	-45	[89]
11	BH_4^-	32	31	21	19	27	[102]
16	NO_2^-	25	25	17	15	6.7	[89]
1	$CH_3CO_2^-$	33	30	17	16	6.4	[89]
12	O_2CPh^-	31	29	17	15	5.8	[89]
19	*pydz*	11	14	15	15	3.5	[89]

otherwise occurring overestimation is due to the fact that standard DFT functionals do not localize the d-states strong enough. Therefore, the resulting overlap of the wave functions is larger resulting in an overestimation of the exchange coupling. B3LYP somewhat corrects for this DFT failure by mixing Hartree-Fock exact exchange into the functional. Consequently, the calculated coupling constants are in better agreement than those obtained from the DFT-PBE calculations. However, they are still off by a factor of two. In the case of L'=BH_4^- the ferromagnetic coupling is even underestimated compared to experiment.

Altogether the comparison revealed that the results obtained from the NRLMOL/PBE calculations are trustworthy and the emerging errors are well understood. Hence all remaining calculations will be done using NRLMOL.

Furthermore, we studied the influence of the geometry on the computation of the exchange coupling. As already mentioned all calculations have been done using the experimentally obtained structure. In order to check our results a full geometry relaxation of the isolated single molecule $[Ni^{II}_2(L^6)(OAc)]^+$ has been carried

out. The calculated exchange coupling constant J of the isolated single molecule ($J = 33.14$ cm^{-1}) and the relaxed structure ($J = 34.89$ cm^{-1}) differ only by about 5%. This deviation is much smaller than the error due to DFT. Hence the results obtained starting directly from the isolated single molecule are deemed trustworthy.

4.1.2 Magnetic properties and electronic structure of $[M_2^{II}(L^6)(OAc)]^+$ as a function of the transition metal ion M

a) magnetic coupling J

As already mentioned a whole family of synthesized type B structures exists. Amongst others also a series of $[M_2^{II}(L^6)(OAc)]^+$ complexes. The transition metals of this series are located in the $3d$ row - namely Co^{II}, Mn^{II}, Fe^{II} and Ni^{II}. As shown in Table 4.2 ferromagnetic coupling is observed only in the case of Ni^{II}. All other complexes show an antiferromagnetic exchange interaction.

Table 4.2: Magnetic properties calculated using NRLMOL (J_{PBE}) and ORCA (J_{B3LYP}) in comparison to experimental coupling constants, the energy difference Δe of the Hay-Thibeault-Hoffmann model and selected structural data of the $[M_2^{II}(L^6)(OAc)]^+$ complexes

No.	M	J_{PBE} [cm^{-1}]	J_{B3LYP} [cm^{-1}]	J_{exp} [cm^{-1}]	Δe [mRyd^2]	d(M-M) [$\AA$]	M-S-M [°]	Refs.
1	Ni^{II}	33	16	6.4	0.014	3.48	89.64(4)	[108, 109]
2	Mn^{II}	-14	-6	-5.1	0.558	3.46	80.41(0)	[101]
3	Fe^{II}	-33	-11	-10	0.979	3.42	85.42(6)	[101]
4	Co^{II}	-141	-2	-1.9	0.068	3.45	81.01(1)	[110]

Although the $M - M$ distance is nearly identical in the considered complexes there exist large differences in the $M^{II} - S - M^{II}$ angle. Here the Goodenough-Kanamori rules can be applied in order to explain the observed coupling. In the case of Ni^{II} a M^{II}-S-M^{II} angle close to 90° is observed. Therefore ferromagnetic coupling is predicted. In the case of smaller angles antiferromagnetic exchange pathways are

opened. These additional pathways will eventually dominate the ferromagnetic exchange contribution.
The Hay-Thibeault-Hoffmann model can also be applied successfully. The calculated energy differences of the orbitals are in good agreement with the experimentally observed coupling. The larger the splitting of d levels in the triplet solution of the system the stronger the antiferromagnetic coupling becomes. For all cases shown in Table 4.2 the usual DFT overestimation of the exchange coupling J as already mentioned in section 2.5.2 is observed. Yet the sign of the magnetic coupling is reproduced in all cases. In the case of Co^{II} the situation is somewhat more complicated. The broken symmetry solutions seems to fail completely while the ferromagnetic solution seems to yield the correct solution. Due to the wrong antiferromagnetic solution the singlet-triplet splitting (which is proportional to the magnetic coupling constant J) is computed to be much bigger than observed in experimental studies. It is known that depending on the exchange correlation functional (and therefore on the level of approximation) a calculation of the electronic ground state configuration yields different solutions[22]. Indeed a significant improvement of the calculated exchange coupling constant J is observed for the B3LYP calculation using ORCA. The B3LYP density functional somewhat corrects for the already mentioned (see section 2.5.2) failure of DFT failure by mixing Hartree - Fock exact exchange into the functional. Therefore, the exchange coupling evaluated from the B3LYP calculations is often in better agreement with the experimental ones[195]. Accordingly, the calculated B3LYP exchange interaction for complex **4** ($J = -2$ cm^{-1}) is closer to the experimental one. For low spin Co^{II} in an octahedral crystal field with one electron occupying the degenerated e_g orbital. The Hamiltonian of the simple form $H = -2J\vec{S_1}\vec{S_2}$ is not correct anymore and additional interaction terms have to be considered[65]. However, a mapping of energies obtained via DFT against a spin Hamiltonian of the above mentioned form is impossible.

b) electronic structure

$Ni^{II}OAc$

Apart from the magnetic properties it is also very interesting to take a closer look at the density of states (DOS) and the electronic structure of the different transition metal complexes. As shown in Figure 4.2 the ferromagnetic coupling complex

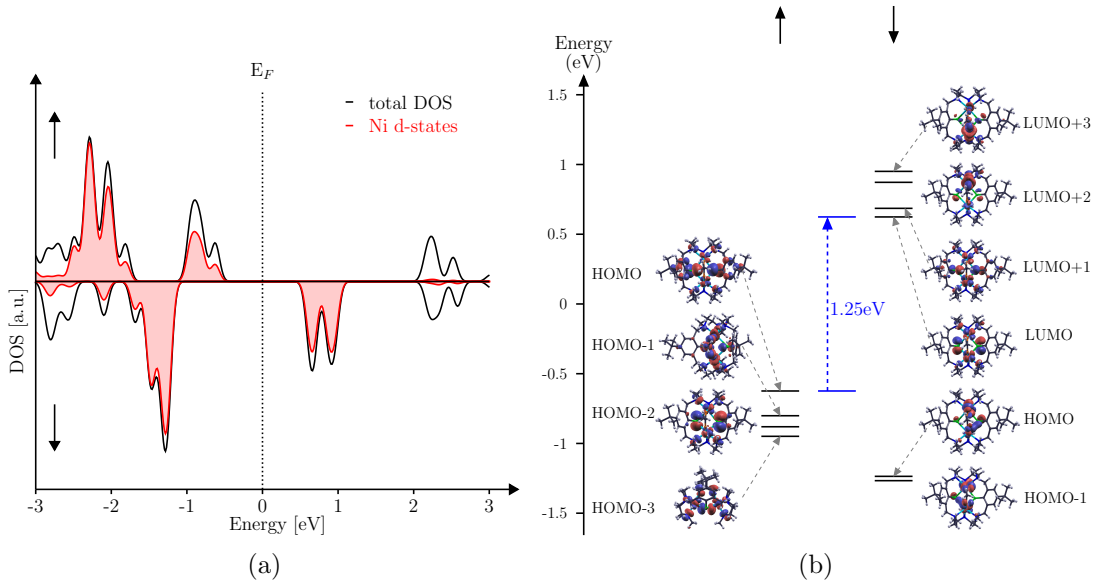

Figure 4.2: (a) DOS $Ni^{II}OAc$; (b) electronic structure of $Ni^{II}OAc$ close to E_F ($\pm$1.5 eV)

$Ni^{II}OAc$ has a rather large HOMO-LUMO gap of 1.25 eV. Since $Ni^{II}OAc$ shows an overall ferromagnetic behavior, it is necessary to consider two distinct spin channels (spin up and spin down) separately. And since the actual HOMO-LUMO gap is between spin up and spin down electrons, this leads immediately to the conclusion that it is essential to take a look at the HOMO-LUMO gap of the respective spin channels as well. The gap for the spin up electrons (2.79 eV) is more than twice of the size the actual HOMO-LUMO gap, whereas the gap for the spin down electrons equals 1.86 eV. It is therefore within the range of the actual HOMO-LUMO gap. This gap for the spin down electrons would also mark the first transition that can be observed in any optical spectra (for example in EELS) since there is no possible optical dipole transition between the HOMO and the LUMO of the molecule. More

accurate there are no allowed optical transitions including a spin flip which would be necessary in this case.
Another fact is that all levels close to E_F are dominated by Ni^{II} d-states as shown in Figure 4.2a. In order to shine some light on the nature of these d-states Figure 4.2b shows the corresponding wave functions close to the Fermi level. Within the spin up channel a ferromagnetic coupling pathway across the sulfur atoms is clearly identified for the HOMO and the HOMO-2 whereas the HOMO-1 and the HOMO-3 indicate that there is an additional exchange pathway across the bridging acetate ligand available that enhances the overall ferromagnetic coupling. The LUMO of the spin up channel consists of ligand states and is not included in Figure 4.2b as it is located well above the Fermi level. Similar pathways can be observed within the spin down channel. Here the HOMO and the HOMO-1 are nearly degenerated and feature a coupling pathway across the third bridging ligand as well as across the sulfur atoms. The LUMO and the LUMO+1 also look nearly the same. The respective wave functions include contributions from the Ni^{II} d-states as well as sulfur p-states and a small amount of carbon p-states from the ligand system. The wave functions that belong to the LUMO+2 and the LUMO+3 consist mainly of states belonging to the acetate ligand and Ni^{II} d-states. All states that are higher in energy belong the the ligand system and do not include any notable amount of Ni^{II} d-states.

$Mn^{II}OAc$

A very similar electronic structure is calculated for the Mn^{II}OAc as can be seen in Figure 4.3. First of all it is no longer necessary to separate the spin channels since there is no difference in these for an antiferromagnetic system. Again a large HOMO-LUMO gap of 1.85 eV is observed and yet again all states close to the Fermi level are dominated by Mn^{II} d-states as shown in Figure 4.3a. It is possible to trace coupling pathways across the sulfur atoms (HOMO) and across the bridging acetate ligand (HOMO-1). A very interesting feature can be found for the LUMO. Here it is possible to track a direct overlap between the Mn^{II} ions. The LUMO+1 consists mainly of states belonging to the acetate ligand and Mn^{II} d-states. Yet again all states that are higher in energy belong the ligand system and do not include any notable amount of Mn^{II} d-states.

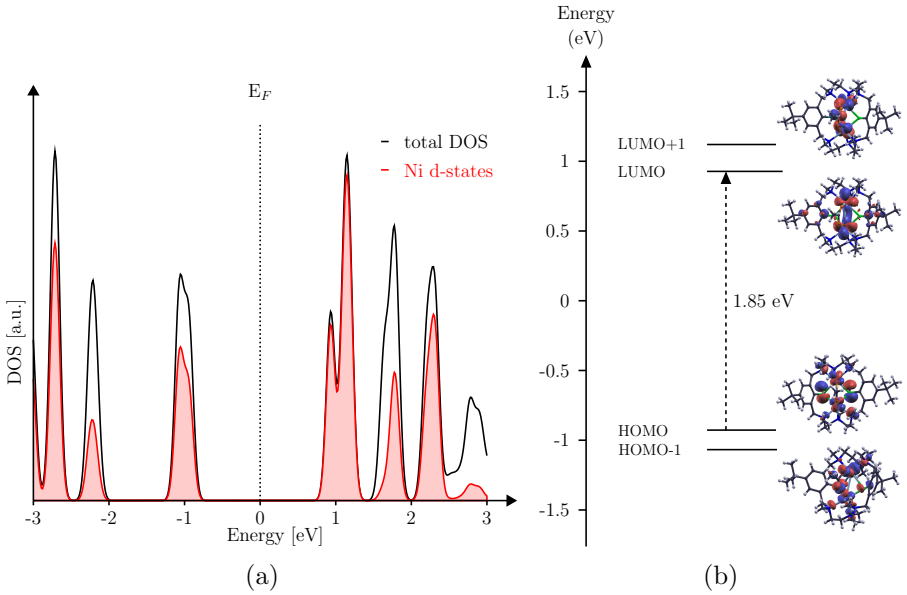

Figure 4.3: (a) DOS $Mn^{II}OAc$; (b) electronic structure of $Mn^{II}OAc$ close to E_F (± 1.5 eV)

$Fe^{II}OAc$

Compared to the already discussed transition metal complexes $Fe^{II}OAc$ comes along with a very small HOMO-LUMO gap of 0.65eV as shown in Figure 4.4. Since the complex shows an overall antiferromagnetic coupling, it is again not necessary to consider the two spin channels separately. As illustrated in Figure 4.4a all states close to the Fermi level are dominated by Fe^{II} d-states which is a common feature for all the regarded transition metal complexes. Focusing at the states close to E_F (see Figure 4.3b) reveals for the HOMO-1 and the HOMO-2 the already known coupling pathways across the sulfur atoms and the bridging acetate ligand. The HOMO however is formed from pure Fe^{II} d-states in contrast to the $Mn^{II}OAc$ and $Ni^{II}OAc$. For the LUMO a mixing of Fe^{II} d-states and p-states belonging to the acetate ligand is observed while for the LUMO+1 a direct overlap of Fe^{II} d-states can be found. Such an unoccupied state was also noticed for the $Mn^{II}OAc$. In the case of $Ni^{II}OAc$ these direct overlap of d-states is observed for states well below the Fermi level.

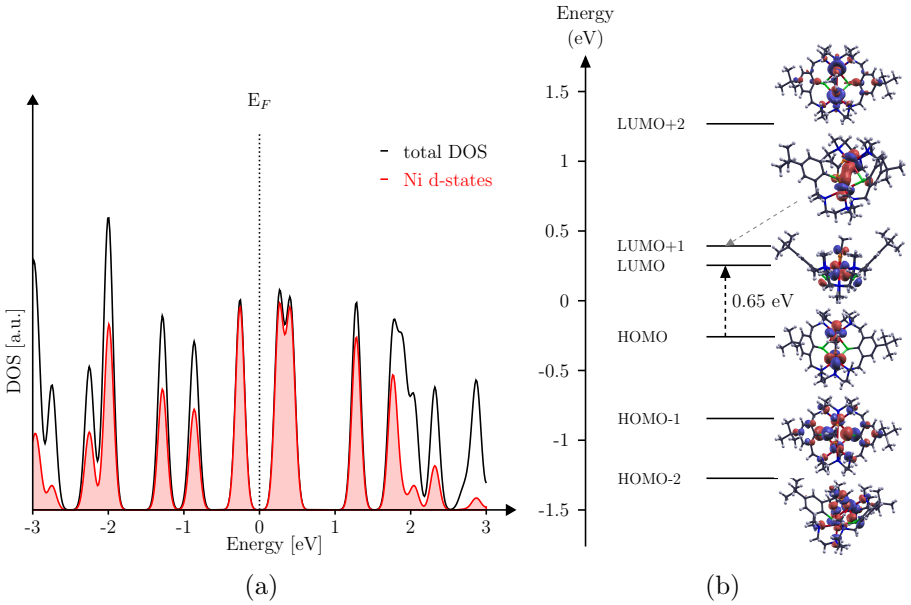

Figure 4.4: (a) DOS $Fe^{II}OAc$; (b) electronic structure of $Fe^{II}OAc$ close to E_F (± 1.5 eV)

$Co^{II}OAc$

We will not discuss the electronic structure of $Co^{II}OAc$ here as NRLMOL yields a wrong antiferromagnetic solution due to the above mentioned reasons. However, one would suspect that it is similar to the electronic structure of $Mn^{II}OAc$ and $Fe^{II}OAc$.

4.1.3 Magnetic and electronic properties of $[Ni^{II}_2(L^6)(L')]^{n+}$ as a function of the third bridging ligand L'

a) magnetic coupling J

It was shown that the variation of transition metal centers allows only for limited changes of the magnetic properties. A far greater variety can be found by changing the third bridging ligand L'. These changes allow a fine tuning of the magnetic interactions. Since only the Ni^{II} complexes show ferromagnetic coupling this section will deal with $[Ni^{II}_2(L^6)(L')]^{n+}$ complexes including the third bridging ligand L'=$EtOCO_2^-$ (**5**), $CH_3OCO_2^-$ (**6**), $\mu_{1,3}$-*meta*-Chlorobenzoato$^-$ (**7**), $\mu_{1,3}$-3,4-Dimethyl-6-phenylcyclohex-3-ene-1-carboxylato$^-$ (**8**), $\mu_{1,3}$-2-(Hydroxyethyl)Carbonato$^-$

(**9**), $CH_3CO_2^-$ (**1**), $\mu_{1,3}$-(2*E*4*E*)-Hexa-2,4-dienoate$^-$ (**10**), BH_4^- (**11**), O_2CPh^- (**12**), NO_3^- (**13**), HCO_2^- (**14**), $\mu_{1,3}$-Bicarbonato (**15**), NO_2^- (**16**), $\mu_{1,2}$-Phthalazine (**17**), $\mu_{1,2}$-Pyrazolato (**18**), *pydz* (**19**), N_2H_4 (**20**), N_3^- (**21**). An overview over the various third bridging ligands is also given in Figure 6.1 in Appendix B (see also Figure I). Note that all of them belong to the conformational type *B* and differ in size and charge. Therefore, it is important to distinguish between structural and electronic effects on the magnetic coupling of the nickel ions. In order to relate the magnetic properties to structural features Table 4.3 also lists the Ni-Ni distance and the average Ni-S-Ni angle (deviations in brackets). The energy differences Δe of the Hay-Thibeault-Hoffmann model are also given in Table 4.3 in order to connect the strength of the magnetic coupling to the electronic structure of the given complex. Nearly all of the complexes show ferromagnetic coupling with varying strength of the exchange coupling constant J. Only in the case of **20** and **21** we observe antiferromagnetic coupling. For **21** the Ni-S-Ni angle is considerably larger than 90° (Ni-S-Ni=94.55°), hence the Goodenough-Kanamori rules predict antiferromagnetic coupling. However, in the case of **18** the deviation of the Ni-S-Ni angle is just the same (Ni-S-Ni=86.38°) and ferromagnetic coupling of the two Ni^{II} is observed. Thus the coupling cannot be explained entirely by the Goodenough-Kanamori rules alone. The energy difference Δe of **21** is also quite large. Therefore, we would expect antiferromagnetic coupling according to the HTH model. Hence, the antiferromagnetic coupling can also be well understood in the terms of the electronic structure of complex **21**. The strong splitting of the magnetic orbitals is here induced by the strong ligand field of the azido bridge. Note that the Ni-Ni distance is also much larger than the average of ~ 3.48 $\mathring{A}$. For complex **18** on the contrary the energy difference Δe of the involved d-orbitals is much smaller. This results in a ferromagnetic coupling predicted by the HTH model. Therefore the electronic effect overrules the structural effect resulting in an overall ferromagnetic coupling. In the case of **20** the energy difference Δe is also considerably larger than the average yet only half as large as the Δe of **21**. Accordingly, a smaller but nevertheless antiferromagnetic coupling is predicted. A closer look at the Ni-S-Ni angle of **20** (87.74°) reveals that the antiferromagnetic behavior of complex **20** can be also understood in the terms of the Goodenough-Kanamori rules. Complex **19** shows nearly identical bridging angles Ni-S-Ni compared to **20**. The Ni-Ni distance is also virtually the same.

Table 4.3: Calculated magnetic coupling J_{calc} using NRLMOL/PBE, the energy difference Δe of the Hay-Thibeault-Hoffmann model and structural data of selected $[\mathrm{Ni}_2^{\mathrm{II}}(\mathrm{L}^6)(\mathrm{L}')]^{\mathrm{n}+}$ complexes. For comparison the experimentally determined magnetic coupling J_{exp} is given as well.

-

complex	J_{calc} [cm^{-1}]	J_{exp} [cm^{-1}]	Δe [mRyd^2]	d(Ni-Ni) [$\mathring{A}$]	Ni-S-Ni [°]	Refs.
5	37	-	0.019	3.49	90.47(5)	[108, 109]
6	35	-	0.007	3.49	90.00(6)	[108, 109]
7	35	-	0.076	3.46	89.95(12)	[88]
8	35	-	0.015	3.49	90.12(12)	[106, 107]
9	34	-	0.049	3.49	89.89(4)	[108, 109]
1	33	6.4	0.014	3.48	89.64(4)	[108, 109]
10	33	-	0.010	3.47	89.46(9)	[106, 107]
11	32	27	0.024	3.49	89.41(5)	[102]
12	31	5.8	0.009	3.47	89.09(4)	[89]
13	27	-	0.016	3.49	90.73(6)	[89]
14	27	-	0.019	3.48	88.95(3)	[102]
15	26	-	0.043	3.47	89.25(8)	[89]
16	25	6.7	0.047	3.40	87.03(4)	[89]
17	22	-	0.030	3.40	88.06(4)	[89]
18	20	-	0.050	3.39	86.38(9)	[89]
19	11	3.5	0.064	3.39	87.58(2)	[89]
20	-6	-	0.145	3.44	87.74(3)	[89]
21	-173	-45	0.313	3.68	94.55(4)	[89]

Nevertheless, ferromagnetic coupling is observed. This can again be understood in the terms of the Hay-Thibeault-Hoffmann model since the energy difference Δe is only 0.064 mRyd^2 and therefore significantly smaller than in complexes **20** and **21**. These facts suggest that the effects on the electronic structure due to the chemical bonding of the third bridging ligand L' becomes the deciding factor and somewhere

between 0.6 mRyd^2 < Δe <0.15 mRyd^2 ferromagnetic interaction becomes favored. A comparison of the remaining energy differences shows that they all display more or less the same values. Without the influence of additional structural effects one expects larger ferromagnetic coupling together with smaller values of Δe. However, there are some exceptions - for example **7**. Despite the large energy difference of Δe = 0.076 mRyd^2 strong ferromagnetic coupling is predicted. This complex also shows a Ni-S-Ni angle of 89.95°. Therefore ferromagnetic coupling is predicted by the Goodenough-Kanamori rules. It seems that in this case the structural effect on the magnetic coupling is stronger than the electronic one. This is again a good example that structural changes and electronic effects affect at the same time the magnetic coupling within these series of nickel complexes.
The discussed relation between the calculated exchange coupling constant J_{calc} and the energy difference Δe is highlighted in Figure 4.5. The data deviate from a per-

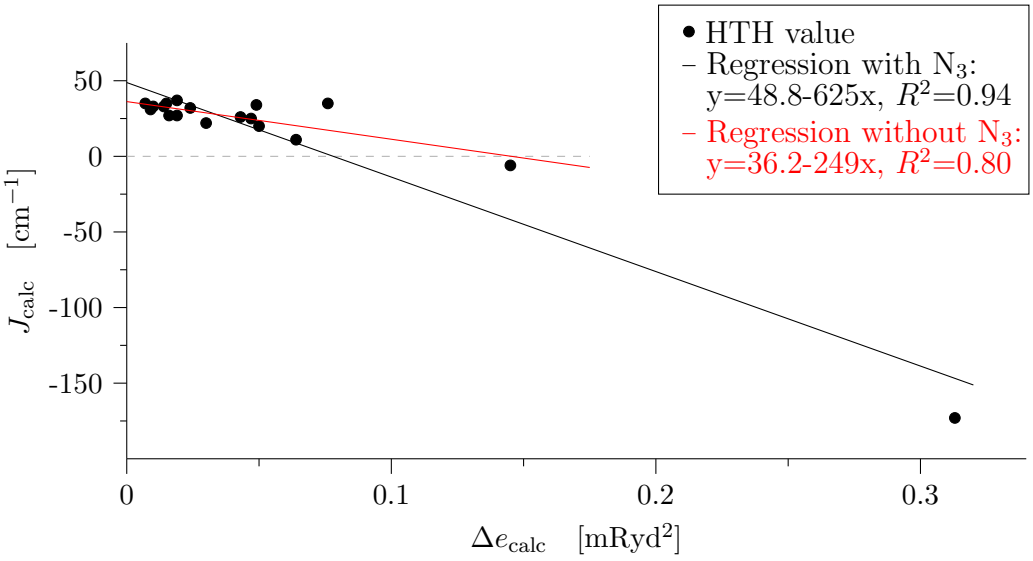

Figure 4.5: Plot of Δe against J_{calc} for $[Ni^{II}_2(L^6)(L')]^{n+}$ complexes including a linear least squares fit for all complexes (black) and for all complexes but **21** (L'=N_3^-) (red)

fect linear dependence due to small differences in the local structural environment of the magnetic Ni^{II} ion. Nevertheless, a least square fit was done in order to predict the maximal possible ferromagnetic J value. The fit yields a maximal possible

ferromagnetic coupling of $J = 48.8$ cm^{-1}. This suggests that within the family of nickel amine-thiophenolat complexes no higher values of the coupling constant J are possible regardless of the third bridging ligand L'. The value for this predicted $J_{\max}$ is even smaller (= 36.2 cm^{-1}) if complex **21** is removed from the fit (see Figure 4.5). However, the regression coefficient becomes quite bad for this fit compared to the fit including all complexes. This is mainly due to a large scattering of the of the HTH values for the ferromagnetically coupling complexes. Here we can clearly see the influence of the ligand field of each L' which does of course influence the splitting of the d-levels at the Ni ions (which is measured by the HTH value). Yet the co-ligand L' is crucial for the magnetic coupling. As shown elsewhere[125] about 70% of the total ferromagnetic coupling are mediated via the bridge. This was proven by model calculations without the third bridging ligand and otherwise unchanged geometry. The results are shown in Table 6.1 in Appendix B. As already mentioned, the only difference between all these models is the changed geometry of the magnetic core. All atoms and chemical bonds are identical. Note that the removal of the third bridging ligand L' will perturb the electronic structure considerably. Therefore the model calculations should only be compared with each other, since all differences in the magnetic coupling will have geometrical reasons.

As shown in Figure 4.6 there exists again a nearly linear dependence of Δe_{model} vs. J_{model}. Interestingly, the linear fit predicts nearly the same theoretical $J_{\max}$ (= 35.2 cm^{-1}) as the fit of the original data excluding complex **21** ($J_{\max} = 36.2$ cm^{-1}). However the regression coefficient is far higher now since the influence of the ligand field of L' is removed. The differences that occur now are only due to the slightly different geometry of each complex. This already indicates the strong link between the electronic structure and the magnetic coupling.

In nearly all model calculations the strength of the ferromagnetic coupling drops to about 1/3 of the coupling with the third bridging ligand. In some cases even weak antiferromagnetic coupling is observed. A closer look at the energy differences Δe_{model} reveals an increased splitting of levels compared to the original calculations (see also 4.1.3). Therefore, the reduced strength of the magnetic coupling can be easily understood in the terms of the Hay-Thibeault-Hoffmann model. Only in the case of the $L' = N_3^-$ co-ligand a strong ferromagnetic coupling is observed for the model calculation together with a reduced energy difference. This indicates that the

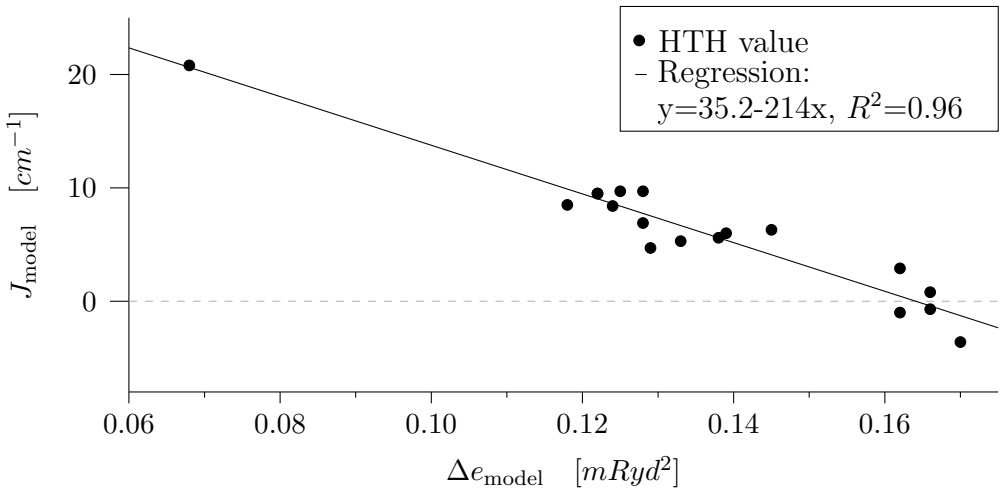

Figure 4.6: Plot of Δe_{model} against J_{model} for $[\text{Ni}_2^{\text{II}}(L^6)(L')]^{n+}$ complexes including a linear least squares fit.

co-ligand L' is either opening a new exchange pathway or it is changing the orbital manifold and therefore the magnetic coupling. In order to clarify the situation some more model calculations have been carried out[124]. To keep track of the change of the magnetic coupling J with respect to the third bridging ligand L' some model calculations of complex **11** are done. Note that there is no change of geometry here since the BH_4^- bridge is simply replaced by some other co-ligands. Therefore all observed changes are due to variations of the electronic structure of the third bridging ligand. Swapping from BH_4^- to halogen ions (F^-, Cl^-, Br^-) results in an increase of the calculated exchange coupling to $J \sim 37$ cm^{-1}. Replacing the BH_4^- ligand by the iso-electronic CH_4 yields a coupling of $J = 30$ cm^{-1}. Finally, Ne was introduced as a bridging ligand resulting in a weak ferromagnetic coupling of $J = 12$ cm^{-1} which is about the value of the model calculation without any co-ligand. These model calculations suggest, that the magnetic coupling basically does not depend on the charge or size of the co-ligand L'. The only important feature is the electronic structure of the third bridging ligand - namely the energetic position of the p-levels because they mediate the superexchange. There exists a direct exchange pathway across the bridge as shown in Figure 4.7 which is most pronounced in complex **11**. In the case of **21** the N_3^- co-ligand changes the orbital energies in such a way, that the

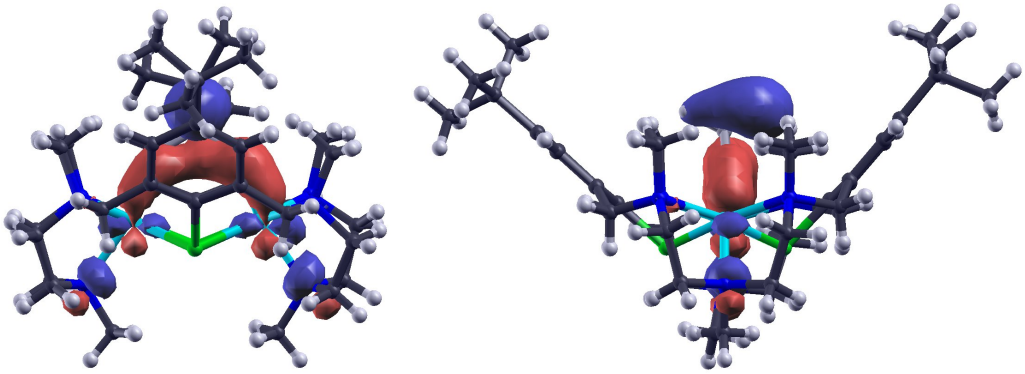

(a) sideview (b) topview

Figure 4.7: Exchange pathway across the BH_4^- bridge **11**. The depicted orbital belongs to the HOMO-15 in the spin up channel.

ferromagnetic exchange pathway across the third bridging ligand becomes blocked. This is not surprising, since N_3^- is known as a ligand inducing a strong ligand field.

All these observations result in some general rules to enhance the magnetic exchange coupling J within these series of Robson-type hexamine-dithiophenolate macrocycles $[M_2^{II}(L^6)(L')]^+$:

- Ferromagnetic coupling is only observed in the case of M=Ni^{II}. All other examined third row transition metal ions yield antiferromagnetic coupling.
- The strength (J) and the kind (ferromagnetic or antiferromagnetic) of the magnetic coupling can be understood in terms of structural as well as electronic effects.
- The influence of the structure on the magnetic coupling is described by the Goodenough-Kanamori rules, whereas the impact of the electronic structure is described within the Hay-Thibeault-Hoffmann model. Both effects compete with each other and may enhance or cancel out their effects.
- The energy splitting of the Hay-Thibeault-Hoffmann model can be understood as a measure of the crystal field strength of L'. Only weak ligands favor ferromagnetic exchange.

- An additional ferromagnetic exchange pathway is provided across the third bridging ligand L'.
- The co-ligand should be of appropriate geometrical size to keep the general structure of type B.
- The largest predicted ferromagnetic coupling J of the $[Ni_2^{II}(L^6)(L')]^{n+}$ complexes is about 50 cm^{-1}.

b) magnetic anisotropy D

While it appears possible to rationalize the observed magnetic exchange properties in terms of structural and electronic elements, the situation changes completely when considering the magnetic anisotropy D. As shown in literature[30, 50, 72, 77, 134, 150, 191] there are basically four parameters that influence the sign and the value of the magnetic anisotropy D:

- the geometric distortion of the metal center environment
- the crystal field strength of the ligand
- the covalence of the metal center
- the HOMO-LUMO gap (which is of course induced by geometric distortions and varying crystal field strength)

In the case of the Robson-type hexamine-dithiophenolate macrocycles the covalence of the metal center is always the same - therefore the magnetic anisotropy should be governed by the crystal field strength of the ligand and the geometric distortion. Both working together do of course also influence the HOMO-LUMO gap of the respective molecule. The crystal field strength of the third bridging ligand can be expressed in terms of the Hay-Thibeault-Hoffmann model. The stronger the crystal field induced by the ligand the larger is the splitting of levels (note that the Hay-Thibeault-Hoffmann model takes only unoccupied levels into account). Yet there is no connection between D and the splitting of the orbital energies as calculated within the HTH model for the original structures as shown in Figure 4.8.

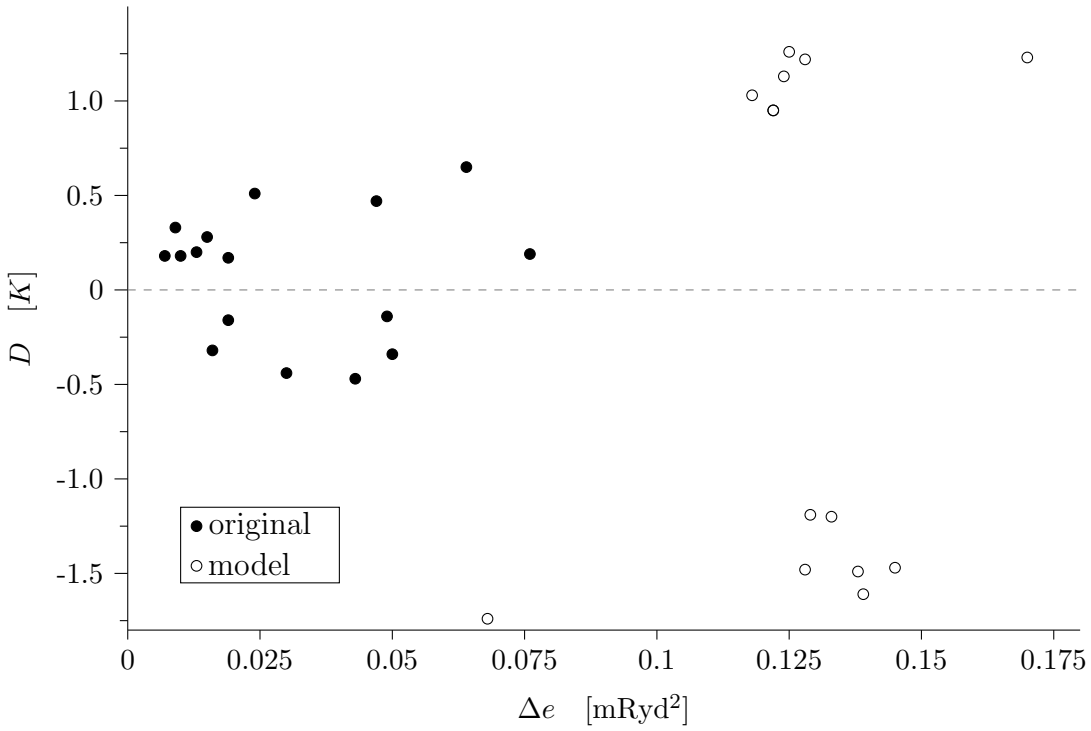

Figure 4.8: Plot of $\Delta e_{\mathrm{orig/model}}$ against $D_{\mathrm{orig/model}}$ (empty/filled triangles) for various $[\mathrm{Ni}_2^{\mathrm{II}}(\mathrm{L}^6)(\mathrm{L}')]^{\mathrm{n}+}$ complexes

Upon the removal of the third bridging ligand (see Table 6.1 in Appendix B) all electronic contributions of this co-ligand vanish and we observe a much higher HTH energy difference and accordingly smaller ferromagnetic coupling or even a change from ferromagnetic coupling to antiferromagnetic coupling (complex **16-19**). For the cases of **20** and **21** we can switch from (strong) antiferromagnetic coupling to ferromagnetic coupling as already explained in more detail in section 4.1.3. Interestingly, this decrease in the strength of the coupling is accompanied by an increase in the strength of the magnetic anisotropy D as shown in Figure 4.9 (red). Apparently, the system tends to high coupling constants and low D values in the case for the original molecules and vice versa in the case of the model calculations. This indicates that a given ferromagnetic system minimizes its energy either by a strong coupling of the spins or a strong magnetic anisotropy.
Furthermore, the removal of the third bridging ligand leads to a tremendous re-

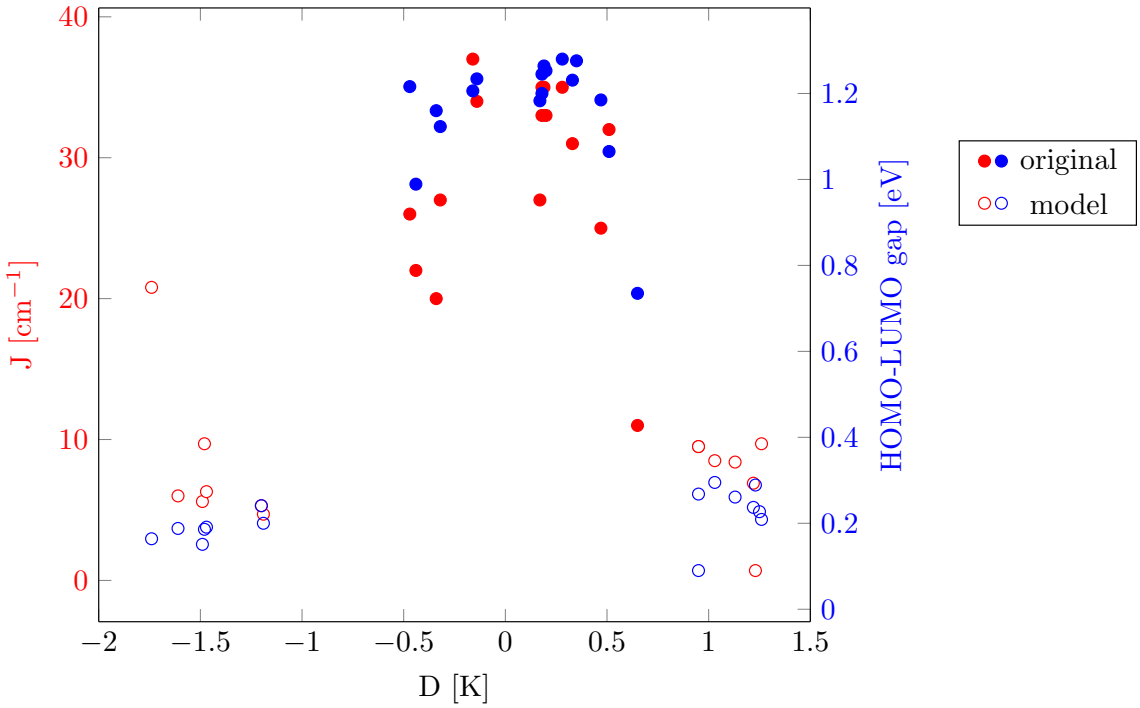

Figure 4.9: Plot of the magnetic anisotropy D against J (red) and the HOMO-LUMO gap (blue) for various $[Ni_2^{II}(L^6)(L')]^{n+}$ (filled circles) and $[Ni_2^{II}(L^6)]^{n+}$ (empty circles) complexes

duction (one order of magnitude) of the HOMO-LUMO gap of any given complex. This can be related to the crystal field splitting induced by the co-ligand which does of course vanish once L' is removed. This reduction of the HOMO-LUMO gap is directly related to an increase of $|D|$ as shown in Figure 4.9 (blue) and in Table 6.1 in Appendix B. As already stated by Goswani and Misra[77] an increasing magnetic anisotropy is related to a decreasing HOMO-LUMO gap which is clearly observed here as well.

A further attempt to relate the magnetic anisotropy to structural parameters is the computation of the mean deviation $\Delta O = \frac{|O_1+O_2|}{2}$ from the octahedral symmetry of both central Ni^{II} ions for the original molecules. These values are obtained by the use of the SHAPE package. As shown in Figure 4.10 the smaller the variation from a perfect octahedron, the more likely is a single molecule magnet behavior. Yet there are deviations from this rule. In the case of **9** a negative magnetic anisotropy is

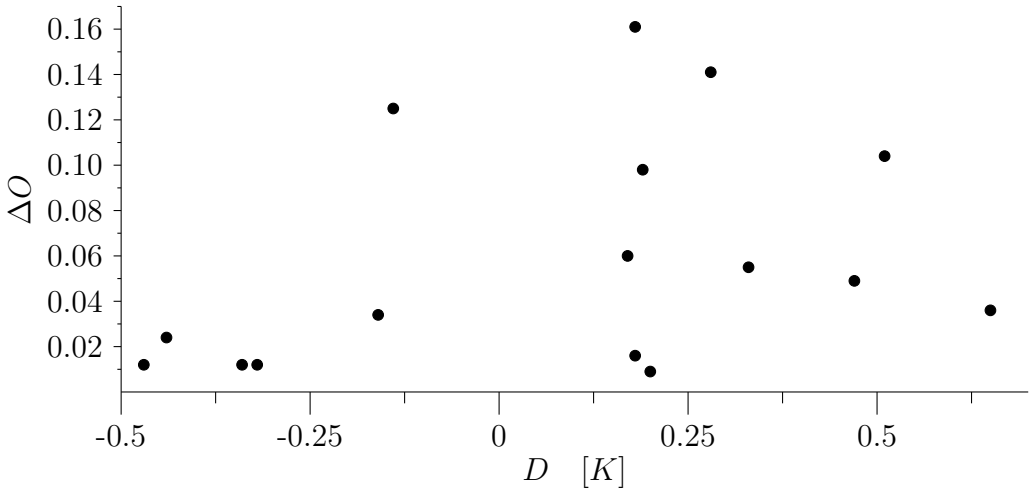

Figure 4.10: Plot of Δe_{orig} against D_{orig} for $[\text{Ni}_2^{\text{II}}(\text{L}^6)(\text{L}')]^{\text{n}+}$ complexes

observed despite the fact that a large geometric distortion is present. In the case of **1** and **10** the reversed behavior can be found. These two complexes exhibit only a small distortion from the octahedral environment of the two central Ni^{II} ions, yet the magnetization prefers an easy plane system. Apparently, an easy axis behavior of a given complex is more likely for nearly undistorted octahedral structures. However, this is not a sufficient condition for the occurrence of an easy axis anisotropy. A detailed overview of all the discussed properties of the original and model systems can be found in Appendix B in Table 6.1.

Summarizing this section it can be concluded that

- there is no connection between the energy difference Δe of the HTH model and the magnetic anisotropy D.
- the magnetic anisotropy D and the strength of the magnetic coupling seem to be connected. For this system it is not possible to maximize both quantities at the same time.
- a decreasing HOMO-LUMO gap results in an increase of the magnetic anisotropy.
- a nearly octahedral environment favors easy axis system but not all "undistorted" structures yield SMM behavior.

c) electronic structure

After the detailed discussion of the magnetic properties this work shall now focus on the electronic properties of the variously bridged $[Ni_2^{II}(L^6)(L')]^{n+}$ complexes. According to experimental data complex **11** (L'= BH_4^-) exhibits the largest ferromagnetic coupling and hence it shall be the first complex whose electronic structure is discussed in more detail.

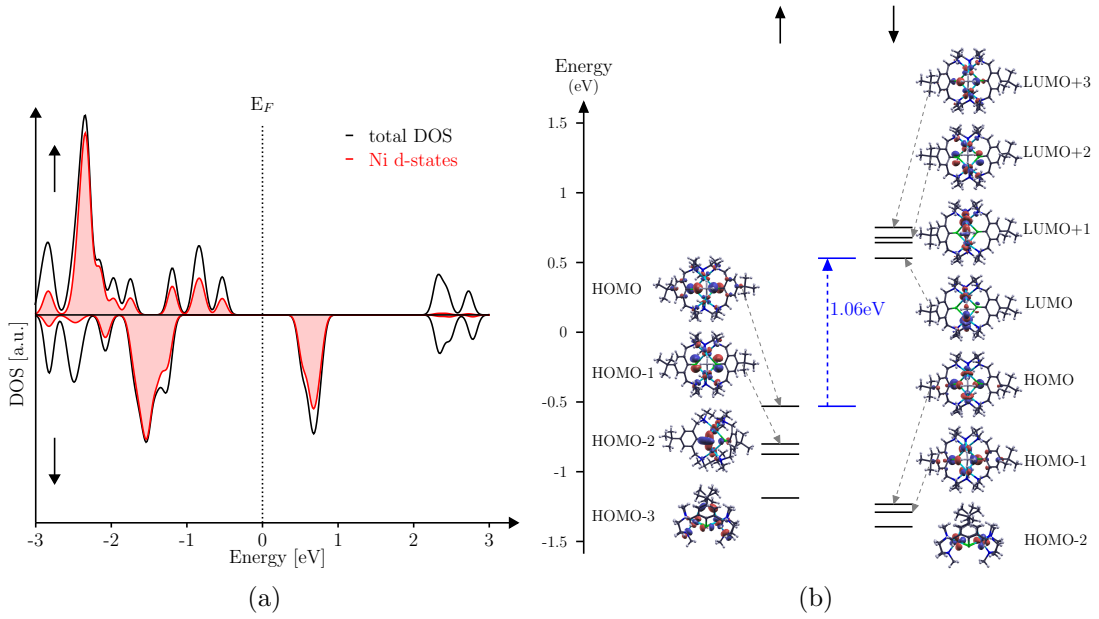

Figure 4.11: (a) DOS of $[Ni_2^{II}(L^6)(BH_4)]^+$;
(b) electronic structure of $[Ni_2^{II}(L^6)(BH_4)]^+$ close to E_F (±1.5 eV)

As shown in Figure 4.11 the ferromagnetic complex $[Ni_2^{II}(L^6)(BH_4)]^+$ has a HOMO-LUMO gap of approximately 1 eV which is between a spin up state (HOMO) and a spin down state (LUMO). The HOMO-LUMO gaps within the spin channels are even larger with 2.84 eV (spin up) and 1.77 eV (spin down). Yet again all levels close to the Fermi level are dominated by Ni^{II} d-states as shown in Figure 4.11a and already observed in case of the $[M_2^{II}(L^6)(OAc)]^+$ macrocycles discussed in section 4.1.2. Consistently, the corresponding wave functions (see Figure 4.11b) are also very similar. Within the spin up channel a ferromagnetic coupling pathway across

the sulfur atoms is clearly identified for the HOMO and the HOMO-1 whereas the HOMO-2 and the HOMO-3 indicate that there is an additional exchange pathway across the bridging BH_4 ligand enhancing the overall ferromagnetic coupling. The LUMO of the spin up channel consists of ligand states and is not included in Figure 4.11b as it is located well above the Fermi level. Similar pathways can be observed within the spin down channel. Here the HOMO, HOMO-1 and the HOMO-2 are very close in energy and feature a coupling pathway across the the sulfur atoms. The LUMO and the LUMO+1 on the other hand include contributions from the Ni^{II} d-states as well as the bridging BH_4 ion. The wave functions that build the LUMO+2 and the LUMO+3 consist mainly of states belonging to the sulfur atoms and Ni^{II} d-states. All states that are higher in energy belong the the ligand system and do not include any notable amount of Ni^{II} d-states. Upon the removal of the BH_4^- bridge the

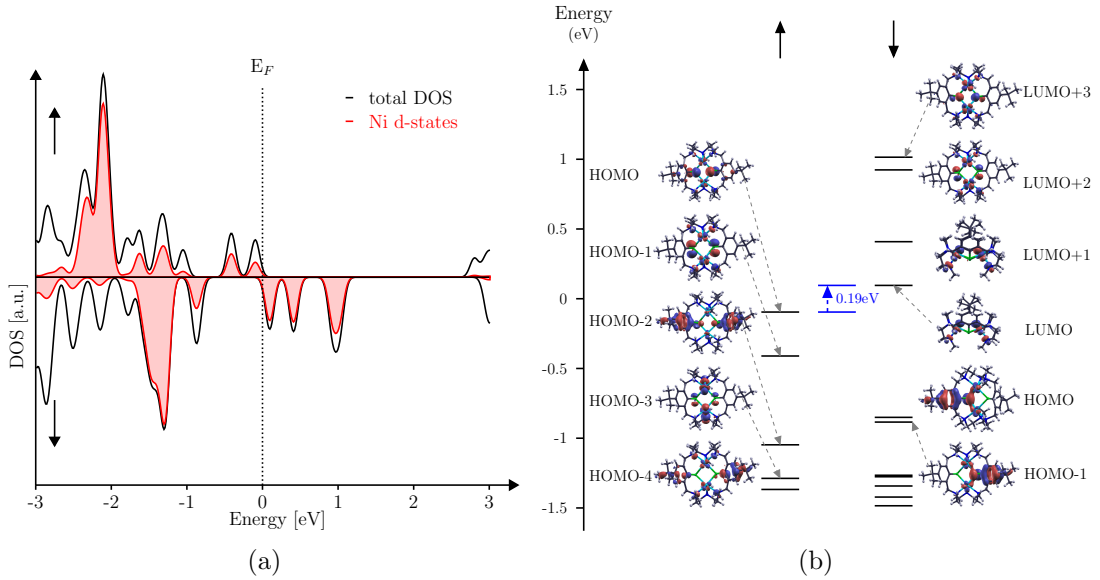

Figure 4.12: (a) DOS of complex **11** without BH_4^- ;
(b) electronic structure of complex **11** without BH_4^- close to E_F ($\pm$1.5 eV). The wave functions belonging to HOMO-6 to HOMO-2 are pure Ni^{II} d-states. For reasons of clarity these states are omitted and instead depicted in Appendix B (Figure 6.2)

electronic structure does change, yet the overall ferromagnetic coupling is preserved

(but weakened). The most outstanding change is the tremendous reduction of the HOMO-LUMO gap by a factor of 5 (1.06 eV $\rightarrow$ 0.19 eV) as shown in Figure 4.12. Taking a closer look at the density of states (Figure 4.12a) it becomes evident that there are also similarities to the density of states of the original complex. Compared to the DOS shown in Figure 4.11a the states close to the Fermi level are shifted towards E_F, while those further away are more or less unaffected. Furthermore, a larger splitting of levels is observed especially for the unoccupied states of the spin down channel close to the Fermi level. Taking a closer look at the wave functions close to E_F confirmed this assumption. As depicted in Figure 4.12b the HOMO and the HOMO-1 in the spin up channel are identical with the respective states for the original complex. The HOMO-2 of the spin up channel is an orbital also present in the original complex, where it is the HOMO-4. As already discussed the HOMO-2 and HOMO-3 of the original include contributions from the BH_4^- bridge. These states do upon the removal of the third bridging ligand. A similar behavior can be observed for the spin down channel.
Summarizing it can be concluded that the removal of the third bridging ligand results in

- a tremendous decrease of the HOMO-LUMO gap ($\sim \frac{1}{5}$ of the original value).
- a larger splitting of levels for the unoccupied states of the spin down channel close to the Fermi level.
- the disappearance of states including contributions from the third bridging ligand.
- an overall preserved level ordering (apart from the states mentioned above).

The density of states for the ferromagnetic coupling complexes looks very alike for all considered complexes, hence a separate discussion for every single complex is omitted. The DOS of the antiferromagnetic coupling complexes is similar to the already discussed DOS of complex **2** (see section 4.1.2) and will be discussed here neither. For comparison the DOS of complexes **1**, **5-10** and **12-21** with and without L' are also depicted in Appendix B in Figures 6.3-6.19.

Overall we have been able to show that

- Ferromagnetic coupling is only observed in the case of M=Ni^{II}. All other examined third row transition metal ions yield antiferromagnetic coupling.
- The influence of the structure on the magnetic coupling is described by the Goodenough-Kanamori rules, whereas the impact of the electronic structure is described within the Hay-Thibeault-Hoffmann model. Both effects compete with each other and may enhance or cancel out their effects.
- The energy splitting of the Hay-Thibeault-Hoffmann model can be understood as a measure of the crystal field strength of L'. Only weak ligands favor ferromagnetic exchange.
- An additional ferromagnetic exchange pathway is provided across the third bridging ligand L'.
- Upon the removal of L' a tremendous decrease of the HOMO-LUMO gap ($\sim \frac{1}{5}$ of the original value) is observed.
- The magnetic anisotropy D and the strength of the magnetic coupling seem to be connected. For this system it is not possible to maximize both quantities at the same time.
- A decreasing HOMO-LUMO gap results in an increase of the magnetic anisotropy.
- A nearly octahedral environment favors easy axis system but not all "undistorted" structures yield SMM behavior.

4.2 Various azido-$\mu_{1,1}$ bridged transition metal complexes

As already observed in the case of the Robson-type hexamine-dithiophenolate macrocycles there seems to be a connection between the magnetic coupling J and the magnetic anisotropy D in a way that we can not have strong coupling and strong magnetic anisotropy at the same time. Now we will focus on the question whether or not it is possible to combine a large spin ground state S and a high magnetic anisotropy. This would of course be preferred in order to build single molecule magnets with a large barrier of magnetization U which is given by $U = S^2|D|$ (see also section 2.4.4). In order to get comparable results we restricted ourselves to octahedral coordinated, azido-bridged copper, nickel and manganese dimers with the general structure shown in Figure 4.13. As shown in literature dinuclear com-

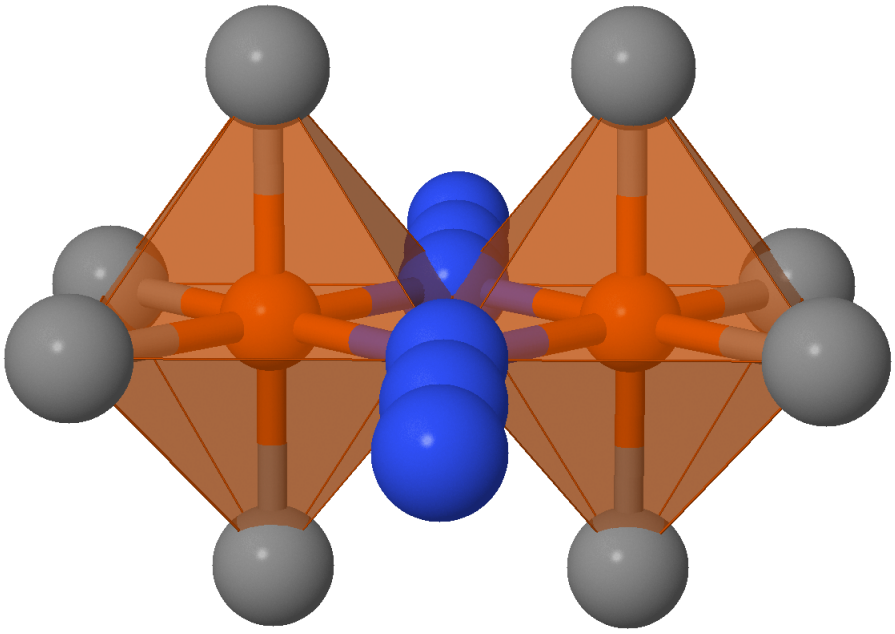

Figure 4.13: octahedral coordinated $\mu_{1,1}$-azido bridged transition metal (TM) dimer; grey: any ligand, orange: TM^{II}, blue: N

plexes including a $TM(\mu_{1,1} - N_3)_2TM$ magnetic fragment are usually expected to couple ferromagnetically due to the orientation of the magnetic orbitals[7, 47, 186, 190] and hence the N_{azide}-TM-N_{azide} angles[59, 129, 197]. Yet this is not always true. In the case of asymmetric complexes the TM-N_{azide} distances become the deciding factor.

Larger TM$-N_{\text{azide}}$ distances result in a damping of the ferromagnetic coupling and may even give rise to antiferromagnetic coupling[197, 218] within the transition metal dimer. Nevertheless these dimers are expected to exhibit largely ferromagnetic coupling and thus a high spin ground state. Hence they are promising candidates to observe a possible connection between the ground state S and the magnetic anisotropy D. Note that all anisotropies presented within this chapter are calculated according to van Wüllen[219] (see equation (2.106)). In order to keep the study comparable only octahedral coordinated transition metal complexes are examined. A more detailed discussion of structural and magnetic trends can be found elsewhere[5, 189].

4.2.1 Cu$(\mu_{1,1} - \mathrm{N}_3)_2$Cu complexes

An intensive search within the Cambridge Structural Database (CSD)[8] yields 11 complexes showing the desired geometry. An overview of the respective structures is given in Figure 6.20 in Appendix C (see also Figure II). The theoretical and (if available) experimental results for the magnetic behavior are summarized in Table 4.4. All results are in fairly good agreement with experimental results except LIZVOF. Here an antiferromagnetic coupling of the two Cu^{II} is predicted, whereas strong ferromagnetic coupling is observed experimentally. It can be assumed that this discrepancy is due to a failure of the broken symmetry approach since the coupling of the nearly identical complex LIZVUL is predicted correctly. For FELZAY and YIBNON very weak antiferromagnetic coupling is predicted experimentally while the calculations yield weak ferromagnetic coupling. Here the divergence may be due to the general overestimation of the exchange coupling within DFT (see also section 2.5.2). In order to overcome these shortcommings further calculations using the B3LYP functional as implemented in ORCA have been done since it is known that B3LYP usually yields better results compared to PBE calculations. These calculations reproduced the correct coupling for all complexes except LIFGAI where a weak antiferromagnetic coupling is predicted instead of the experimentally observed ferromagnetic coupling. For comparison further PBE calculations using ORCA have been carried out for all considered complexes. However, those calculations only confirm the results obtained from the NRLMOL/PBE calculations.
Based on these findings the magnetic anisotropy D has been calculated as imple-

Table 4.4: Magnetic properties of various $Cu(\mu_{1,1}-N_3)_2Cu$ complexes. Given are experimental J_{exp} and calculated J_{PBE}/J_{B3LYP} coupling constants as well as magnetic anisotropy $D_{exp/calc}$ (D_{corr} is the corrected magnetic anisotropy according to Van Wüllen[219]) and the barrier of magnetization U which is calculated based on the corrected magnetic anisotropies. For the calculation of the coupling constant NRLMOL(PBE)/ORCA(B3LYP) have been used. *=relaxed structure

complex	J_{exp} [cm^{-1}]	J_{PBE} [cm^{-1}]	J_{B3LYP} [cm^{-1}]	D_{exp} [cm^{-1}]	D_{calc} [K]	D_{corr} [K]	U [K]	Refs.
BATHUZ10	35 ± 10	49	54	-	0.31	0.62	-	[52]
FELZAY	-1.5	3	1	-	-	-	-	[203]
LIFGAI*	20.1	10	-3	-12.5	-2.10	-4.20	4.2	[53]
LIZVOF	115	-10	70	-	-2.50	-5.00	5.0	[67]
LIZVUL*	112	40	97	-	-2.50	-5.00	5.0	[67]
PIDYEG	-2.9	-7	17	-	-	-	-	[54]
PIVMOX	-	-21	-20	-	-	-	-	[122]
WEVKUD	-	20	75	-	-2.75	-5.50	5.5	[135]
WIDNUS	-	13	78	-	-2.68	-5.36	5.4	[136]
YIBNON	-2.46	4	-1	-	-	-	-	[6]
ZUBYUQ	-	-1	-4	-	-	-	-	[74]

mented in NRLMOL. It has been determined for all complexes where a ferromagnetic coupling is observed experimentally or where PBE and B3LYP calculations agree on the ferromagnetic coupling for those complexes with no experimental data available. All of them - except BATHUZ10 - show an easy axis behavior and are therefore single molecule magnets (SMMs). The magnetic anisotropy of the six SMMs is nearly identical with $|D| \sim 5$ K. Only LIFGAI ($D = -10$ K) and LIZVUL ($D = -18$ K) show a significant higher anisotropy. However upon the relaxation of these two structures a much smaller magnetic anisotropy of $D = -4.2/-5$ K (LIFGAI*/LIZVUL*) is observed. Note that this decrease of the magnetic anisotropy is accompanied by a decrease of the total energy (i.e. the solution with a high energy yields a high magnetic anisotropy whereas the solution with the lowest energy yields

a low magnetic anisotropy). Summarizing it can be stated that complexes show a resulting barrier of ~ 5 K.

4.2.2 Ni($\mu_{1,1} - N_3)_2$Ni complexes

In the case of Ni($\mu_{1,1} - N_3)_2$Ni complexes only eight complexes of the required geometry can be found within the CSD. An overview of the respective structures is given in Figure 6.21 in Appendix C (see also Figure III). The theoretical and (if available) experimental results are summarized in Table 4.5. All of them exhibit a $S = 2$ ground state in the calculations. Again there is a good the agreement between

Table 4.5: Magnetic properties of various Ni($\mu_{1,1} - N_3)_2$Ni complexes. Given are experimental J_{exp} and calculated J_{PBE}/J_{B3LYP} coupling constants as well as magnetic anisotropy $D_{exp/calc}$ (D_{corr} is the corrected magnetic anisotropy according to Van Wüllen[219]) and the barrier of magnetization U which is calculated based on the corrected magnetic anisotropies. For the calculation of the coupling constant NRLMOL(PBE)/ORCA(B3LYP) have been used.

complex	J_{exp} [cm^{-1}]	J_{PBE} [cm^{-1}]	J_{B3LYP} [cm^{-1}]	D_{exp} [cm^{-1}]	D_{calc} [K]	D_{corr} [K]	U [K]	Refs.
CALWUH	13.6	26	33	-19.2	0.88	1.17	-	[21]
DAWTUR	1.2	13	26	-	-0.73	-0.97	3.8	[27]
GUWJIR	21.8	32	36	-	1.25	1.66	-	[61]
IXUFEM	39.0	25	28	7.3	-0.59	-0.78	3.1	[62]
JEDHIK	11.5	29	30	5.27	-0.77	-1.02	4.0	[202]
JEXCIY	20.1	16	27	-12.5	1.37	1.82	-	[16]
PEJNAT	33.8	20	30	-21.5	0.43	0.57	-	[221]
TEQNEJ	-1.8	9	11	0(fixed)	-0.83	-1.11	3.3	[48]

experimentally obtained coupling constants and the calculated ones. Only in the case of TEQNEJ ferromagnetic coupling is predicted whereas antiferromagnetic coupling is observed experimentally. However, the ferromagnetic ground state is confirmed

by the B3LYP calculations, hence it is assumed that the ferromagnetic coupling is indeed present. Hence a magnetic anisotropy for TEQNEJ was calculated despite the fact that the experimentally obtained coupling was weakly antiferromagnetic. The agreement between the calculated and experimentally obtained anisotropies on the other hand is rather bad. However, a similar behavior has been observed by Zein et al.[229]. They found that a mismatch of the calculated and experimentally obtained anisotropies is observed for large $\frac{E}{D}$ ratios, i.e. for cases where a large biaxial anisotropy E is present. For Mn complexes these "critical" ratio is $\frac{E}{D} > 0.2$. Nearly all of the here considered $\mathrm{Ni}(\mu_{1,1}-\mathrm{N}_3)_2\mathrm{Ni}$ complexes show a $\frac{E}{D} > 0.1$ ratio. So it might well be that the "critical" ratio for the $\mathrm{Ni}(\mu_{1,1}-N_3)_2\mathrm{Ni}$ is smaller compared to the Mn complexes investigated by Zein et al.[229].

Note that that not all of the dimers show SMM behavior, nevertheless the absolute value of the magnetic anisotropy is within an order of magnitude 0.57 K$< |D| <$ 1.82 K. In the case of the SMMs the deviation is even smaller 0.78 K$< |D| <$ 1.11 K. Therefore, it is not surprising that the barrier of magnetization U differs only slightly $U \sim 3.6$ K. Interestingly this is the same order of magnitude as the barrier height observed in the case of the Cu-dimers. It is remarkably smaller than the barrier calculated for the copper complexes. This is rather surprising since we would expect a higher barrier for complexes with a higher total spin according to $U = S^2|D|$. Here the total spin S enters quadratically whereas it is linearly dependend on the magnetic anisotropy D. Hence one would expect a higher barrier for larger total spins. On the other hand one could argue that there is a "hidden" $[S \cdot (S-0.5)]^{-1}$ dependency in the computation of D as pointed out by van Wüllen[219]. As explained in more detail in section 2.5.3 we actually calculate an axial magnetic anisotropy energy (MAE) which is divided by $S \cdot (S-0.5)$ in order to obtain the magnetic anisotropy D (see equation (2.106). Taking that into account the actual formula for the calculation of the barrier of magnetization U should read:

$$U = |D| \cdot S^2 = \mathrm{MAE}\frac{\mathrm{S}^2}{\mathrm{S}(\mathrm{S}-0.5)} = \mathrm{MAE}\frac{\mathrm{S}}{\mathrm{S}-0.5}. \tag{4.1}$$

Using this connection one could define the ratio Δ_1 of the different barriers of magnetization of the copper dimers and the nickel dimers according to:

$$\begin{aligned} \Delta_1 = \frac{U_{\mathrm{Cu}}}{U_{\mathrm{Ni}}} &= \frac{\mathrm{MAE_{Cu}} \cdot \mathrm{S_{Cu}}(\mathrm{S_{Ni}} - 0.5)}{(S_{\mathrm{Cu}} - 0.5) \cdot \mathrm{MAE_{Ni}} \cdot \mathrm{S_{Ni}}} \\ &= \frac{\mathrm{MAE_{Cu}} \cdot 1 \cdot (2 - 0.5)}{(1 - 0.5) \cdot \mathrm{MAE_{Ni}} \cdot 2} \\ &= \frac{3 \cdot \mathrm{MAE_{Cu}}}{2 \cdot \mathrm{MAE_{Ni}}} \end{aligned} \tag{4.2}$$

Apparently, the ratio Δ depends only on a pre-factor given by the respective transition metal species and the axial magnetic anisotropy energy. A very crude approximation for the MAE can for example be extracted from the free ion single electron spin-orbit coupling parameters ζ. Here we find $\zeta_{\mathrm{Ni}} = 630$ cm^{-1} and $\zeta_{\mathrm{Cu}} = 830$ cm^{-1}[127]. The free ion single electron spin-orbit coupling parameter of copper is larger than the one of nickel which is to be expected as the value of ζ increases with increasing nuclear charge. As pointed out by Neese et al[151] for iron-complexes ζ is reduced due to the relativistic nephelauxetic effect (enhanced covalent metal-ligand bond). Note that the relativistic nephelauxetic effect depends on the nature of the ligand[18, 19, 130] as well as on the nature of the central metal ion[63, 95]. The effect of the ligands should be negligible within the present study since we deliberately choose complexes with nearly identical ligands. As for the different transition metal centers we expect a larger relativistic nephelauxetic effect for copper compared to nickel.[95]. Summarizing can be stated that we would expect an overall ratio Δ_1 of roughly two when taking into account the pre-factor $\frac{3}{2}$ and the free ion single electron spin-orbit coupling parameters ζ as a first approximation for the axial magnetic anisotropy energy. In other words we expect the barrier of magnetization to be twice as large for the copper complexes compared to the nickel complexes. However, we observe

$$\frac{U_{\mathrm{Cu}}}{U_{\mathrm{Ni}}} \sim 1.4 \tag{4.3}$$

for the ratio Δ_1. This damping might by due to the relativistic nephelauxetic effect which leads to a larger reduction of the free ion single electron spin-orbit coupling parameters ζ in copper compared to nickel. Thus, the advantage gained by having

a larger spin ground state is destroyed by the much smaller magnetic anisotropy. The drop in the anisotropy is even larger than the increase given by the larger spin ground state resulting in an overall smaller barrier of magnetization. The interesting question is now how the manganese complexes behave.

4.2.3 $\mathbf{Mn}(\mu_{1,1}-\mathrm{N}_3)_2\mathbf{Mn}$ complexes

There are several Mn_2 complexes exhibiting the desired structure. The theoretical and (if available) experimentally obtained magnetic properties are summarized in Table 4.6. An overview of the respective structures is given in Figure 6.22 in Appendix C (see also Figure IV). All of them exhibit either a $S = 5$ ground state or - in the case of antiferromagnetic coupling - a $S = 0$ ground state. All manganese complexes show a rather weak coupling and the experimental results are in no agreement to the coupling constants calculated using a PBE xc-functional. For comparison we also did PBE calculations using the ORCA program packages, however the results are identical to those obtained using NRLMOL. The B3LYP calculations on the other hand predict the ferromagnetic coupling correctly and hence the magnetic anisotropy is calculated for all complexes regardless of the magnetic coupling predicted by the PBE calculations. Interestingly we observe for all the complexes a barrier $U \sim 2 \pm 1$ K which is in the range of the barrier observed for the nickel and copper dimers. The barrier is even somewhat lower compared to the other transition metal complexes. Again this is surprising. At first glance one would expect the highest barrier of magnetization for the manganese complexes since we get here the highest spin ground state of $S = 5$ (remember: $U = S^2|D|$). However, here we also have to bear in mind the "hidden" $[S \cdot (S - 0.5)]^{-1}$ dependency in the computation of D[219] within second order perturbation theory. Taking that into account we can again define the ratio Δ of the different barriers of magnetization. This time for the copper/manganese and the nickel/manganese dimers. This should read as:

$$\Delta_3 = \frac{U_{\mathrm{Cu}}}{U_{\mathrm{Mn}}} = \frac{\mathrm{MAE_{Cu}} \cdot \mathrm{S_{Cu}}(\mathrm{S_{Mn}} - 0.5)}{(S_{\mathrm{Cu}} - 0.5) \cdot \mathrm{MAE_{Mn}} \cdot \mathrm{S_{Mn}}} = \frac{9 \cdot \mathrm{MAE_{Cu}}}{5 \cdot \mathrm{MAE_{Mn}}} \quad \text{and} \quad \Delta_4 = \frac{U_{\mathrm{Ni}}}{U_{\mathrm{Mn}}} = \frac{\mathrm{MAE_{Ni}} \cdot \mathrm{S_{Ni}}(\mathrm{S_{Mn}} - 0.5)}{(S_{\mathrm{Ni}} - 0.5) \cdot \mathrm{MAE_{Mn}} \cdot \mathrm{S_{Mn}}} = \frac{6 \cdot \mathrm{MAE_{Ni}}}{5 \cdot \mathrm{MAE_{Mn}}}$$

Table 4.6: Magnetic properties of various $Mn(\mu_{1,1}-N_3)_2Mn$ complexes. Given are experimental J_{exp} and calculated J_{PBE}/J_{B3LYP} coupling constants as well as magnetic anisotropy $D_{exp/calc}$ (D_{corr} is the corrected magnetic anisotropy according to Van Wüllen[219]) and the barrier of magnetization U which is calculated based on the corrected magnetic anisotropies. For the calculation of the coupling constant NRLMOL(PBE)/ORCA(B3LYP) have been used. FM: ferromagnetic, AFM: antiferromagnetic

complex	J_{exp} [cm^{-1}]	J_{PBE} [cm^{-1}]	J_{B3LYP} [cm^{-1}]	D_{exp} [cm^{-1}]	D_{calc} [K]	D_{corr} [K]	U [K]	Refs.
FIBJIK	intra: weak FM	1	4	-	0.04	0.04	-	[121]
	inter: weak AFM			-				
LEXPOU	-	2	4	-	0.06	0.07	-	[184]
LIMLAV	1.31	-1	4	-	-0.09	-0.10	2.5	[226]
PIVQOB	2.46	-2	4	0.019	0.86	0.95	-	[228]
PIVQUH	2.26	-1	4	0.017	0.07	0.08	-	[228]
PIVRAO	1.92	1	4	-	-0.12	-0.13	3.2	[228]
RALKAR	0.77	1	3	-	0.03	0.03	-	[105]
RALKEV	2.04	3	5	-	-0.13	-0.14	3.5	[105]
RALKIZ	1.75	3	5	-	-0.11	-0.12	3.0	[105]
RASHID	0.65	2	4	-	-0.03	-0.03	0.7	[153]
RASHOJ	0.55	-1	3	-	-0.04	-0.04	1.0	[153]
RASHUP	0.68	1	4	-	-0.04	-0.04	1.0	[153]

Again we observe that the ratio of the respective barriers of magnetization depends on a prefactor given by the involved transition metal ions and the axial magnetic anisotropy energy. Taking the free ion single electron spin-orbit coupling parameters $\zeta_{Mn} = 300\ cm^{-1}$ as a first crude approximation we get:

$$\Delta_3 = 5 \qquad \text{and} \qquad \Delta_4 = 2.5$$

But already here we see that the barrier of the dimers containing manganese ions is always expected to be the smallest out of the three regarded transition metals.

Now we compare these to the actual calculated barriers and we get:

	$\Delta_1 = \frac{U_{\mathrm{Cu}}}{U_{\mathrm{Ni}}}$	$\Delta_3 = \frac{U_{\mathrm{Cu}}}{U_{\mathrm{Mn}}}$	$\Delta_4 = \frac{U_{\mathrm{Ni}}}{U_{\mathrm{Mn}}}$
estimated:	$\Delta_1 = 2$	$\Delta_3 = 5$	$\Delta_4 = 2.5$
calculated:	$\Delta_1 \sim 1.4$	$\Delta_3 \sim 3$	$\Delta_4 \sim 1.5$

Apparently, we observe the same trend for the calculated barriers of magnetization and the respective ratios as predicted by the estimations. The barrier U of the copper complexes is always larger than the respective barrier of the nickel and manganese complexes. The ratio of the calculated barriers is smaller than those obtained from the estimations which might again be due to the damping evoked by the relativistic nephelauxetic effect as already discussed in the previous section. Note that the damping of the free ion single electron spin-orbit coupling parameters ζ due to the relativistic nephelauxetic effect is strongest for copper followed by nickel and manganese. Hence it is not surprising that the calculated ratio Δ_4 is furthest away from the predicted one.

Summarizing it can be concluded that the barrier of magnetization U is within an order of magnitude ($U = 1 - 5K$) for all regarded complexes. As shown in Figure 4.14a the computed magnetic anisotropy D goes down for increasing magnetic moments, i.e. upon changing the transition metal center of the complexes from copper via nickel to manganese. Furthermore, we observe a nearly linear dependency of D and $\frac{1}{S^2}$ (regression yields $y = 0.18426 - 5.1796x, R^2 = 0.99$). In other words we can increase S^2 by a factor of 25 (by replacing the copper centers with manganese centers) and we get a decrease of the magnetic anisotropy of a factor of approximately five. For comparison the results obtained from NRLMOL calculations without the correction proposed by Van Wüllen[219] are plotted (red line) in Figure 4.14a as well. Here we also observe a linear dependency (regression yields $y = -0.021934 - 2.46x, R^2 = 0.98$), however the pre-factors have changed. Furthermore we see that the correction of Van Wüllen[219] got the strongest effect for the copper system with a small total spin S. This is to be expected as the correction acts strongest on systems with small spin as explained in more detail in section 2.5.3. In this section we can also find the explanation for the nearly linear behavior of D vs. $\frac{1}{S^2}$. As stated there and shown in equation 2.106 and 4.1 the barrier of

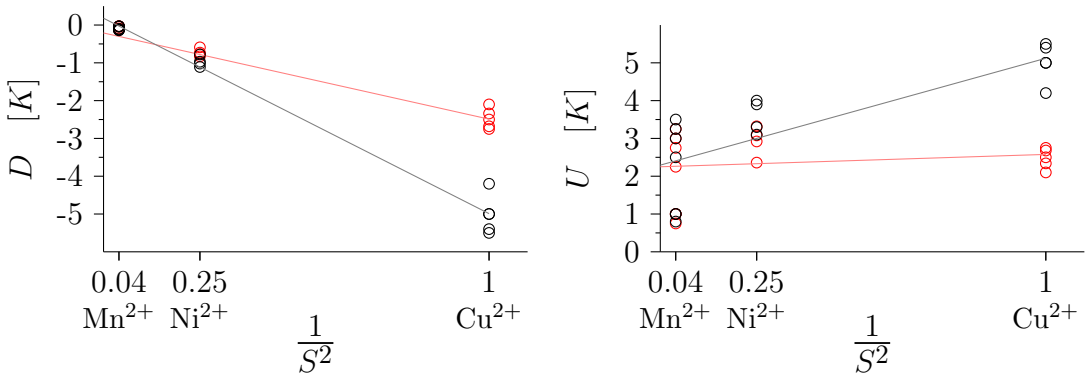

(a) D vs. $\frac{1}{S^2}$ (b) U vs. $\frac{1}{S^2}$

Figure 4.14: Figure 4.14a: Magnetic anisotropy D depending on $\frac{1}{S^2}$;
red: magnetic anisotropy D as calculated in NRLMOL;
red line: regression $y = -0.02 - 2.46x, R^2 = 0.98$;
black: corrected magnetic anisotropy (according to Van Wüllen[219]);
black line: regression $y = 0.18 - 5.186x, R^2 = 0.99$
Figure 4.14b: barrier of magnetization U depending on $\frac{1}{S^2}$
red: barrier of magnetization U;
red line: regression $y = 2.2496 + 0.32735x, R^2 = 0.17$;
black: corrected barrier (according to Van Wüllen[219]);
black line: regression $y = 2.2935 + 2.8271x, R^2 = 0.80$

magnetization does ultimately depend on the calculated axial magnetic anisotropy energy MAE and the total spin of the given system:

$$U = \frac{S \cdot \text{MAE}}{S - 0.5}.$$

Here we observe by no means a quadratic dependency on the total spin ground state S as indicated by $U = S^2|D|$ - the common formula used for the calculation of the barrier of magnetization. Rather we have a $\frac{S}{S-0.5}$ dependency which converges to one for large S

$$\lim_{S \to \infty} \frac{S}{S - 0.5} = 1. \tag{4.4}$$

Thus, the barrier does ultimately depend only on the axial magnetic anisotropy energy as calculated within NRLMOL for our test cases. (On a side note - equation 4.1

would read $U = \text{MAE}$ without the correction of Van Wüllen[219] to the computation of the magnetic anisotropy energy.) As already mentioned the MAE is proportional to the free ion single electron spin-orbit coupling parameter ζ, which does increase with increasing nuclear charge (see Figure 4.15). Hence, we got a pre-factor in equa-

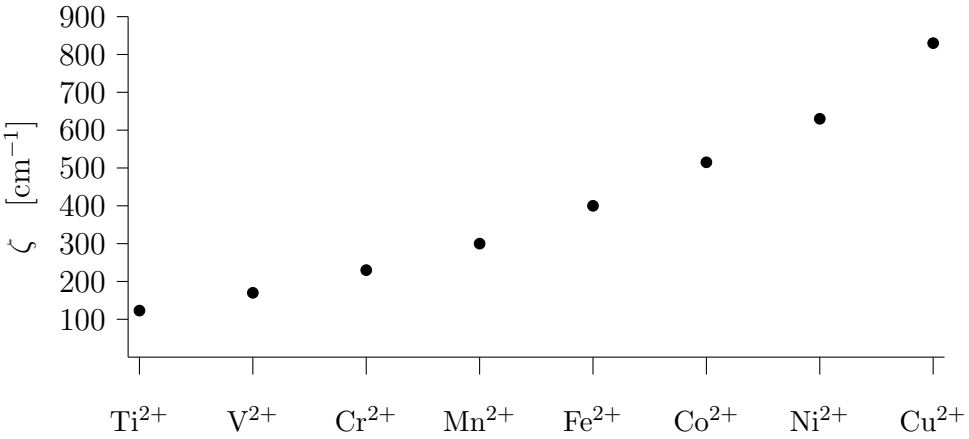

Figure 4.15: The free ion single electron spin-orbit coupling parameter ζ of various first row transition metal ions[127]. For configurations with more than one unpaired electron it is also common to use λ which is given by $\lambda = \pm\frac{\zeta}{2S}$ where S is the total spin. By definition $\lambda < 0$ applies for less than half filled shells ($d^1 - d^4$) whereas $\lambda > 0$ applies elsewhere. Note that the same trend is observed for higher (+3, +4, ...) and lower (+1, 0) charged ions. The only difference is that larger charges increase the free ion single electron spin-orbit coupling parameter systematically whereas the opposite trend is observed for smaller charged ions.

tion 4.1 that goes to one for large S and a MAE that can be estimated by the free ion single electron spin-orbit coupling parameter ζ which increases from manganese via nickel to copper. Accordingly it is not surprising that we do indeed observe the largest barrier of magnetization for the copper complexes ($S = 1$) and not for the nickel ($S = 2$) or manganese ($S = 5$) complexes which is summarized in Figure 4.14b. The advantage of a large spin ground state S is destroyed by the decrease of the free ion single electron spin-orbit coupling parameter. The pre-factor $\frac{S}{S-0.5}$ even enhances the barrier of complexes with a small spin ground state (i.e. copper) in addition to the already larger ζ.

Summarizing this section we can state that

- all considered complexes exhibit a barrier $U = 1 - 5K$.
- the barrier decreases from copper via nickel to manganese complexes.
- due to a "hidden" dependency on S in the calculation of the magnetic anisotropy D the barrier of magnetization should be calculated according to $U = \frac{S \cdot \mathrm{MAE}}{S-0.5}$ instead of $U = S^2|D|$.
- the magnetic anisotropy energy (MAE) scales roughly with the free ion single electron spin-orbit coupling parameter ζ as long as one stays within one group of the periodic table (i.e. first row TMs or second row TMs) and within the same oxidation form (i.e. TM^{2+} or TM^{3+} or TM^{1+}).
- the free ion single electron spin-orbit coupling parameter ζ increases with increasing nuclear charge.
- the advantage of a large spin ground state S is destroyed by the decrease of the free ion single electron spin-orbit coupling parameter ζ.
- a high spin ground state does not necessarily result in a larger barrier (due to the above mentioned points).

4.3 The family of hexametallic $[Mn_6^{III}O_2(R\text{-sao})_6]^{2+}$

There exist further experimental evidence that a given magnetic system minimizes its energy either by magnetic coupling or magnetic anisotropy. The family of polynuclear Mn_6 complexes of the general formula $[Mn_6^{III}O_2(R\text{-sao})_6(O_2CR')_2(sol)_{4-6}]$ (where sao^{2-} is the dianion of salicylaldoxime or 2-hydroxybenzaldeyhyde oxime; R=H, Me, Et; R'=H, Me, Ph, etc; sol=EtOH, MeOH and/or H_2O), synthesized by Brechin and coworkers[138–142], shows appealing magnetic properties. Yet all of them show basically the same magnetic core configuration. Two Mn_3 triangles are linked together via oxygen bridges as shown in Figure 4.16. Note that there are two structure motifs.

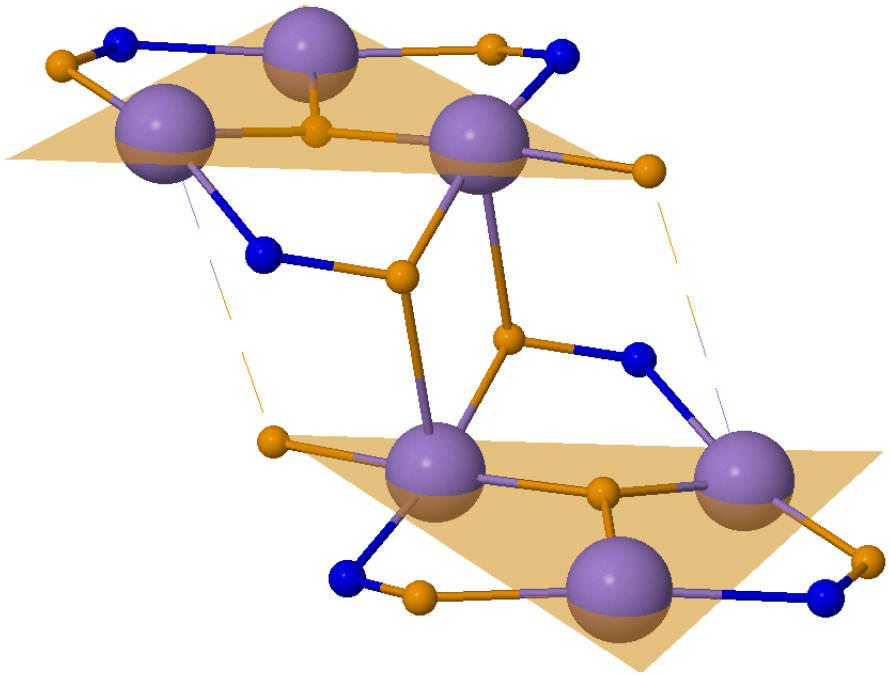

Figure 4.16: Core configuration of the Mn_6 clusters - two Mn_3 triangles linked together via oxygen bridges. The dotted bonds are not always present and depend on the size of R and R'; purple:Mn, blue:N, yellow:O

Depending on the size of R and R' the dotted bridge may or may not be developed. For of small ligands the bridge is formed resulting in an octahedral environment of all Mn ions. More bulky ligands distort the structure and the two Mn-O-Mn bridges are destroyed. In this case four of the manganese ions are in an octahedral

environment and the remaining two are in a square pyramidal environment. Table 4.7 shows a selection of some members of the family giving an impression about the wide range of possible ground states depending on the ligands R and R'. There

Table 4.7: Magnetic properties of the family of Mn_6 complexes (references: **A-H**[138], **I-L**[100]) and the energy barrier U_{eff}

No.		S	D_{exp} [cm^{-1}]	$U_{\text{eff}}^{\text{exp}}$ [K]
A	$[Mn_6O_2(H-sao)_6(O_2CH)_2(MeOH)_4]$	4	-1.39	28.0
B	$[Mn_6O_2(Me-sao)_6(O_2CCPh_3)_2(EtOH)_4]$	4	n.a.	31.7
C	$[Mn_6O_2(Et-sao)_6(O_2CCMe_3)_2(EtOH)_5]$	6	-0.75	30.0
D	$[Mn_6O_2(Et-sao)_6(O_2CPh^4OPh)_2(EtOH)_4(H_2O)_2]$	9	-0.37	56.9
E	$[Mn_6O_2(Me-sao)_6(O_2CPhBr)_2(EtOH)_6]$	11	-0.50	50.2
F	$[Mn_6O_2(Et-sao)_6(O_2CPh)_2(EtOH)_4(H_2O)_2]$	12	-0.43	53.1
G	$[Mn_6O_2(Et-sao)_6(O_2CPh(Me)_2)_2(EtOH)_6]$	12	-0.43	86.4
H	$[Mn_6O_2(Et-sao)_6(O_2CPhMe)_2(EtOH)_4(H_2O)_2]$	12	-0.44	69.9
I	$[Mn_6O_2(Et-sao)_6(O_2C_{12}H_{17})_2(EtOH)_4(H_2O)_2]$	5±1	n.a.	31.2
K	$[Mn_6O_2(Et-sao)_6(O_2CNapth)_2(EtOH)_4(H_2O)_2]$	12	-0.34	60.1
L	$[Mn_6O_2(Et-sao)_6(O_2CAnth)_2(EtOH)_4(H_2O)_2]$	12	-0.44	60.1

are many more complexes available whose magnetic properties are discussed elsewhere[97, 100, 132, 133, 138, 217]. Within the selection nearly all magnetic ground states ranging from $S = 4$ to $S = 12$ are present. A detailed discussion of the magnetic coupling J within this family of Mn_6 complexes can be found in literature[55, 97, 100, 138] and will be discussed here only briefly. The coupling seems to depend strongly on the Mn-N-O-Mn torsion angle. Above a torsion angle of approximately 31° the coupling is ferromagnetic while smaller torsion angles lead to an antiferromagnetic coupling between Mn_2 pairs[55, 132]. The coupling in between the Mn_3 triangles on the other hand is always ferromagnetic[138]. Hence it is possible to tune the ground state depending on the ligands R and R'. A $S = 4$ ground state for example can be described by a spin-flip of two Mn^{III} cations[200]. As the molecules are relatively sta-

ble it is possible to deposit them for example on Au(111) surfaces[145] which might be an interesting application for spintronics. As shown by Cremades and co-workers[56] in a purely theoretical work the Mn_6 complexes are well suited for applications for spintronics. It is also possible to influence the ground state by pressure. Increasing the pressure results in a reduction of the total S[182]. Furthermore, there are several examples in literature[97, 117, 213] that report mixed valence species showing interesting properties.

Table 4.8: Barrier of magnetization U [K] for different possible ground states, namely $S = 4, 8, 12$ calculated using NRLMOL. Furthermore, it is shown in a schematic way how the respective ground states can be explained by spin inversion of certain Mn^{3+} atoms (red).

No.	S=4	S=8	S=12
A	62	57	54
B	62	56	53
C	55	57	53
D	65	59	56
E	62	56	53
F	65	59	55
G	65	58	54
H	65	59	56
I	64	58	54
K	52	46	42
L	45	43	39

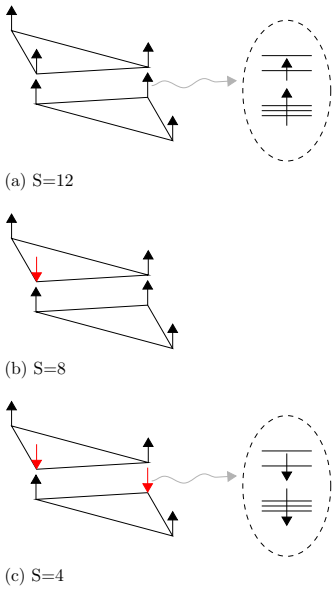

(a) S=12

(b) S=8

(c) S=4

Undoubtedly there is a broad range of experimentally available magnetic ground states within this family of Mn_6 complexes, however the magnetic barrier U is within a factor of two for all of them. For example the magnetic barrier U for the $S = 12$ ground state is only twice as large as the barrier for the $S = 4$ ground state. This would not to be expected considering the rather simple formula $U = S^2 |D|$, which

indicates that a large magnetic groundstate S leads to a large barrier U. However, as evident from the experimental data, this is clearly not the case. This can of course be understood in terms of the discussion introduced in section 4.2. Assuming that the MAE does not change (due to the same magnetic core of all structures) we would indeed expect the experimentally observed behavior. Moreover, we would expect to see the largest barriers U for the smaller spin ground states. This behavior is observed in the calculations as shown in Table 4.8. First of all it is remarkable that all considered complexes show nearly identical barriers of magnetization in the calculation. This is in some contradiction to the experimental results shown in Table 4.7. An explanation for the difference could be that the experimental D values are averaged over the low-lying states[200] which is not the case for the calculated ones. Only complex **L** and **M** show a significantly smaller barrier U which will be discussed later. The highest barrier U is always observed for the $S = 4$ ground state as already predicted based on our simple estimation. If we now consider the ratio Δ of the different ground states (remember, we are still under the assumption that the MAE does not change), we get:

	$\Delta_5 = \frac{U_{S=4}}{U_{S=12}}$	and	$\Delta_6 = \frac{U_{S=8}}{U_{S=12}}$	and	$\Delta_7 = \frac{U_{S=4}}{U_{S=8}}$
estimated:	$\Delta_5 = 1.10$		$\Delta_6 = 1.02$		$\Delta_7 = 1.07$
calculated:	$\Delta_5 \sim 1.16$		$\Delta_6 \sim 1.07$		$\Delta_7 \sim 1.08$

Here we already observe a good agreement between our estimated Δ and the ones obtained from the actual calculations. However, a slight misfit remains. In order to understand this Table 4.9 shows the computed magnetic anisotropies D as well as the spin channel contributions (see section 2.5.3) of selected Mn_6 complexes. An overview over all considered complexes is given in Table 6.2 in Appendix D. What we observe is a magnetic anisotropy for the lowest spin states ($S = 4$) that is one order of magnitude smaller than in the highest spin state ($S = 12$). This is consistent with the findings of Ruiz et al.[200] who investigated some other members of the same class of molecules as well as Mn_{12}[123] and Martinez-Lillo et al[133] who reported a similar behavior for a closely related class of molecules.

The electronic structure of each Mn^{3+} ion is not altered by the spin flip since the most important contributions to the magnetic anisotropy come from M_{ij} terms in-

Table 4.9: magnetic anisotropy D [K] of the Mn_6 complexes **A**,**G** and **L** indicating the spin channel contributions (see also equation 2.99. Shown are results for S =4,8 and 12. All D values are corrected according to Van Wüllen[219]. MAE=magnetic anisotropy energy, α= spin up electrons, β= spin down electrons

complex	S	D_{calc}	MAE	$\alpha-\alpha$	$\alpha-\beta$	$\beta-\alpha$	$\beta-\beta$	$\lvert D\rvert \cdot S^2$
A	4	-3.855	-53.9	-0.793	-1.879	-0.818	-0.430	61.7
	8	-0.884	-53.0	-0.221	-0.521	-0.096	-0.049	56.6
	12	-0.378	-52.1	-0.112	-0.264	0.002	0.002	54.3
G	4	-4.125	-57.7	-0.922	-1.744	-0.913	-0.568	66.0
	8	-0.929	-55.7	-0.247	-0.508	-0.099	-0.077	59.4
	12	-0.384	-52.9	-0.121	-0.262	0.009	-0.010	55.3
L	4	-3.304	-46.2	-0.277	-1.281	-1.260	-0.534	52.8
	8	-0.731	-43.8	-0.191	-0.463	-0.045	-0.030	46.7
	12	-0.292	-40.2	-0.049	-0.205	0.060	-0.009	42.0

volving excitations within d orbitals of the same metal[200] (see equation (2.99)). The only effect of a spin flip is the replacement of $\alpha-\alpha$ and $\alpha-\beta$ by $\beta-\alpha$ and $\beta-\beta$ contributions at the respective Mn^{3+} ions that are involved in the spin flip. Note that $\alpha-\alpha$ refers here to a transition of an α spin occupied to an α spin unoccupied orbital. These concepts are reflected in Table 4.9. For the low spin state $S=4$ we see significant contributions from all spin channels. The weights of the $\alpha-\alpha$ and $\alpha-\beta$ terms are approximately twice as large as the $\beta-\beta$ and $\beta-\alpha$ which is consistent with the number of Mn^{3+} with spin up (α) and spin down (β) electrons. This can also be seen nicely in Figure 4.8. For the high spin state $S=12$ we observe only contributions from the $\alpha-\alpha$ and $\alpha-\beta$ channel which is also consistent with this picture since there are no β electrons in the metal d manifold. The small $\beta-\beta$ and $\beta-\alpha$ contributions that appear in Table 4.9 are mainly due to low lying β electrons localized at the ligands. However, these contributions are fairly small due to a large denominator in equation 2.99 in section 2.5.3. For the intermediate case of $S=8$ we observe contributions from all spin channels, however the $\alpha-\alpha$ and

$\alpha - \beta$ contribution are approximately five times larger than the $\beta - \beta$ and $\beta - \alpha$ contributions. This is again consistent with the number of Mn^{3+} with spin up (α) and spin down (β) electrons (see also Figure 4.8).
All this suggests that the magnetic anisotropy D and the ground state of a given system are closely related. Another conclusion that can be made is that the magnetic anisotropy does not depend crucially on the structural details. Although all complexes are very similar there are small differences in the actual environment of every Mn^{3+} ion. For example, there are different ligands surrounding the Mn^{3+} ions resulting in slightly shorter or longer bond length. Furthermore, the coordination number of selected Mn^{3+} ions can change depending on the ligand. However, the calculations reveal that there is only a small impact of these changes in the computed magnetic anisotropy. The ground state of the molecule varies the value of the magnetic anisotropy in a far greater range compared to the effect of the small changes of structural details. This leads ultimately to the conclusion that a high spin ground state and a large magnetic anisotropy seem to be incompatible. The common approach to raise the barrier U simply by maximizing the ground state S of a given system is also not very promising as we observe similar energy barriers for different spin states of a given system. Due to the previously mentioned fact that the barrier should actually be calculated as

$$U = \frac{S \cdot \mathrm{MAE}}{S - 0.5} \qquad \text{and} \qquad \lim_{S \to \infty} \frac{S}{S - 0.5} = 1. \tag{4.5}$$

It is even to be expected that lower ground states yield a higher barrier U. This is exactly the behavior we observe in Table 4.9. As shown there the MAE does not stay constant upon a change of the ground state. In fact, it decreases linearly with increasing S as shown in Figure 4.17.

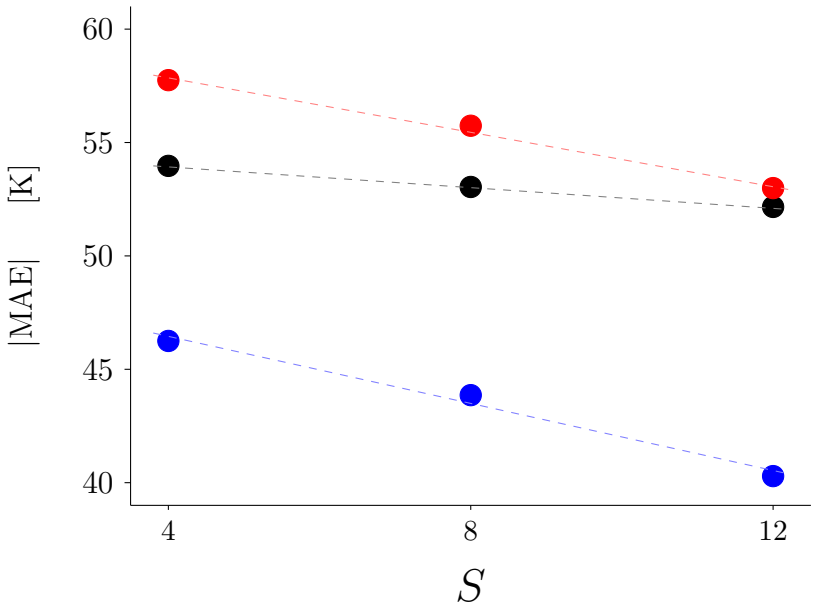

Figure 4.17: black: complex **A**; regression: $y = 54.86 - 0.23x, R^2 = -0.999$
blue: complex **G**; regression: $y = 60.25 - 0.60x, R^2 = -0.995$
red: complex **L**; regression: $y = 49.42 - 0.74x, R^2 = -0.993$

Hence, we get two effects. We expect

- a (slightly) higher barrier U for small ground states S due to equation 4.5
- a higher barrier U for small ground states S due to a decrease of the MAE for higher ground states S as shown in Figure 4.17

Both effects favor a decrease of the barrier with increasing S which is indeed observed in the calculations.
One might argue that this effect is not observed for the experimental data. As shown in Table 4.7 the barrier for a low ground state ($S = 4$) complex is approximately three times smaller compared to the barrier of a large ground state ($S = 12$) complex. However, here you have to keep in mind that all the experimental structures differ slightly in the composition. Hence we expect slightly different bond length, bond angles and so on for each complex. This small differences may of course have a large effect on the actual barrier observed for each of the complexes as especially the magnetic anisotropy depends crucially on such structural parameters[19, 191]. In the

theoretical considerations done in the present work we assumed different possible ground states for each complex and calculated the respective magnetic anisotropy. This is not direct comparable to the experimental results as there only the "real" ground state of the complex is accessible. Yet, the experimental data agree with the theoretical observation that the barrier U is by no means quadratically dependent on the ground state S as indicated by $U = S^2|D|$.

5 Conclusion

As already explained single molecule magnets (SMMs) are very interesting candidates for storage devises of the next generation. Unfortunately it is not yet possible to operate them at room temperature which would be favorable in order to build up devises for the everyday use. In order to do that it is necessary to enhance the barrier U for a flip $S \rightarrow -S$. As the barrier is given by $U = S^2|D|$ it is essential to understand and control each of the parameters as well as the interplay of the ground state S and the magnetic anisotropy D. While the well known Goodenough-Kanamori rules[75, 76, 104] yield an accurate description of the magnetic coupling and hence the ground state of a given molecule there are no such easy to understand rules that might explain or predict the magnetic anisotropy.

In order to gain some insight in the underlying mechanisms the present work will deal with the electronic and magnetic properties of various transition metal complexes. Furthermore we will address the issue of a dual optimization of the magnetic anisotropy D and the ground state S in more detail. All results are based on density functional theory[93, 111] within the generalized gradient approximation (GGA) using mainly the PBE[168] functional.

As shown in section 4.1 the magnetic coupling and respectively also the ground state of a given system (here $[M^{II}_2(L^6)(L')]^{n+}$ (L^6=polyamine-dithiophenolate ligand ($C_{38}H_{64}N_6S_2$), L'= variable third bridging ligand) is tuneable by L' and M. Ferromagnetic coupling is only observed in the case of M=Ni^{II}, all other examined third row transition metal ions (manganese, iron, copper) yield antiferromagnetic coupling. As we are only interested in ferromagnetically coupling systems we focused our studies on the nickel complexes. Experimentally there is a wide range of third bridging ligands realized which were studied here in great detail with respect to the electronic structure and the magnetic coupling. The largest predicted ferromagnetic coupling J within this family of the $[Ni^{II}_2(L^6)(L')]^{n+}$ complexes is about 50 cm^{-1}. We have been able to relate the strength (given by the coupling constant J) and the kind (ferromagnetic or antiferromagnetic) of the magnetic coupling in terms of structural as well as electronic effects. The influence of the structure can be explained

in terms of the Goodenough-Kanamori rules, whereas the impact of the electronic structure is described within the Hay-Thibeault-Hoffmann model[90]. Both effects compete with each other and may enhance or cancel out their effects. Furthermore, it was shown that the coupling depends crucially on the the crystal field strength of L'. In order to tune J to higher ferromagnetic couplings only weak co-ligands should be considered. In addition to the already mentioned facts we noted that the third bridging ligand opens a new pathway for a ferromagnetic exchange between the two nickel ions which is most pronounced for L'=BH_4. This has been proved by model calculations without L' where a tremendous reduction of J is observed. Furthermore, for these calculations a large decrease of the HOMO-LUMO gap was observed ($\sim \frac{1}{10}$ of the original value), while the overall level ordering (apart from the states belonging to L') is preserved. In addition to the magnetic coupling we also took a closer look at the magnetic anisotropy and found that the magnetic anisotropy D and the strength of the magnetic coupling are not independent of each other. For this system it is not possible to maximize both quantities. You can either have a strong coupling or a large magnetic anisotropy. Furthermore, we observed that a decreasing HOMO-LUMO gap results in an increase of the magnetic anisotropy in accordance with literature[77]. The magnetic anisotropy could also be related to the environment of the Ni^{2+} ions. An nearly octahedral environment favors easy plane systems but not all "undistorted" structures yield SMM behavior.

In section 4.2 we focused on the question whether or not it is possible to combine a large spin ground state S and a high magnetic anisotropy D in order to achieve a large barrier of magnetization $U = S^2|D|$. In order to get comparable results we restricted ourselves to octahedral coordinated, azido-bridged copper, nickel and manganese dimers. As shown by the calculations all of them exhibit a barrier $U = 1 - 5K$ and the barrier decreases from copper via nickel to manganese complexes. Furthermore we explained in detail that due to a "hidden" dependency on S in the calculation of the magnetic anisotropy D the barrier of magnetization should be calculated with respect to the magnetic anisotropy energy (MAE) as

$$U = \frac{S}{S - 0.5}\mathrm{MAE}$$

with

$$\lim_{S\to\infty} \frac{S}{S-0.5} = 1.$$

The MAE on the other hand scales roughly with the free ion single electron spin-orbit coupling parameter ζ as long as one stays within one group of the periodic table (i.e. first row transition metals (TMs) or second row transition metals) and within the same oxidation form (i.e. TM^{2+} or TM^{3+} or TM^{1+}). An other interesting fact is that the free ion single electron spin-orbit coupling parameter ζ increases with increasing nuclear charge. Therefore the advantage of a large spin ground state S is destroyed by the simultaneous decrease of the free ion single electron spin-orbit coupling parameter ζ. Hence a high spin ground state does not necessarily result in a larger barrier (due to the above mentioned points). It is rather the other way around. The advantage of having a higher spin ground state S ($S_{Cu} < S_{Ni} < S_{Mn}$) is completely destroyed by the reduction of the MAE ($MAE_{Cu} > MAE_{Ni} > MAE_{Mn}$) resulting in an overall reduced barrier U for the complex with the largest spin ground state ($U_{Cu} > U_{Ni} > U_{Mn}$). It is also notable that all calculated barriers are within an order of magnitude $U = 1-5$ K which seems to be the maximum barrier obtainable within this system.

Finally the present work focused on a family of hexametallic $[Mn_6^{III}O_2(R-sao)_6]^{2+}$ complexes in section 4.3. As shown experimentally there is a wide range of possible ground states obtainable within this family. Therefore, it is a good test system to study the influence of the ground state S on the magnetic anisotropy D. Similarly to the octahedral coordinated, azido-bridged copper, nickel and manganese dimers we have been able to show that there is an overall reduction of the barrier U with increasing ground state S. However, here the effect is not due to different transition metal centers but purely on account of different ground states. This can be understood by the overlap of two effects. On the one hand we expect a (slightly) higher barrier U for small ground states S and on the other hand there is a decrease of the MAE for higher ground states S as shown in Figure 4.17. Both effects favor a decrease of the barrier with increasing S which is indeed observed in the calculations.

Summarizing all these facts we conclude that there is a dependency of S within

the magnetic anisotropy which (over)compensates the seemingly quadratic dependency on the ground state in the calculation of the barrier $U = S^2|D|$. There are several examples within the available literature[150, 200] where a similar conclusion is reached. It does not seem possible to consider the magnetic anisotropy D and the spin state S as two distinct features of a given system. From the experimental as well as computational point of view it appears that they are closely related in an inverse relation. Hence, a dual optimization of both parameters is not possible. In general a high spin ground state S is accompanied by a small magnetic anisotropy D and vice versa.

List of Tables

List of Figures

6 Appendix

6.1 Appendix A

Calculation of the spin Hamiltonian for the Ising model:

$\vec{S} = (0, 0, S_z)$

$S_z|\uparrow> = \frac{1}{2}|\uparrow>$ $\qquad$ $<\uparrow|\uparrow> = 1$

$S_z|\downarrow> = -\frac{1}{2}|\downarrow>$ $\qquad$ $<\uparrow|\downarrow> = 0$

Given two interacting spins $\vec{S}_1 = \vec{S}_2 = \frac{1}{2}$ and the hamiltonian $H = -2JS_{1z}S_{2z}$ the following spin Hamiltonian is obtained:

	$\uparrow\uparrow$	$\uparrow\downarrow$	$\downarrow\uparrow$	$\downarrow\downarrow$
$\uparrow\uparrow$	1			
$\uparrow\downarrow$	2			
$\downarrow\uparrow$				
$\downarrow\downarrow$				

(6.1)

The entry in position number **1** is given by:

$$\begin{aligned} <\uparrow\uparrow|H|\uparrow\uparrow> &= <\uparrow\uparrow|-2JS_{1z}S_{2z}|\uparrow\uparrow> \\ &= -2J <\uparrow\uparrow|S_{1z}S_{2z}|\uparrow\uparrow> \\ &= -2J <\uparrow\uparrow|\frac{1}{2}\frac{1}{2}|\uparrow\uparrow> \\ &= -\frac{J}{2} <\uparrow\uparrow|\uparrow\uparrow> \\ &= -\frac{J}{2} \end{aligned}$$

The entry in position number **2** is given by:

$$\begin{aligned} <\uparrow\uparrow|H|\uparrow\downarrow> &= <\uparrow\uparrow|-2JS_{1z}S_{2z}|\uparrow\downarrow> \\ &= -2J <\uparrow\uparrow|S_{1z}S_{2z}|\uparrow\downarrow> \\ &= -2J <\uparrow\uparrow|\frac{1}{2}\left(-\frac{1}{2}\right)|\uparrow\downarrow> \\ &= \frac{J}{2} <\uparrow\uparrow|\uparrow\downarrow> \\ &= 0 \end{aligned}$$

accordingly all the other position are evaluated resulting in the spin Hamiltonian shown in 2.57

Calculation of the spin Hamiltonian for the Heisenberg model:

$\vec{S} = (S_x, S_y, S_z)$
$H = -2J\vec{S}_1\vec{S}_2 = -2J(S_{1x}S_{2x} + S_{1y}S_{2y} + S_{1z}S_{2z})$

The discussion will again be for two interacting spins $\vec{S}_1 = \vec{S}_2 = \frac{1}{2}$ and $\vec{S}_{1z} = \vec{S}_{2z} = \frac{1}{2}$ For reasons already discussed in section 2.4.1 the generation and annihilation operator S_+ and S_- are defined.

$$\begin{aligned} S_+ &= S_x + iS_y \\ S_- &= S_x - iS_y. \end{aligned}$$

The products $S_+ \cdot S_-$ and $S_- \cdot S_+$ are given by:

$$\begin{aligned} S_+ \cdot S_- &= S_x^2 + iS_yS_x - S_xiS_y + S_y^2 \\ S_- \cdot S_+ &= S_x^2 + S_xiS_y - iS_yS_x + S_y^2. \end{aligned}$$

The sum of these products yields

$$\begin{aligned} (S_+ \cdot S_-) + (S_- \cdot S_+) &= 2S_x^2 + 2S_y^2 \\ (S_{1+} \cdot S_{2-}) + (S_{1-} \cdot S_{2+}) &= 2S_{1x}S_{2x} + 2S_{1y}S_{2y}. \end{aligned}$$

Hence the hamiltonian can be rewritten:

$$H = -2J\left(\frac{(S_{1+} \cdot S_{2-}) + (S_{1-} \cdot S_{2+})}{2} + S_{1z}S_{2z}\right).$$

Furthermore it is known that:

$S_\pm|S, S_z> = \sqrt{S(S+1) - S_z(S_z \pm 1)}|S, S_z \pm 1>$

Taking all these considerations into account we get for $S = \frac{1}{2}$ and $S_z = \frac{1}{2}$:

$S_z|\uparrow> = \frac{1}{2}|\uparrow>$ $\qquad$ $<\uparrow|\uparrow> = 1$
$S_z|\downarrow> = -\frac{1}{2}|\downarrow>$ $\qquad$ $<\uparrow|\downarrow> = 0$

$$
\begin{aligned}
S_+|\uparrow> &= \sqrt{\frac{1}{2}\left(\frac{3}{2}\right) - \frac{1}{2}\left(\frac{3}{2}\right)}\left|\frac{1}{2},\frac{3}{2}\right.>= 0 \\
S_+|\downarrow> &= \sqrt{\frac{1}{2}\left(\frac{3}{2}\right) - \left(-\frac{1}{2}\right)\left(\frac{1}{2}\right)}\left|\frac{1}{2},\frac{1}{2}\right.>= 1|\uparrow> \\
S_-|\uparrow> &= \sqrt{\frac{1}{2}\left(\frac{3}{2}\right) - \frac{1}{2}\left(-\frac{1}{2}\right)}\left|\frac{1}{2},-\frac{1}{2}\right.>= 1|\downarrow> \\
S_-|\downarrow> &= \sqrt{\frac{1}{2}\left(\frac{3}{2}\right) - \left(-\frac{1}{2}\right)\left(-\frac{3}{2}\right)}\left|\frac{1}{2},-\frac{3}{2}\right.>= 0.
\end{aligned}
$$

Note that $S_z = \frac{3}{2}$ is forbidden. Only $S_z \pm \frac{1}{2}$ is allowed for $S = \frac{1}{2}$ spins.
The basis of the spin Hamiltonian is similar to the Ising model:

$$
\begin{array}{c|cccc}
 & \uparrow\uparrow & \uparrow\downarrow & \downarrow\uparrow & \downarrow\downarrow \\
\uparrow\uparrow & 1 & & & \\
\uparrow\downarrow & & & & \\
\downarrow\uparrow & & & & \\
\downarrow\downarrow & & & &
\end{array}
\tag{6.2}
$$

The entry in position number **1** is given by:

$$
\begin{aligned}
& <\uparrow\uparrow|H|\uparrow\uparrow> \\
= \; & <\uparrow\uparrow| - 2J\left(\frac{(S_{1+}\cdot S_{2-}) + (S_{1-}\cdot S_{2+})}{2} + S_{1z}S_{2z}\right)|\uparrow\uparrow> \\
= \; & <\uparrow\uparrow| - JS_{1+}S_{2-} - JS_{1-}S_{2+} - 2JS_{1z}S_{2z}|\uparrow\uparrow> \\
= \; & -J<\uparrow\uparrow|S_{1+}S_{2-}|\uparrow\uparrow> - J<\uparrow\uparrow|S_{1-}S_{2+}|\uparrow\uparrow> - 2J<\uparrow\uparrow|S_{1z}S_{2z}|\uparrow\uparrow>
\end{aligned}
$$

Each of the three terms will now be treated separately:

$$
\begin{aligned}
-J<\uparrow\uparrow|S_{1+}S_{2-}|\uparrow\uparrow> &= -J<\uparrow\uparrow|0\cdot 1|\uparrow\downarrow> \\
&= 0
\end{aligned}
$$

$$
\begin{aligned}
-J<\uparrow\uparrow|S_{1-}S_{2+}|\uparrow\uparrow> &= -J<\uparrow\uparrow|1\cdot 0|\downarrow\uparrow> \\
&= 0
\end{aligned}
$$

$$-2J <\uparrow\uparrow |S_{1z}S_{2z}| \uparrow\uparrow> = -2J <\uparrow\uparrow |\frac{1}{2}\cdot\frac{1}{2}| \uparrow\uparrow> = -\frac{J}{2}$$

Hence

$$<\uparrow\uparrow |H| \uparrow\uparrow> = -\frac{J}{2}$$

Accordingly all other all the other position are evaluated resulting in the spin Hamiltonian shown in 2.64

6.2 Appendix B

- Figure 6.1: third bridging ligands L' - overview of the various structures
- Figure 6.2: electronic structure of complex **11** without BH_4^-; focused on energy window -1 eV to -1.5 eV
- Table 6.1: properties of various original/model Ni_2^{II} complexes
- Figures 6.3-6.19: density of states of **1**, **5-10** and **12-21** a) with and b) without the respective third bridging ligand

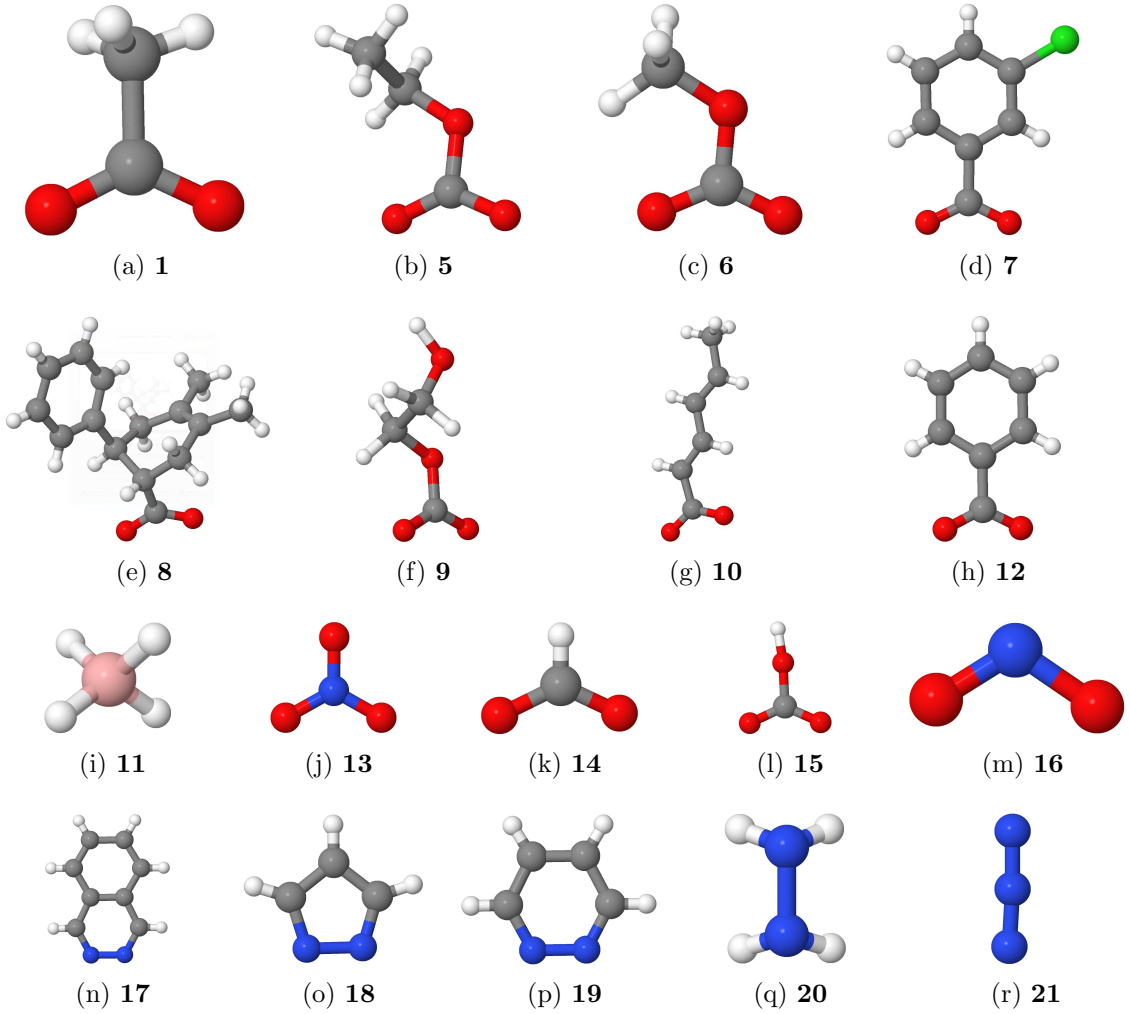

(a) **1** (b) **5** (c) **6** (d) **7**

(e) **8** (f) **9** (g) **10** (h) **12**

(i) **11** (j) **13** (k) **14** (l) **15** (m) **16**

(n) **17** (o) **18** (p) **19** (q) **20** (r) **21**

Figure 6.1: Overview of the various third bridging ligands L' of the Robson-type hexamine-dithiophenolate macrocycles: L'=$CH_3CO_2^-$ (**1**), $EtOCO_2^-$ (**5**), $CH_3OCO_2^-$ (**6**), $\mu_{1,3}$-*meta*-Chlorobenzoato$^-$ (**7**), $\mu_{1,3}$-3,4-Dimethyl-6-phenylcyclohex-3-ene-1-carboxylato$^-$ (**8**), $\mu_{1,3}$-2-(Hydroxyethyl)Carbonato$^-$ (**9**), $\mu_{1,3}$-(2*E*4*E*)-Hexa-2,4-dienoate$^-$ (**10**), BH_4^- (**11**), O_2CPh^- (**12**), NO_3^- (**13**), HCO_2^- (**14**), $\mu_{1,3}$-Bicarbonato (**15**), NO_2^- (**16**), $\mu_{1,2}$-Phthalazine (**17**), $\mu_{1,2}$-Pyrazolato (**18**), *pydz* (**19**), N_2H_4 (**20**), N_3^- (**21**); grey: C; blue: N; red: O; green: Cl, pink: B

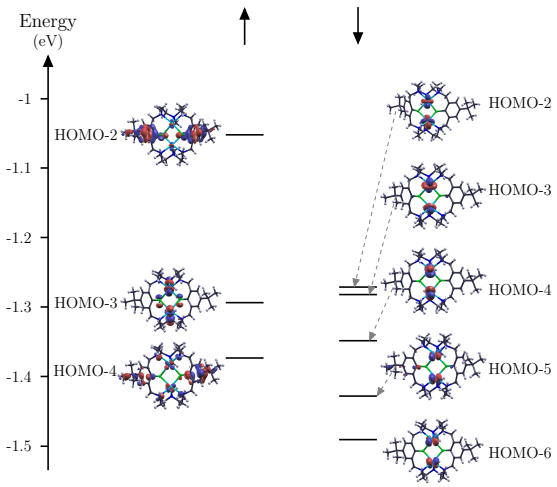

Figure 6.2: electronic structure of complex **11** without BH_4^-; focused on energy window -1 eV to -1.5 eV

Table 6.1: Magnetic coupling $J_{orig/model}$, magnetic anisotropy $D_{orig/model}$, the HOMO-LUMO gap $HLG_{orig/model}$, the mean deviation ΔO from the perfect octahedral environment and the energy differences $\Delta e_{orig/model}$ of the HTH model of various $[Ni_2^{II}(L^6)(L')]^{n+}$ complexes.

complex	J_{orig} [cm^{-1}]	J_{model} [cm^{-1}]	D_{orig} [K]	D_{model} [K]	HLG_{orig} [eV]	HLG_{model} [eV]	ΔO	Δe_{orig} [$mRyd^2$]	Δe_{model} [$mRyd^2$]
5	37	9.7	-0.16	-1.48	1.206	0.186	0.034	0.019	0.128
6	35	9.5	0.18	0.95	1.200	0.090	0.161	0.007	0.122
7	35	4.7	0.19	-1.19	1.264	0.200	0.098	0.076	0.129
8	35	9.7	0.28	1.26	1.280	0.209	0.141	0.015	0.125
9	34	9.5	-0.14	0.95	1.234	0.268	0.125	0.049	0.122
1	33	5.6	0.20	-1.49	1.253	0.151	0.009	0.014	0.138
10	33	6.9	0.18	1.22	1.245	0.237	0.016	0.010	0.128
11	32	6.3	0.51	-1.47	1.065	0.191	0.104	0.024	0.145
12	31	8.5	0.33	1.03	1.231	0.295	0.055	0.009	0.118
13	27	6.0	-0.32	-1.61	1.123	0.188	0.012	0.016	0.139
14	27	8.4	0.17	1.13	1.183	0.261	0.060	0.019	0.124
15	26	5.3	-0.47	-1.20	1.216	0.241	0.012	0.043	0.133
16	25	-3.6	0.47	-	1.185	0.497	0.049	0.047	0.170
17	22	-0.7	-0.44	-	0.989	0.505	0.024	0.030	0.166
18	20	-2.5	-0.34	-	1.160	0.484	0.012	0.050	0.162
19	11	-1.0	0.65	-	0.735	0.533	0.036	0.064	0.162
20	-6	0.7	-	1.23	1.259	0.289	0.063	0.145	0.166
21	-173	20.8	-	-1.74	1.208	0.164	0.038	0.313	0.068

DOS of various $[Ni_2^{II}(L^6)(L')]^{n+}$ (**1, 5-21** except **11**) complexes with and without the respective third bridging ligand L'. For ferromagnetically coupling complexes the spin up and spin down channel for the electrons is presented, whereas such a distinction is not necessary for the antiferromagnetic coupling complexes. Hence only the total density of states is presented. The scaling of the y-axis is the same for all shown DOS. The electronic structure of the ferromagnetically coupling complexes is very similar for each of the complexes and a representative, detailed discussion of the electronic structure of $[\mathrm{Ni}_2^{II}(L^6)(BH_4)]^+$ can be found in section 4.1.3 The DOS of the antiferromagnetically coupling complexes is also very similar for all complexes and is described in more detail for the $\mathrm{Fe^{II}}$OAc and $\mathrm{Mn^{II}}$OAc complex in section 4.1.2.

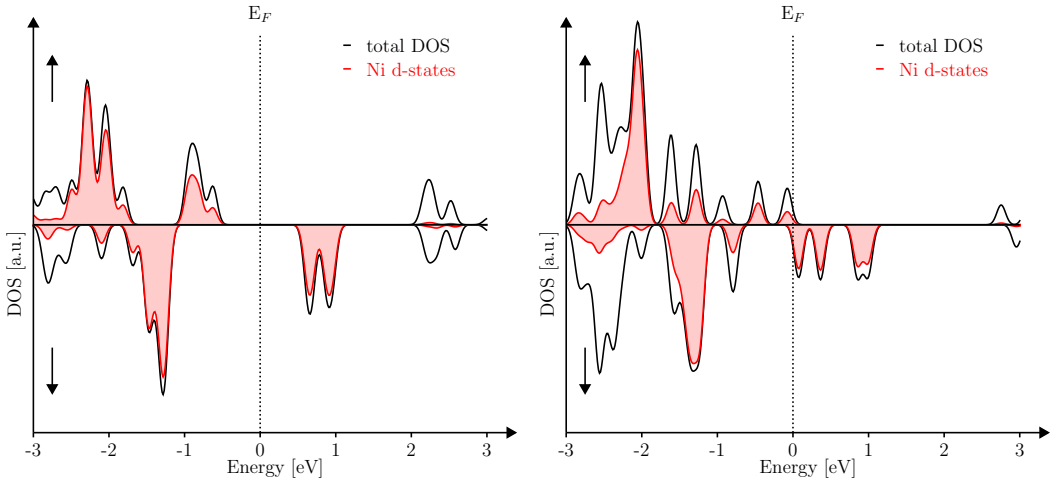

(a) with $CH_3CO_2^-$ (b) without $CH_3CO_2^-$

Figure 6.3: DOS of $[Ni_2^{II}(L^6)(CH_3CO_2)]^+$ (**1**)

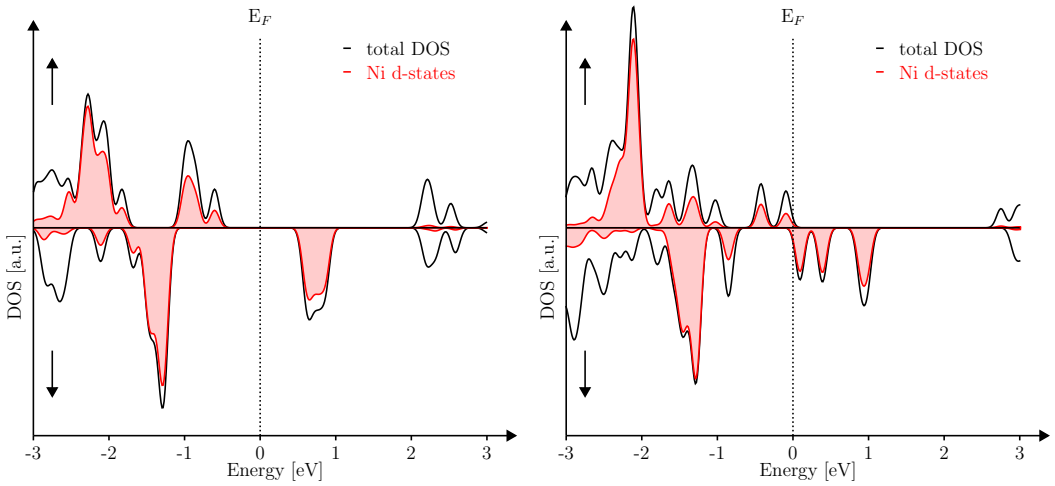

(a) with $EtOCO_2^-$ (b) without $EtOCO_2^-$

Figure 6.4: DOS of $[Ni_2^{II}(L^6)(EtOCO_2)]^+$(**5**)

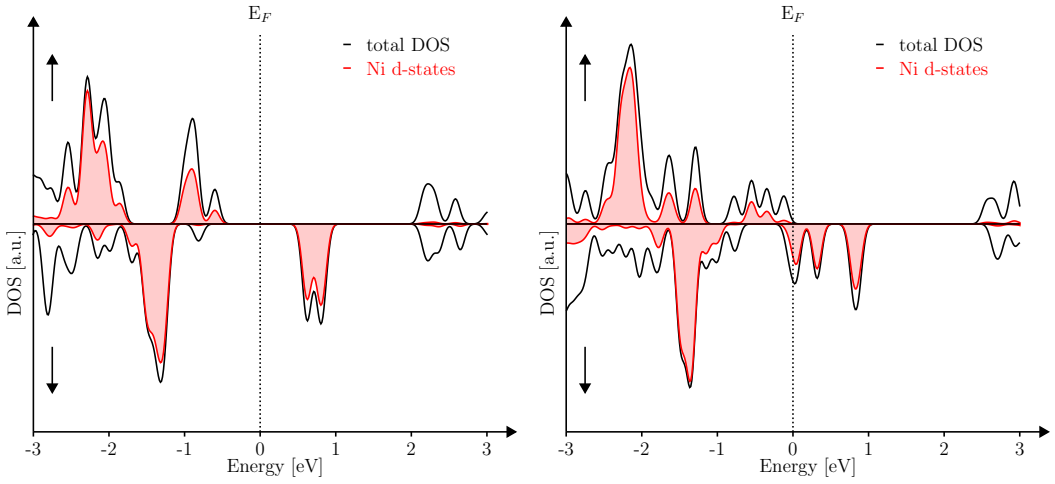

(a) with $CH_3OCO_2^-$ (b) without $CH_3OCO_2^-$

Figure 6.5: DOS of $[Ni_2^{II}(L^6)(CH_3OCO_2)]^+$ (**6**)

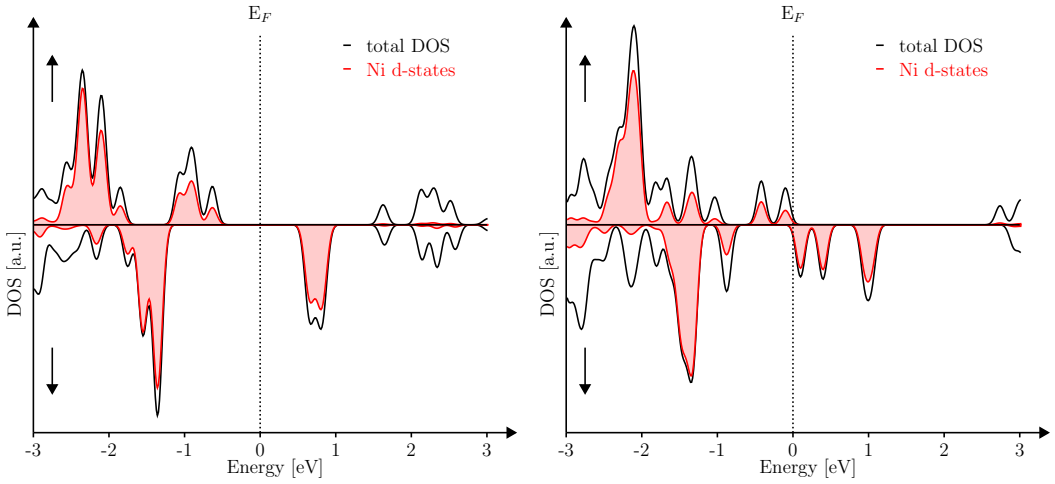

(a) with $m - CL - C_6H_4CO_2^-$ (b) without $m - CL - C_6H_4CO_2^-$

Figure 6.6: DOS of $[Ni_2^{II}(L^6)(m - Cl - C_6H_4CO_2)]^+$ (**7**)

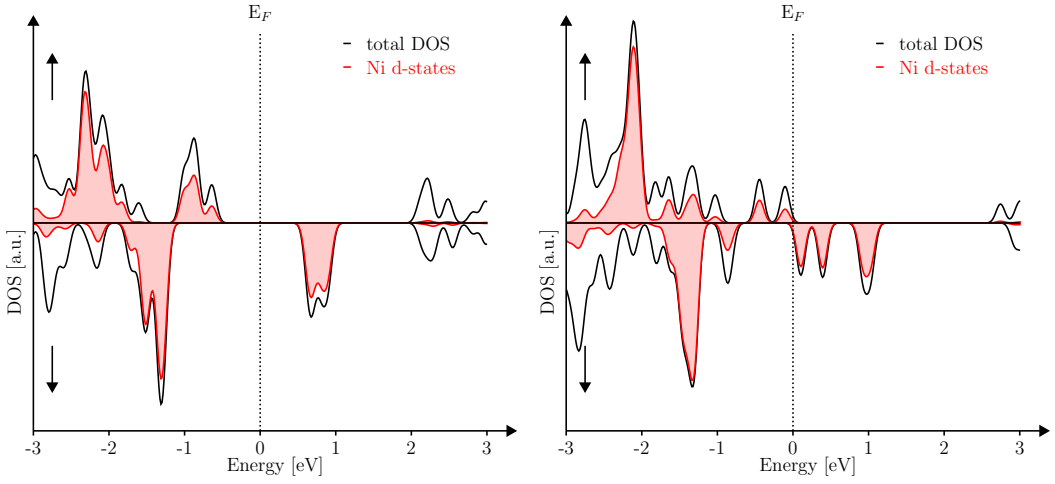

(a) with $C_{15}H_{17}O_2^-$ (b) without $C_{15}H_{17}O_2^-$

Figure 6.7: DOS of $[Ni_2^{II}(L^6)(C_{15}H_{17}O_2)]^+$ (**8**)

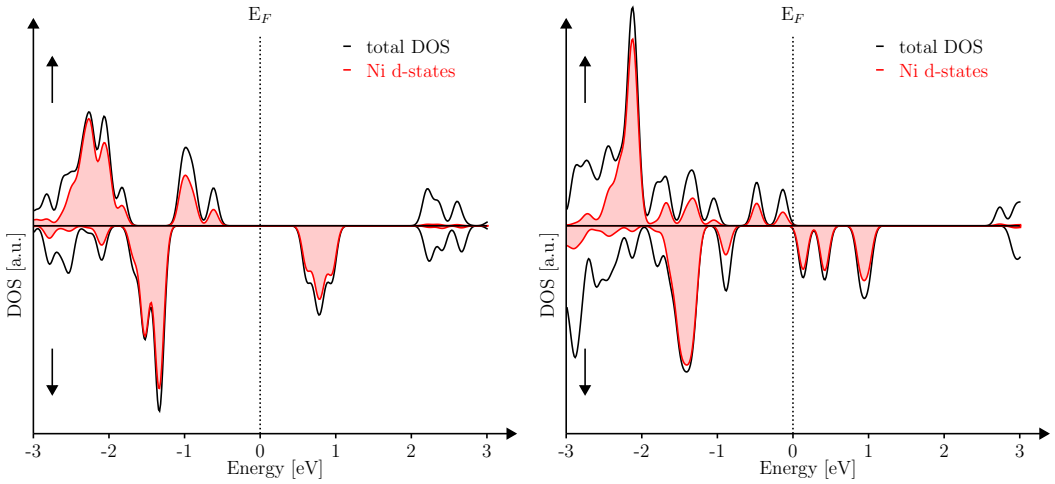

(a) with $HO(CH_2)_2OCO_2^-$ (b) without $HO(CH_2)_2OCO_2^-$

Figure 6.8: DOS of $[Ni_2^{II}(L^6)(HO(CH_2)_2OCO_2)]^+$ (**9**)

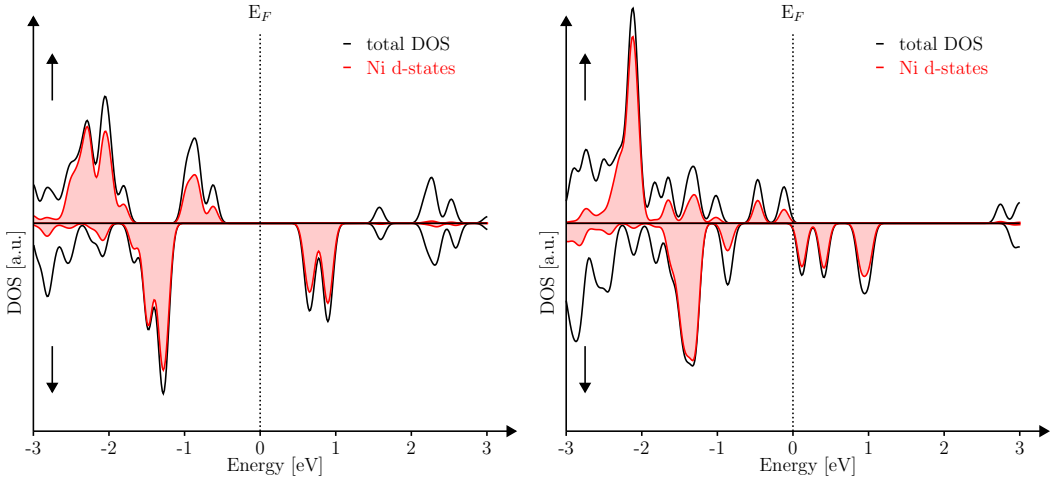

(a) with $C_5H_8CO_2^-$ (b) without $C_5H_8CO_2^-$

Figure 6.9: DOS of $[Ni_2^{II}(L^6)(C_5H_8CO_2)]^+$ (**10**)

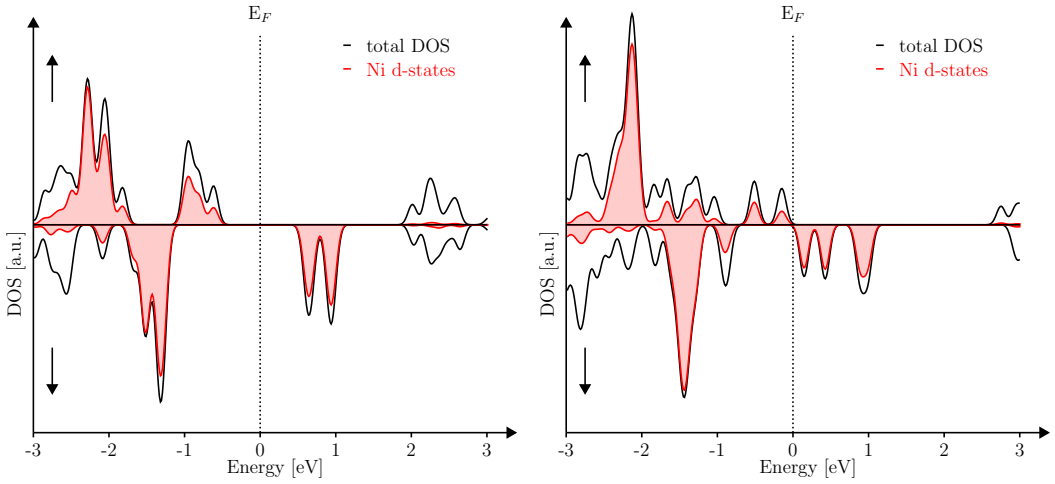

(a) with O_2CPh^- (b) without O_2CPh^-

Figure 6.10: DOS of $[Ni_2^{II}(L^6)(O_2CPh)]^+$ (**12**)

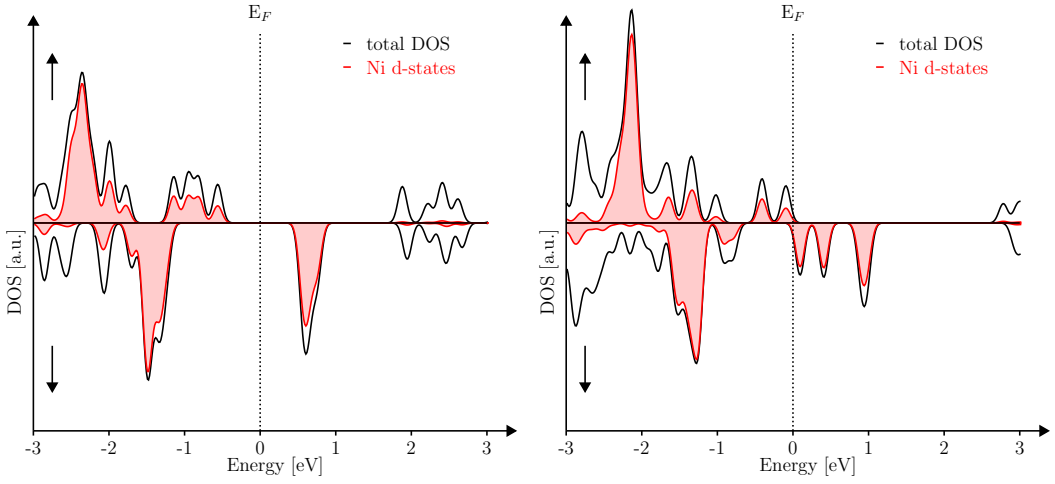

(a) with NO_3^- (b) without NO_3^-

Figure 6.11: DOS of $[Ni_2^{II}(L^6)(NO_3)]^+$ (**13**)

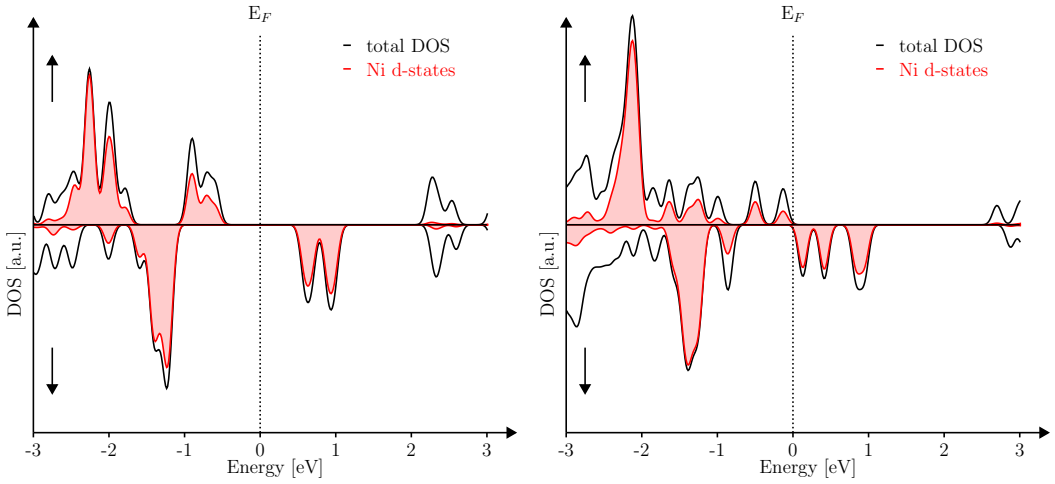

(a) with HCO_2^- (b) without HCO_2^-

Figure 6.12: DOS of $[Ni_2^{II}(L^6)(HCO_2)]^+$ (**14**)

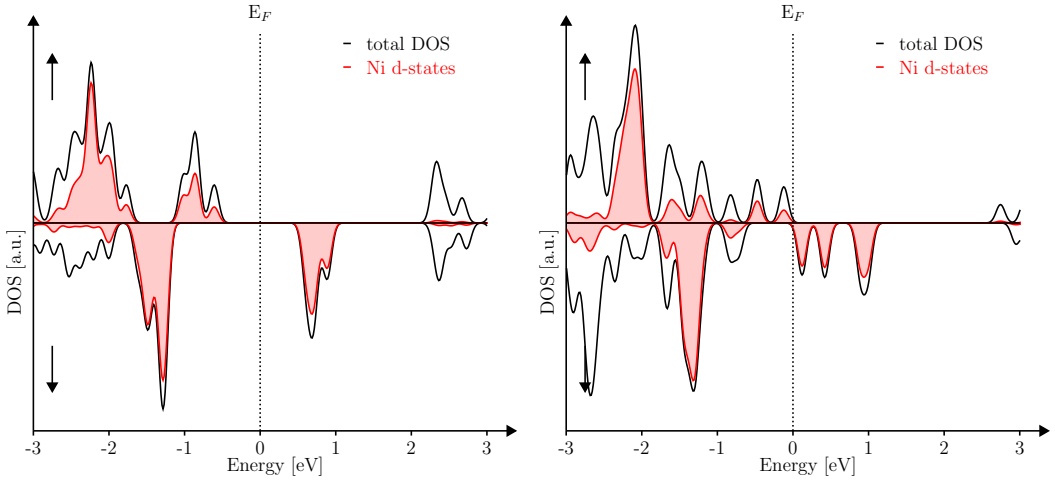

(a) with CO_2OH^- (b) without CO_2OH^-

Figure 6.13: DOS of $[Ni_2^{II}(L^6)(CO_2OH)]^+$ (**15**)

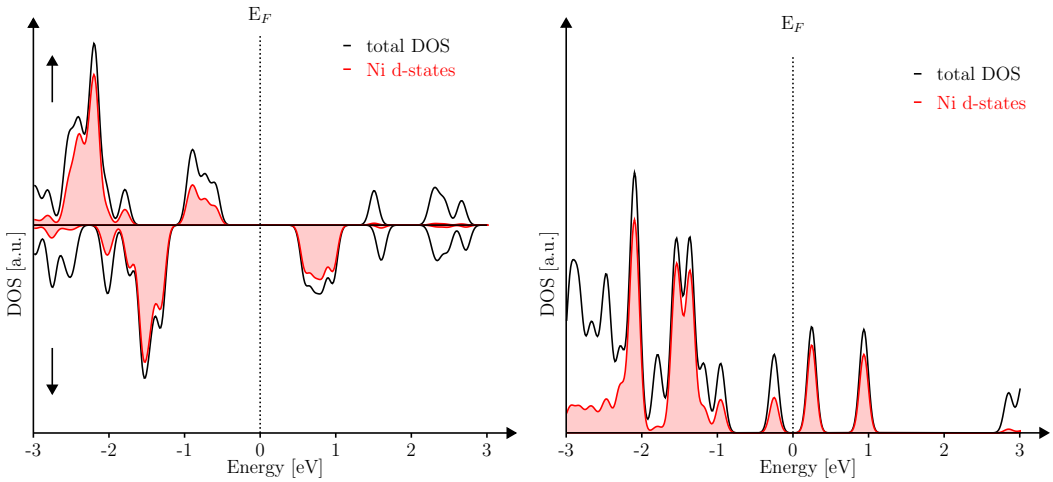

(a) with NO_2^- (b) without NO_2^-

Figure 6.14: DOS of $[Ni_2^{II}(L^6)(NO_2^-)]^+$ (**16**)

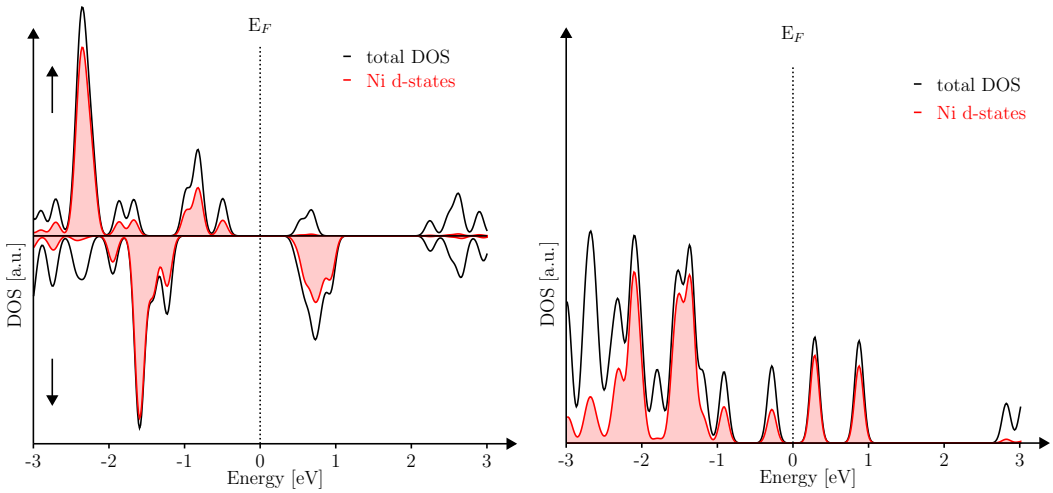

(a) with $C_8H_6N_2$ (b) without $C_8H_6N_2$

Figure 6.15: DOS of $[Ni_2^{II}(L^6)(C_8H_6N_2)]^{2+}$ (**17**)

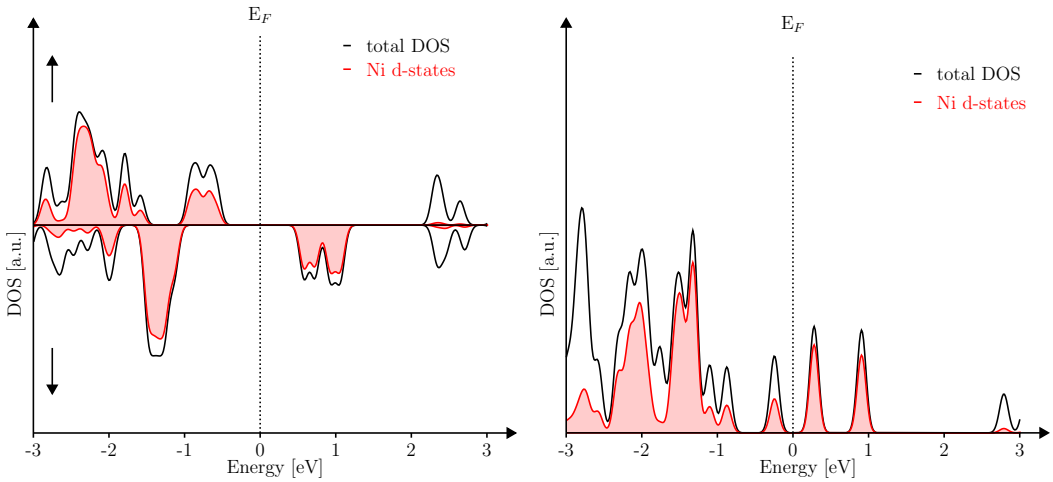

(a) with $C_3H_4N_2^-$ (b) without $C_3H_4N_2^-$

Figure 6.16: DOS of $[Ni_2^{II}(L^6)(C_3H_4N_2)]^+$ (**18**)

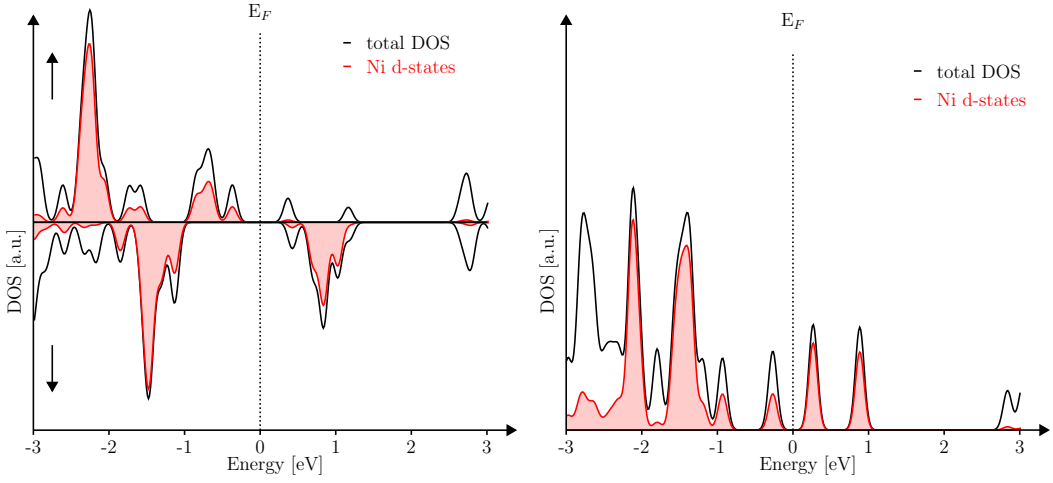

(a) with *pydz* (b) without *pydz*

Figure 6.17: DOS of $[Ni_2^{II}(L^6)(pydz)]^{2+}$ (**19**)

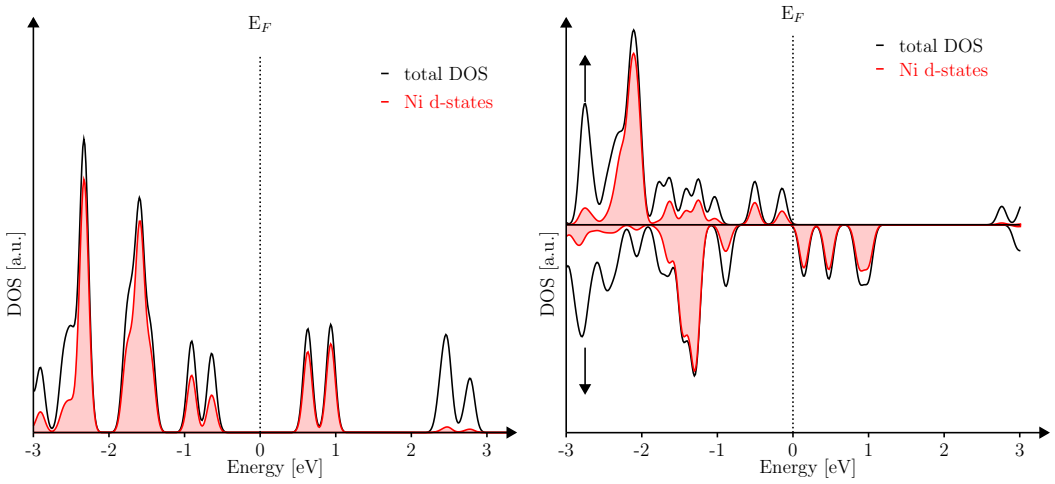

(a) with N_2H_4 (b) without N_2H_4

Figure 6.18: DOS of $[Ni_2^{II}(L^6)(N_2H_4)]^{2+}$ (**20**)

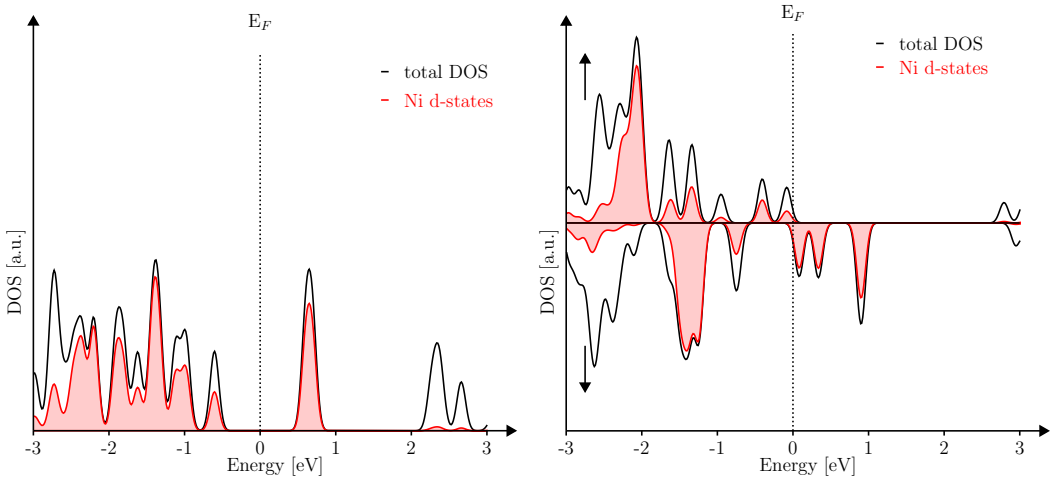

(a) with N_3^- (b) without N_3^-

Figure 6.19: DOS of $[Ni_2^{II}(L^6)(N_3)]^{+}$ (**21**)

6.3 Appendix C

Overview of the various azido-bridged copper, nickel and manganese dimers including structure and chemical formulas of the respective complexes:

- Figure 6.20: copper dimers
- Figure 6.21: nickel dimers
- Figure 6.22: manganese dimers

color code:

- grey: C
- blue: N
- red: O
- orange: Cu
- green: Ni
- purple: Mn
- H is omitted for reasons of clarity

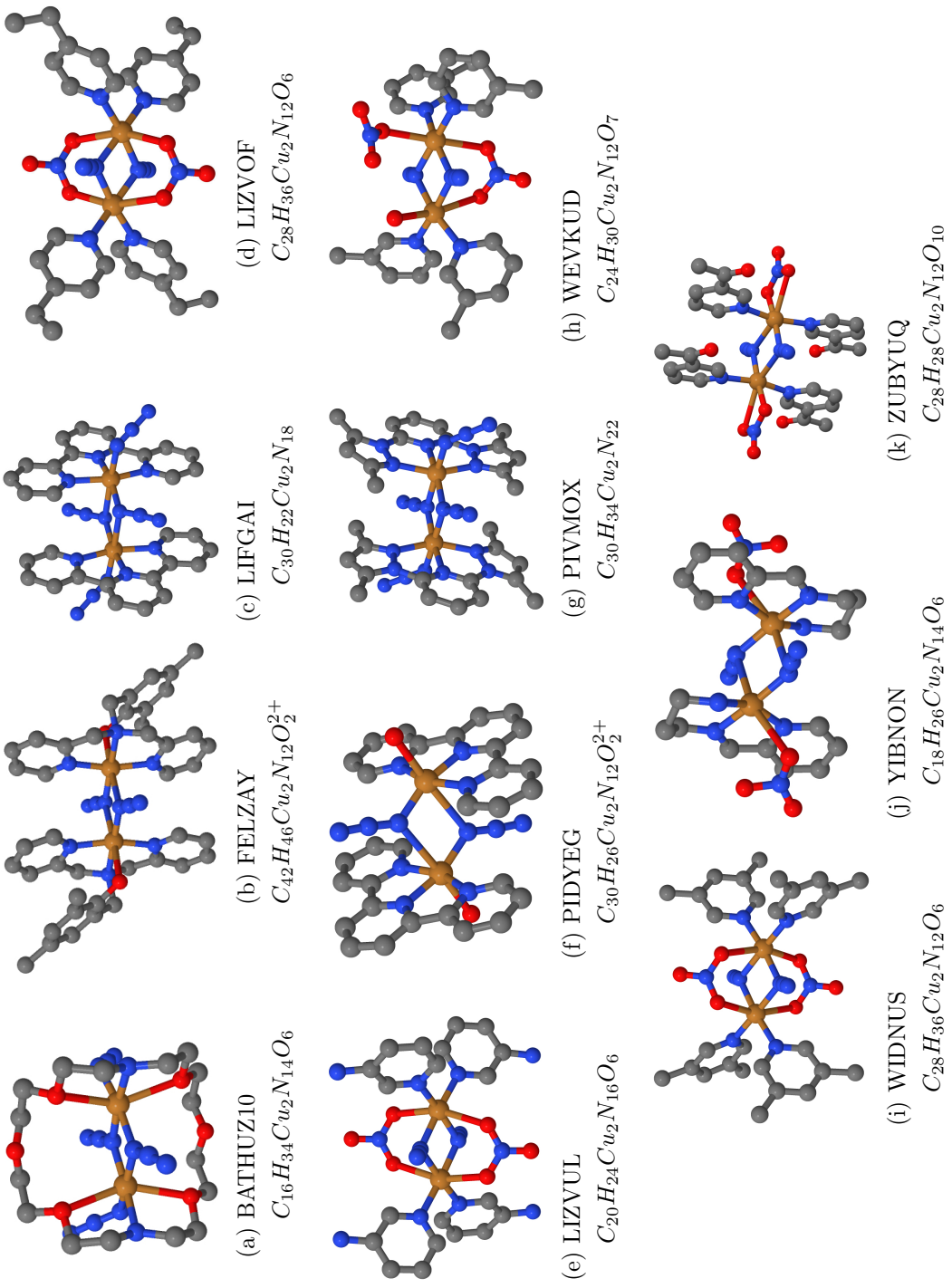

Figure 6.20: Overview of the various azido-bridged copper dimers including structure and chemical formulas of the respective complexes; grey: C; blue: N; red: O; orange: Cu; H is omitted for reasons of clarity

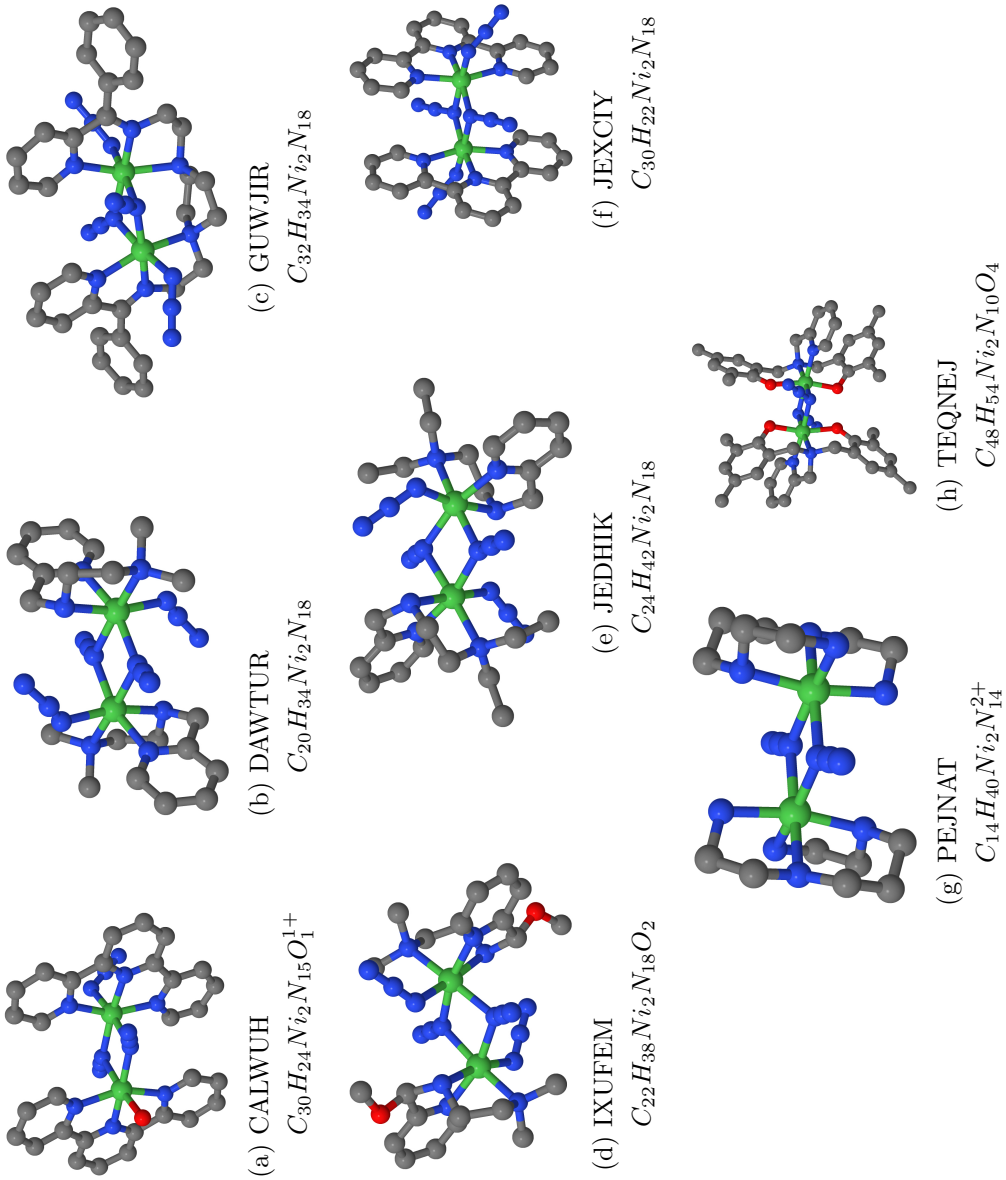

(a) CALWUH $C_{30}H_{24}Ni_2N_{15}O_1^{1+}$

(b) DAWTUR $C_{20}H_{34}Ni_2N_{18}$

(c) GUWJIR $C_{32}H_{34}Ni_2N_{18}$

(d) IXUFEM $C_{22}H_{38}Ni_2N_{18}O_2$

(e) JEDHIK $C_{24}H_{42}Ni_2N_{18}$

(f) JEXCIY $C_{30}H_{22}Ni_2N_{18}$

(g) PEJNAT $C_{14}H_{40}Ni_2N_{14}^{2+}$

(h) TEQNEJ $C_{48}H_{54}Ni_2N_{10}O_4$

Figure 6.21: Overview of the various azido-bridged nickel dimers including structure and chemical formulas of the respective complexes; grey: C; blue: N; red: O; green: Ni; H is omitted for reasons of clarity

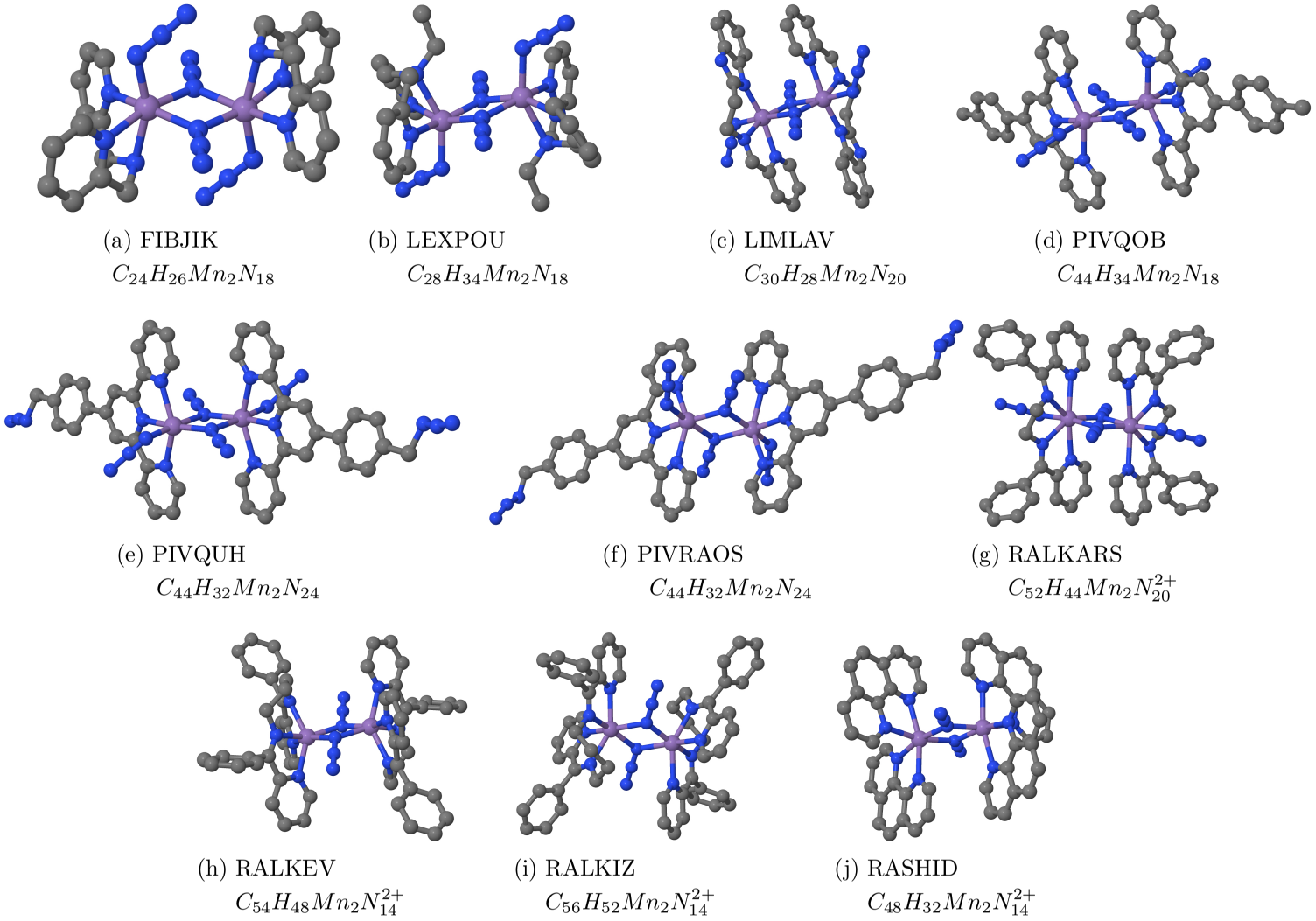

(a) FIBJIK $C_{24}H_{26}Mn_2N_{18}$

(b) LEXPOU $C_{28}H_{34}Mn_2N_{18}$

(c) LIMLAV $C_{30}H_{28}Mn_2N_{20}$

(d) PIVQOB $C_{44}H_{34}Mn_2N_{18}$

(e) PIVQUH $C_{44}H_{32}Mn_2N_{24}$

(f) PIVRAOS $C_{44}H_{32}Mn_2N_{24}$

(g) RALKARS $C_{52}H_{44}Mn_2N_{20}^{2+}$

(h) RALKEV $C_{54}H_{48}Mn_2N_{14}^{2+}$

(i) RALKIZ $C_{56}H_{52}Mn_2N_{14}^{2+}$

(j) RASHID $C_{48}H_{32}Mn_2N_{14}^{2+}$

Figure 6.22: Overview of the various azido-bridged manganese dimers including structure and chemical formulas of the respective complexes. RASHID, RASHOJ and RASHUP differ only in the counter ion, hence only RASHID is depicted here; grey: C; blue: N; purple: Mn; H is omitted for reasons of clarity

6.4 Appendix D

Table 6.2: magnetic anisotropy D [K] of various Mn_6 complexes indicating the spin channel contributions. Shown are results for S =4,8 and 12. All values are corrected according to Van Wüllen[219]

complex	S	D_{calc}	$\alpha-\alpha$	$\alpha-\beta$	$\beta-\alpha$	$\beta-\beta$	$\lvert D\rvert \cdot S^2$
A	4	-3.855	-0.793	-1.879	-0.818	-0.430	61.7
	8	-0.884	-0.221	-0.521	-0.096	-0.049	56.6
	12	-0.378	-0.112	-0.264	0.002	0.002	54.3
B	4	-3.835	-0.844	-1.763	-0.731	-0.505	61.3
	8	-0.877	-0.065	-0.107	-0.477	-0.235	56.1
	12	-0.363	-0.115	-0.248	0.007	-0.006	52.3
C	4	-3.912	-0.859	-1.720	-0.822	-0.507	62.5
	8	-0.894	-0.238	-0.496	-0.098	-0.067	57.2
	12	-0.370	-0.116	-0.253	0.006	-0.006	53.2
D	4	-4.155	-0.922	-1.762	-0.923	-0.576	66.4
	8	-0.935	-0.078	-0.099	-0.512	-0.247	59.8
	12	-0.386	-0.121	-0.263	0.009	-0.010	55.5
E	4	-3.882	1.520	-2.563	-2.058	1.471	62.1
	8	-0.878	0.361	-0.684	-0.413	0.348	56.1
	12	-0.369	0.161	-0.336	-0.158	0.157	53.2
F	4	-4.125	-0.922	-1.744	-0.913	-0.568	66.0
	8	-0.929	-0.247	-0.508	-0.099	-0.077	59.4
	12	-0.384	-0.121	-0.262	0.009	-0.010	55.3
G	4	-4.130	-0.914	-1.769	-0.900	-0.567	66.0
	8	-0.928	-0.245	-0.511	-0.097	-0.076	59.3
	12	-0.383	-0.120	-0.262	0.009	-0.009	55.1
H	4	-4.157	-0.935	-1.806	-0.888	-0.565	66.5
	8	-0.934	-0.247	-0.518	-0.094	-0.077	59.7
	12	-0.385	-0.120	-0.264	0.010	-0.010	55.4
I	4	-4.067	-0.912	-1.774	-0.841	-0.555	65.0
	8	-0.917	-0.245	-0.508	-0.090	-0.074	58.6
	12	-0.381	-0.120	-0.260	0.008	-0.008	54.8
K	4	-3.304	-0.277	-1.281	-1.260	-0.534	52.8

	8	-0.731	-0.191	-0.463	-0.045	-0.030	46.7
	12	-0.292	-0.049	-0.205	0.060	-0.009	42.0
L	4	-2.953	-0.300	-1.112	-1.185	-0.458	47.2
	8	-0.680	-0.092	-0.375	-0.151	-0.065	43.5
	12	-0.277	-0.051	-0.201	0.034	0.009	39.8

7 Bibliography

[1] `http://www.thch.uni-bonn.de/tc/orca`.

[2] Jmol: an open-source java viewer for chemical structures in 3d. `http://www.jmol.org`.

[3] N.S. Ostlund A. Szabo. *Modern Quantum Chemistry*. Dover Publishing, Mineola, New York, 1996.

[4] C. Adamo, V. Barone, A. Bencini, R. Broer, M. Filatov, N. M. Harrison, F. Illas, J. P. Malrieu, and I. de P. R. Moreira. Comment on "about the calculation of exchange coupling constants using density-functional theory: The role of the self-interaction error" [j. chem. phys. [bold 123], 164110 (2005)]. *J. Chem. Phys.*, 124(10):107101, 2006.

[5] C. Adhikary and S. Koner. Structural and magnetic studies on copper(II) azido complexes. *Coordin. Chem. Rev.*, 254(23-24):2933 – 2958, 2010.

[6] C. Adhikary, D. Mal, R. Sen, A. Bhattacharjee, P. Guetlich, S. Chaudhuri, and S. Koner. Synthesis, X-ray crystal structure and magnetic study of a novel μ_2-1,1-azido bridged dimeric copper(II) complex. *Polyhedron*, 26(8):1658–1662, 2007.

[7] M.A. Aebersold, B. Gillon, O. Plantevin, L. Pardi, O. Kahn, P. Bergerat, I. von Seggern, F. Tuczek, L. Ohrstrom, A. Grand, and E. Lelievre-Berna. Spin density maps in the triplet ground state of $[Cu_2(t-Bupy)_4(N_3)_2](ClO_4)_2$ (t-bupy = p-tert-butylpyridine): A polarized neutron diffraction study. *J. Am. Chem. Soc.*, 120(21):5238–5245, 1998.

[8] F.H. Allen. The Cambridge Structural Database: A quarter of a million crystal structures and rising. *Acta Crystallographica Section B: Structural Science*, 58(3 PART 1):380388, 2002.

[9] S. Alvarez, D. Avnir, M. Llunell, and M. Pinsky. Continuous symmetry maps and shape classification. the case of six-coordinated metal compounds. *New J. Chem.*, 26(8):996–1009, 2002.

[10] S. Alvarez and M. Llunell. Continuous symmetry measures of penta-coordinate molecules: Berry and non-berry distortions of the trigonal bipyramid. *J. Chem. Soc., Dalton Trans.*, (19):3288–3303, 2000.

[11] O.K. Andersen. Linear methods in band theory. *Phys. Rev. B*, 12(8):3060–3083, 1975.

[12] P. W. Anderson. *Theory of Magnetic Exchange Interactions: Exchange in Insulators and Semiconductors*, volume 14 of *Solid State Physics*. Academic Press, 1963.

[13] P. W. Anderson. More is different. *Science*, 177(4047):393–396, April 1972.

[14] V. I. Anisimov, I. V. Solovyev, M. A. Korotin, M. T. Czyżyk, and G. A. Sawatzky. Density-functional theory and nio photoemission spectra. *Phys. Rev. B*, 48:16929–16934, Dec 1993.

[15] Vladimir I. Anisimov, Jan Zaanen, and Ole K. Andersen. Band theory and mott insulators: Hubbard U instead of stoner I. *Phys. Rev. B*, 44:943–954, Jul 1991.

[16] M.I. Arriortua, A.R. Cortes, L. Lezam, T. Rojo, X. Solans, and M. Fontbardia. Crystal-structure and magetnic properties of $[Ni(terpy)(N_3)_2]_2 * 2H_2O$, a Nickel(II) dinuclear complex with ferromagnetic interaction. *Inorg. Chim. Acta*, 174(2):263–269, 1990.

[17] H. Astheimer and W. Haase. Direct theoretical ab initio calculations in exchange coupled copper(II) dimers: Influence of structural and chemical parameters in modeled copper dimers. *J. Chem. Phys.*, 85(3):1427–1432, 1986.

[18] M. Atanasov, P. Comba, S. Helmle, D. Mller, and F. Neese. Zero-field splitting in a series of structurally related mononuclear ni ii-bispidine complexes. *Inorg. Chem.*, 51(22):12324–12335, 2012.

[19] M. Atanasov, J.M. Zadrozny, J.R. Long, and F. Neese. A theoretical analysis of chemical bonding, vibronic coupling, and magnetic anisotropy in linear iron(ii) complexes with single-molecule magnet behavior. *Chem. Sci.*, 4:139–156, 2013.

[20] P. S. Bagus and B. I. Bennett. Singlet–triplet splittings as obtained from the x-scattered wave method: A theoretical analysis. *Int. J. Quantum Chem.*, 9(1):143–148, 1975.

[21] M.G. Barandika, R. Cortes, L. Lezama, M.K. Urtiaga, M.I. Arriortua, and T. Rojo. Synthesis and magnetostructural characterization of two ferromagnetic nickel(II) dimers. *J. Chem. Soc. - Dalton Trans.*, (17):2971–2976, 1999.

[22] C.J. Barden, J.C. Rienstra-Kiracofe, and H.F. Schaefer. Homonuclear 3d transition-metal diatomics: A systematic density functional theory study. *J. Chem. Phys.*, 113(2):690, 2000.

[23] A.D. Becke. Density-functional exchange-energy approximation with correct asymptotic behavior. *Phys. Rev. A*, 38(6):3098–3100, 1988.

[24] A.D. Becke. Density-functional thermochemistry. I. the effect of the exchange-only gradient correction. *J. Chem. Phys.*, 96(3):2155–2160, 1992.

[25] A.D. Becke. Density-functional thermochemistry. III. the role of exact exchange. *J. Chem. Phys.*, 98(7):5648–5652, 1993.

[26] A.D. Becke. A new mixing of hartree–fock and local density-functional theories. *J. Chem. Phys.*, 98(2):1372–1377, 1993.

[27] H.D. Bian, W. Gu, Q. Yu, S.P. Yan, D.Z. Liao, Z.H. Jiang, and P. Cheng. Synthesis, crystal structure, and magnetic properties of three nickel(II) complexes with the tridentate ligand N,N-dimethyl-N ‘-(pyrid-2-ylmethyl)-ethylenediamine. *Polyhedron*, 24(15):2002–2008, 2005.

[28] S. Blügel, G. Gompper, E. Koch, H. Müller-Krumbhaar, R. Spatschek, and R.G. Winkler. *Computational Condensed Matter Physics*. Forschungszentrum Jülich GmbH Institut für Festkörperforschung, 2006.

[29] R. Boca. *Theoretical Foundations of Molecular Magnetism*. Elsevier, 1999.

[30] R. Boca. Zero-field splitting in metal complexes. *Coordin. Chem. Rev.*, 248(9-10):757 – 815, 2004.

[31] D. Bohm and D. Pines. A collective description of electron interactions. i. magnetic interactions. *Phys. Rev.*, 82:625–634, Jun 1951.

[32] D. Bohm and D. Pines. A collective description of electron interactions: Iii. coulomb interactions in a degenerate electron gas. *Phys. Rev.*, 92:609–625, Nov 1953.

[33] N. Bohr. Über die Serienspektra der Elemente. *Z. Physik*, 2(5):423469, 1920.

[34] M. Born and R. Oppenheimer. Zur quantentheorie der molekeln. *Ann. Phys. (Berlin)*, 389(20):457–484, 1927.

[35] S.F. Boys. Electronic wave functions. I. a general method of calculation for the stationary states of any molecular system. *Proc. R. Soc. A*, 200(1063):542–554, 1950.

[36] R. Caballol, O. Castell, F. Illas, I. de P. R. Moreira, and J. P. Malrieu. Remarks on the proper use of the broken symmetry approach to magnetic coupling. *J. Phys. Chem. A*, 101(42):7860–7866, 1997.

[37] C.J. Calzado, C. Angeli, D. Taratiel, R. Caballol, and J.P. Malrieu. Analysis of the magnetic coupling in binuclear systems. iii. the role of the ligand to metal charge transfer excitations revisited. *J. Chem. Phys.*, 131(4):044327, 2009.

[38] C.J. Calzado, J. Cabrero, J.P. Malrieu, and R. Caballol. Analysis of the magnetic coupling in binuclear complexes. ii. derivation of valence effective hamiltonians from ab initio ci and dft calculations. *J. Chem. Phys.*, 116(10):3985–4000, 2002.

[39] C.J. Calzado, J.Cabrero, J.P. Malrieu, and R. Caballol. Analysis of the magnetic coupling in binuclear complexes. i. physics of the coupling. *J. Chem. Phys.*, 116(7):2728–2747, 2002.

[40] K. Capelle. A bird's-eye view of density-functional theory. *Braz. J. Phys.*, 36(4A):1318–1343, 2006.

[41] R. Car and M. Parrinello. Unified approach for molecular dynamics and density-functional theory. *Phys. Rev. Lett.*, 55(22):2471–2474, 1985.

[42] S. Carretta, T. Guidi, P. Santini, G. Amoretti, O. Pieper, B. Lake, J. van Slageren, F. El Hallak, W. Wernsdorfer, H. Mutka, M. Russina, C. J. Milios, and E. K. Brechin. Breakdown of the giant spin model in the magnetic relaxation of the Mn_6 nanomagnets. *Phys. Rev. Lett.*, 100(15):157203, 2008.

[43] D. Casanova, P. Alemany, J.M. Bofill, and S. Alvarez. Shape and symmetry of heptacoordinate transition-metal complexes: Structural trends. *Chem. Eur. J.*, 9(6):1281–1295, 2003.

[44] D. Casanova, M. Llunell, P. Alemany, and S. Alvarez. The rich stereochemistry of eight-vertex polyhedra: A continuous shape measures study. *Chem. Eur. J.*, 11(5):1479–1494, 2005.

[45] D. Ceperley, G. V. Chester, and M. H. Kalos. Monte carlo simulation of a many-fermion study. *Phys. Rev. B*, 16:3081–3099, Oct 1977.

[46] D. M. Ceperley and B. J. Alder. Ground state of the electron gas by a stochastic method. *Phys. Rev. Lett.*, 45:566–569, Aug 1980.

[47] M.F. Charlot, O. Kahn, M. Chaillet, and C. Larrieu. Interaction between copper(II) ions through the azido bridge: concept of spin polarization and ab initio calculations on model systems. *J. Am. Chem. Soc.*, 108(10):2574–2581, 1986.

[48] P. Chaudhuri, R. Wagner, S. Khanra, and T. Weyhermueller. Ferromagnetic vs. antiferromagnetic coupling in bis(μ_2-1,1-azido)dinickel(II) with syn- and anti-conformations of the end-on azide bridges. *Dalton Trans.*, (41):4962–4968, 2006.

[49] J. Cirera, P. Alemany, and S. Alvarez. Mapping the stereochemistry and symmetry of tetracoordinate transition-metal complexes. *Chem. Eur. J.*, 10(1):190–207, 2007.

[50] J. Cirera, E. Ruiz, S. Alvarez, F. Neese, and J. Kortus. How to build molecules with large magnetic anisotropy. *Chem. Eur. J.*, 15(16):4078–4087, 2009.

[51] D. Collison, M. Murrie, V.S. Oganesyan, S. Piligkos, N.R.J. Poolton, G. Rajaraman, G.M. Smith, A.J. Thomson, G.A. Timko, W. Wernsdorfer, R.E.P. Winpenny, and E.J.L. McInnes. Magnetic and optical studies on an S=6 ground-state cluster $[Cr_{12}O_9(OH)_3(O_2CCMe_3)_{15}]$: Determination of, and the relationship between, single-ion and cluster spin hamiltonian parameters. *Inorg. Chem.*, 42(17):5293–5303, 2003. PMID: 12924901.

[52] J. Comarmond, P. Plumere, J.M. Lehn, Y. Agnus, R. Louis, R. Weiss, O. Kahn, and I. Morgensternbadarau. Dinuclear copper(II) cryptates of macrocyclic ligands: synthesis, crystal structure, and magnetic properties. Mechanism of the exchange interaction through bridging azido ligands. *J. Am. Chem. Soc.*, 104(23):6330–6340, 1982.

[53] R. Cortes, L. Lezama, J.I.R. Larramendi, M. Inausti, J.V. Folgado, G. Madariaga, and T. Rojo. Crystal-structure, spectroscopic and magnetic properties of 2 unsual compounds - $[Cu(terpy)(N_3)Cl]$ and $[(Cu_{0.75}Ni_{0.25}(terpy)(N_3)_2)]*2H_2O$ (terpy = 2,2'/6',2"-terpyridine). *J. Chem. Soc. - Dalton Trans.*, (17):2573–2579, 1994.

[54] R. Cortes, M.K. Urtiaga, L. Lezama, J.I.R Larramendi, M.I. Arriortua, and T. Rojo. Synthetic strategy, magnetic and spectroscopic properties of the terpyridine complexes $[Cu(terpy)X(H_2O)n]Y$ (X = NCO, NCS or N_3; n= 0 or 1; Y = NO_3 or PF_6). Crystal structures of the azidenitrate and azidehexafluorophosphate. *J. Chem. Soc. - Dalton Trans.*, (24):3685–3694, DEC 21 1993.

[55] E. Cremades, J. Cano, E. Ruiz, G. Rajaraman, C.J. Milios, and E.K. Brechin. Theoretical Methods Enlighten Magnetic Properties of a Family of Mn6 Single-Molecule Magnets. *Inorg. Chem.*, 48(16):8012–8019, 2009. PMID: 19624160.

[56] E. Cremades, C.D. Pemmaraju, S. Sanvito, and E. Ruiz. Spin-polarized transport through single-molecule magnet mn6 complexes. *Nanoscale*, 5(11):4751–4757, 2013.

[57] D. Cremer. Density functional theory: Coverage of dynamic and non-dynamic electron correlation effects. *Molec. Phys.*, 99(23):1899–1940, 2001. cited By (since 1996)139.

[58] G.I. Csonka, O.A. Vydrov, G.E. Scuseria, A. Ruzsinszky, and J.P. Perdew. Diminished gradient dependence of density functionals: Constraint satisfaction and self-interaction correction. *J. Chem. Phys.*, 126(24):244107, 2007.

[59] F.F. de Biani, E. Ruiz, J. Cano, J.J. Novoa, and S. Alvarez. Magnetic coupling in end-to-end azido-bridged copper and nickel binuclear complexes: A theoretical study. *Inorg. Chem.*, 39(15):3221–3229, 2000.

[60] W. Demtröder. *Molecular Physics: Theoretical Principles and Experimental Methods*. Wiley-VCH, Weinheim, 2005.

[61] S. Deoghoria, S. Sain, M. Soler, W.T. Wong, G. Christou, S.K. Bera, and S.K. Chandra. Synthesis, crystal structure and magnetic properties of a new ferromagnetic nickel(II) dimer derived from a hexadentate Schiff base ligand. *Polyhedron*, 22(2):257–262, 2003.

[62] S.K. Dey, N. Mondal, M.S. El Fallah, R. Vicente, A. Escuer, X. Solans, M. Font-Bardia, T. Matsushita, V. Gramlich, and S. Mitra. Crystal structure and magnetic interactions in nickel(II) dibridged complexes formed by two azide groups or by both phenolate oxygen-azide, -thiocyanate, -carboxylate, or -cyanate groups. *Inorg. Chem.*, 43(7):2427–2434, 2004.

[63] Shriver D.F and Atkins P.W. *Inorganic Chemistry*. Oxford University Press, 4th edition, 2006.

[64] P. A. M. Dirac. On the theory of quantum mechanics. *Proc. R. Soc. London, Ser. A*, 112(762):661–677, 1926.

[65] M. Drillon and R. Georges. New approach for the exchange hamiltonian of an orbitally degenerate ground-state system (T_2g_2 or T_1g_3). *Phys. Rev. B*, 24(3):1278–1286, 1981.

[66] L.A. Eriksson, L.G.M. Pettersson, P.E.M. Siegbahn, and U. Wahlgren. On the accuracy of gradient corrected density functional methods for transition metal complexes. *J. Chem. Phys.*, 102(2):872–878, 1995.

[67] A. Escuer, M.A.S. Goher, F.A. Mautner, and R. Vicente. Three new polynuclear copper(II) complexes with the symmetric $[Cu(\mu(1,1)-N_3)_2Cu]^{2+}$ core and pyridine derivatives: Syntheses, structure, and magnetic behavior. *Inorg. Chem.*, 39(10):2107–2112, 2000.

[68] E. Fermi. Eine statistische methode zur bestimmung einiger eigenschaften des atoms und ihre anwendung auf die theorie des periodischen systems der elemente. *Z. Physik*, 48(1-2):73–79, 1928.

[69] C.F. Fischer. *The Hartree-Fock Method for Atoms: A Numerical Approach.* John Wiley and Sons Inc, New York, 1977.

[70] V. Fock. Approximation method for the solution of the quantum mechanical multibody problems. *Z. Physik*, 61(1-2):126–148, January 1930.

[71] J.R. Friedman, M. P. Sarachik, J. Tejada, and R. Ziolo. Macroscopic measurement of resonant magnetization tunneling in high-spin molecules. *Phys. Rev. Lett.*, 76:3830–3833, May 1996.

[72] D. Gatteschi and R. Sessoli. Quantum tunneling of magnetization and related phenomena in molecular materials. *Angew. Chem. Int. Ed.*, 42(3):268–297, 2003.

[73] D. Gatteschi, R. Sessoli, and J. Villain. *Molecular Nanomagnets.* Oxford University Press, 2006.

[74] M.A.S. Goher and F.A. Mautner. Structural and spectroscopic investigation of di-$\mu_{1,1}$-azido-di(O,O'-nitrato)tetrakis(3-acetylpyridine) dicopper(II). *J. Coord. Chem.*, 34(3):221–228, 1995.

[75] J.B. Goodenough. Theory of the role of covalence in the perovskite-type manganites [La, M(II)] MnO_3. *Phys. Rev.*, 100(2):564–573, 1955.

[76] J.B. Goodenough. An interpretation of the magnetic properties of the perovskite-type mixed crystals La_1-xSrXCoO$_3$-[λ]. *J. Phys. Chem. Solids*, 6(2-3):287 – 297, 1958.

[77] T. Goswami and A. Misra. Ligand effects toward the modulation of magnetic anisotropy and design of magnetic systems with desired anisotropy characteristics. *J. Phys. Chem. A*, 116(21):5207–5215, 2012.

[78] J. Gräfenstein and D. Cremer. The self-interaction error and the description of non-dynamic electron correlation in density functional theory. *Theor. Chem. Acc.*, 123(3-4):171–182, 2009.

[79] J. Gräfenstein, E. Kraka, and D. Cremer. Effect of the self-interaction error for three-electron bonds: On the development of new exchange-correlation functionals. *Phys. Chem. Chem. Phys.*, 6:1096–1112, 2004.

[80] J. Gräfenstein, E. Kraka, and D. Cremer. The impact of the self-interaction error on the density functional theory description of dissociating radical cations: Ionic and covalent dissociation limits. *J. Chem. Phys.*, 120(2):524–539, 2004.

[81] J.J. Griffin and J.A. Wheeler. Collective motions in nuclei by the method of generator coordinates. *Phys. Rev.*, 108:311–327, Oct 1957.

[82] S. Grimme. Accurate calculation of the heats of formation for large main group compounds with spin-component scaled mp2 methods. *J. Phys. Chem. A*, 109(13):3067–3077, 2005.

[83] O. Gunnarsson and B.I. Lundqvist. Exchange and correlation in atoms, molecules, and solids by the spin-density-functional formalism. *Phys. Rev. B*, 13(10):4274–4298, 1976.

[84] D. R. Hamann. Generalized gradient theory for silica phase transitions. *Phys. Rev. Lett.*, 76(4):660–663, 1996.

[85] B. Hammer, K.W. Jacobsen, and J.K. Nørskov. Role of nonlocal exchange correlation in activated adsorption. *Phys. Rev. Lett.*, 70(25):3971–3974, 1993.

[86] B. Hammer and M. Scheffler. Local chemical reactivity of a metal alloy surface. *Phys. Rev. Lett.*, 74(17):3487–3490, 1995.

[87] D. R. Hartree. The wave mechanics of an atom with a non-Coulomb central field part i theory and methods. *Proc. Cambridge Philos. Soc.*, 24:89–110, July 1928.

[88] J. Hausmann, S. Kass, S. Klod, E. Kleinpeter, and B. Kersting. Binucleating aza-sulfonate and aza-sulfinate macrocycles - synthesis and coordination chemistry. *Eur. J. Inorg. Chem.*, 2004(22):4402–4411, 2004.

[89] J. Hausmann, M.H. Klingele, V. Lozan, G. Steinfeld, D. Siebert, Y. Journaux, J.J. Girerd, and B. Kersting. Realization of unusual ligand binding motifs in metalated container molecules: Synthesis, structures, and magnetic properties of the complexes $[(\mathrm{LMe})\mathrm{Ni}_2(\mu - \mathrm{L}')]^{n+}$ with L'=NO_3^-, NO_2^-, N_3^-, $\mathrm{N}_2\mathrm{H}_4$ pyridazine, phthalazine, pyrazolate, and benzoate. *Chem. Eur. J.*, 10(7):1716–1728, 2004.

[90] P.J. Hay, J.C. Thibeault, and R. Hoffmann. Orbital interactions in metal dimer complexes. *J. Am. Chem. Soc.*, 97(17):4884–4899, 1975.

[91] W. Heisenberg. Zur theorie des ferromagnetismus. *Z. Physik*, 49(9-10):619–636, 1928.

[92] D.L. Hill and J.A. Wheeler. Nuclear constitution and the interpretation of fission phenomena. *Phys. Rev.*, 89:1102–1145, Mar 1953.

[93] P. Hohenberg and W. Kohn. Inhomogeneous electron gas. *Phys. Rev.*, 136(3B):B864–B871, Nov 1964.

[94] R. Hotzelmann, K. Wieghardt, U. Floerke, H.-J. Haupt, D. C. Weatherburn, J. Bonvoisin, G. Blondin, and J.-J. Gired. Spin exchange coupling in asymmetric heterodinuclear complexes containing the μ-oxo-bis(μ-acetato)dimetal core. *J. Am. Chem. Soc.*, 114(5):1681–1696, 1992.

[95] C.E. Housecroft and A.G. Sharpe. *Inorganic Chemistry*. Pearson Education Limited, 2nd edition, 2005.

[96] Shavitt I. and Bartlett R-J. *Many-Body Methods in Chemistry and Physics: MBPT and Coupled-Cluster Theory*. Cambridge University Press, Cambridge, 2009.

[97] R. Inglis, L.F. Jones, C.J. Milios, S. Datta, A. Collins, S. Parsons, W. Wernsdorfer, S. Hill, S.P. Perlepes, S. Piligkos, and E.K. Brechin. Attempting to understand (and control) the relationship between structure and magnetism in an extended family of Mn6 single-molecule magnets. *Dalton Trans.*, (18):3403–3412, 2009.

[98] K. Jackson and M.R. Pederson. Accurate forces in a local-orbital approach to the local-density approximation. *Phys. Rev. B*, 42(6):3276–3281, 1990.

[99] H. J. F. Jansen. Magnetic anisotropy in density-functional theory. *Phys. Rev. B*, 59:4699–4707, Feb 1999.

[100] L.F. Jones, M.E. Cochrane, B.D. Koivisto, D.A. Leigh, S.P. Perlepes, W. Wernsdorfer, and E.K. Brechin. Tuning magnetic properties using targeted structural distortion: New additions to a family of mn6 single-molecule magnets. *Inorg. Chim. Acta*, 361(12-13):3420 – 3426, 2008.

[101] Y. Journaux, T. Glaser, G. Steinfeld, V. Lozan, and B. Kersting. Preparation and characterization of CrIII, MnII, FeII, CoII and NiII complexes of a hexaazadithiophenolate macrocycle. *Dalton Trans.*, (14):1738–1748, 2006.

[102] Y. Journaux, V. Lozan, J. Klingele, and B. Kersting. Stabilisation of a paramagnetic BH_4-bridged dinickel(ii) complex by a macrodinucleating hexaazadithiophenolate ligand. *Chem. Commun.*, (1):83–84, 2006.

[103] O. Kahn. Magnetism of heterobimetallics: Toward molecular-based magnets. volume 43 of *Advan. Inorg. Chem.*, pages 179 – 259. Academic Press, 1995.

[104] J. Kanamori. Superexchange interaction and symmetry properties of electron orbitals. *J. Phys. Chem. Solids*, 10(2-3):87 – 98, 1959.

[105] T.K. Karmakar, B.K. Ghosh, A. Usman, H.K. Fun, E. Riviere, T. Mallah, G. Aromi, and S.K. Chandra. Magneto-structural correlations: Synthesis of a

family of end-on azido-bridged manganese(II) dinuclear compounds with S=5 spin ground state. *Inorg. Chem.*, 44(7):2391–2399, 2005.

[106] S. Kass, T. Gregor, and B. Kersting. Diels-alder reactivity of binuclear complexes with calixarene-like structures. *Angew. Chem.*, 118(1):107–110, 2006.

[107] S. Kass, T. Gregor, and B. Kersting. Diels-alder reactivity of binuclear complexes with calixarene-like structures. *Angew. Chem. Int. Ed.*, 45(1):101–104, 2006.

[108] B. Kersting. Carbon dioxide fixation by binuclear complexes with hydrophobic binding pockets. *Angew. Chem. Int. Ed.*, 40(21):3987–3990, 2001.

[109] B. Kersting. Kohlendioxid-fixierung an zweikernkomplexen mit hydrophoben bindungstaschen. *Angew. Chem.*, 113(21):4109–4112, 2001.

[110] B. Kersting and G. Steinfeld. Carboxylate and alkyl carbonate coordination at the hydrophobic binding site of redox-active dicobalt amine thiophenolate complexes. *Angew. Chem.*, 41(5):1140–1150, 2002.

[111] W. Kohn and L. J. Sham. Self-consistent equations including exchange and correlation effects. *Phys. Rev.*, 140(4A):A1133–A1138, 1965.

[112] A. Kokalj. Xcrysden a new program for displaying crystalline structures and electron densities. *J. Mol. Graphics Modell.*, 17(34):176 – 179, 1999.

[113] A. Kokalj. Computer graphics and graphical user interfaces as tools in simulations of matter at the atomic scale. *Comp. Mat. Sci.*, 28(2):155 – 168, 2003.

[114] J. Kortus, C.S. Hellberg, and M.R. Pederson. Hamiltonian of the V_{15} spin system from first-principles density-functional calculations. *Phys. Rev. Lett.*, 86(15):3400–3403, 2001.

[115] J. Kortus and M.R. Pederson. Magnetic and vibrational properties of the uniaxial $Fe_{13}O_8$ cluster. *Phys. Rev. B*, 62(9):5755–5759, 2000.

[116] J. Kortus, M.R. Pederson, T. Baruah, N. Bernstein, and C.S. Hellberg. Density functional studies of single molecule magnets. *Polyhedron*, 22(14-17):1871 – 1876, 2003.

[117] C. Kozoni, E. Manolopoulou, M. Siczek, T. Lis, E.K. Brechin, and C.J. Milios. Polynuclear manganese amino acid complexes. *Dalton Trans.*, 39:7943–7950, 2010.

[118] S. Kümmel and L. Kronik. Orbital-dependent density functionals: Theory and applications. *Rev. Mod. Phys.*, 80:3–60, Jan 2008.

[119] C. Lee, W. Yang, and R.G. Parr. Development of the colle-salvetti correlation-energy formula into a functional of the electron density. *Phys. Rev. B*, 37(2):785–789, 1988.

[120] M. Levy. Universal variational functionals of electron densities, first-order density matrices, and natural spin-orbitals and solution of the v-representability problem. *Proc. Natl. Acad. Sci. U.S.A.*, 76(12):6062–6065, Dec 1979.

[121] C.-M. Liu, S. Gao, D.-Q. Zhang, Z.-L. Liu, and D.-B. Zhu. Solvothermal synthesis, crystal structure and magnetic property of a new dinuclear manganese(II)-azido complexes: $[Mn(2,2'-dpa)(N_3)_2]_2$ (2,2'-dpa=2,2'-dipicolylamine). *Inorg. Chim. Acta*, 358(3):834 – 838, 2005.

[122] G.-F. Liu, Z.-G. Ren, H.-X. Li, Y. Chen, Q.-H. Li, Y. Zhang, and J.-P. Lang. Homo- and heterometallic coordination oligomers and polymers derived from the preformed complexes $[Cu(bdmpp)(MeCN)_2](ClO_4)_2$, $[Cu(bdmpp)(N_3)_2]$, and $[Cu(bdmpp)(N_3)(\mu - N_3)]_2$, [bdmpp=2,6-bis(3,5-dimethyl-1H-pyrazol1-yl)pyridine]: Syntheses, structures, and redox properties. *Eur. J. Inorg. Chem.*, (35):5511–5522, 2007.

[123] T. Liz. Preparation, structure, and magnetic properties of a dodecanuclear mixed-valence manganese carboxylate. *Acta Crystallogr. Soc. B*, 36:2042, 1980.

[124] C. Loose. Berechnung der magnetischen austauschkopplung in molekularen magneten. Diplomarbeit, TU Bergakademie Freiberg, 2006.

[125] C. Loose, E. Ruiz, B. Kersting, and J. Kortus. Magnetic exchange interaction in triply bridged dinickel(ii) complexes. *Chem. Phys. Lett.*, 452(1-3):38 – 43, 2008.

[126] V. Lozan, C. Loose, J. Kortus, and B. Kersting. Coordination chemistry of robson-type polyamine-dithiophenolate macrocycles: Syntheses, structures and magnetic properties of dinuclear complexes of first-row transition metals. *Coordin. Chem. Rev.*, 253(19-20):2244 – 2260, 2009.

[127] H. Lueken. *Magnetochemie*. Teubner, 1999.

[128] M. Lundberg and P.E.M. Siegbahn. Quantifying the effects of the self-interaction error in dft: When do the delocalized states appear? *J. Chem. Phys.*, 122(22):224103, 2005.

[129] G. Manca, J. Cano, and E. Ruiz. Exchange Interactions in Azido-Bridged Ligand Ni-II Complexes: A Theoretical Analysis. *Inorg. Chem.*, 48(7):3139–3144, 2009.

[130] J.L. Manson, S.H. Lapidus, P.W. Stephens, P.K. Peterson, K.E. Carreiro, H.I. Southerland, T. Lancaster, S.J. Blundell, A.J. Steele, P.A. Goddard, F.L. Pratt, J. Singleton, Y. Kohama, R.D. McDonald, R.E. Del Sesto, N.A. Smith, J. Bendix, S.A. Zvyagin, J. Kang, C. Lee, M. Whangbo, V.S. Zapf, and A. Plonczak. Structural, Electronic, and Magnetic Properties of Quasi-1D Quantum Magnets $[Ni(HF_2)(pyz)_2]X$ (pyz = pyrazine; X = PF_6, SbF_6) Exhibiting Ni-FHF-Ni and Ni-pyz-Ni Spin Interactions. *Inorg. Chem.*, 50(13):59906009, 2011.

[131] R.M. Martin. *Electronic structure: Basic Theory and Practical Methods*. Cambridge Univ. Press, Cambridge, 2008.

[132] J. Martinez-Lillo, A. Tomsa, Y. Li, L. Chamoreau, E. Cremades, E. Ruiz, A. Barra, A. Proust, M. Verdaguer, and P. Gouzerh. Synthesis, crystal structure and magnetism of new salicylamidoxime-based hexanuclear manganese(III) single-molecule magnets. *Dalton Trans.*, 41:13668–13681, 2012.

[133] J. Martnez-Lillo, L.-M. Chamoreau, A. Proust, M. Verdaguer, and P. Gouzerh. Hexanuclear manganese(iii) single-molecule magnets from derivatized salicylamidoximes. *Comptes Rendus Chimie*, 15(10):889–894, 2012.

[134] R. Maurice, C. de Graaf, and N. Guihéry. Magnetostructural relations from a combined ab initio and ligand field analysis for the nonintuitive zero-field splitting in Mn(III) complexes. *J. Chem. Phys.*, 133(8):084307, 2010.

[135] F.A. Mautner and M.A.S. Goher. Synthesis, spectroscopic and crystal structure study of di-$\mu(1,1)$-azido-$\mu_{O,O}$-nitrato(O-nitrato)tetrakis(3-picoline)aquadicopper(II) and catena-di-$\mu_{1,3}$-aziod-[di-$\mu_{1,1}$-azido-bis(4-picoline)dicopper(II)], $Cu_2(N_3)_2(NO_3)_2(3-picoline)_4(H_2O)$ and $Cu(4-picoline)(N_3)_2$. *Polyhedron*, 12(23):2823–2829, 1993.

[136] F.A. Mautner and M.A.S. Goher. Crystal-structure and spectroscopic study of di-$\mu_{1,1}$-azido-di$\mu_{0,0}$ -nitrato)tetrakis(3,5-lutidine)dicopper(II), $[Cu(N_3)(NO_3)(3,5-Lutidine)_2]_2$. *Struct. Chem.*, 5(3):171–175, 1994.

[137] W. L. McMillan. Ground state of liquid he^4. *Phys. Rev.*, 138:A442–A451, Apr 1965.

[138] C.J. Milios, R. Inglis, A. Vinslava, R. Bagai, W. Wernsdorfer, S. Parsons, S.P. Perlepes, G. Christou, and E.K. Brechin. Toward a Magnetostructural Correlation for a Family of Mn6 SMMs. *J. Am. Chem. Soc.*, 129(41):12505–12511, 2007.

[139] C.J. Milios, A. Vinslava, W. Wernsdorfer, S. Moggach, S. Parsons, S.P. Perlepes, G. Christou, and E.K. Brechin. A record anisotropy barrier for a single-molecule magnet. *J. Am. Chem. Soc.*, 129(10):2754–2755, 2007.

[140] C.J. Milios, A. Vinslava, W. Wernsdorfer, A. Prescimone, P.A. Wood, S. Parsons, S.P. Perlepes, G. Christou, and E.K. Brechin. Spin switching via targeted structural distortion. *J. Am. Chem. Soc.*, 129(20):6547–6561, 2007.

[141] C.J. Milios, A. Vinslava, A.G Whittaker, S. Parsons, W. Wernsdorfer, G. Christou, S.P. Perlepes, and E.K. Brechin. Microwave-Assisted Synthesis

of a Hexanuclear MnIII Single-Molecule Magnet. *Inorg. Chem.*, 45(14):5272–5274, 2006.

[142] C.J. Milios, A. Vinslava, P.A. Wood, S. Parsons, W. Wernsdorfer, G. Christou, S.P. Perlepes, and E.K. Brechin. A single-molecule magnet with a twist. *J. Am. Chem. Soc.*, 129(1):8–9, 2007.

[143] C. Møller and M.S. Plesset. Note on an approximation treatment for many-electron systems. *Phys. Rev.*, 46:618–622, Oct 1934.

[144] G.E. Moore. Cramming more components onto integrated circuits. *Electronics Magazine*, 1:6, 1965.

[145] F. Moro, V. Corradini, M. Evangelisti, V. De Renzi, R. Biagi, U. del Pennino, C. J. Milios, L. F. Jones, and E. K. Brechin. Grafting Derivatives of Mn6 Single-Molecule Magnets with High Anisotropy Energy Barrier on Au(111) Surface. *J. Phys. Chem. B*, 112(32):9729–9735, 2008. PMID: 18646796.

[146] F. Neese. Configuration interaction calculation of electronic g tensors in transition metal complexes. *Int. J. Quantum Chem.*, 83(3-4):104–114, 2001.

[147] F. Neese. A spectroscopy oriented configuration interaction procedure. *J. Chem. Phys.*, 119(18):9428–9443, 2003.

[148] F. Neese. Calculation of the zero-field splitting tensor on the basis of hybrid density functional and hartree-fock theory. *J. Chem. Phys.*, 127(16):164112, 2007.

[149] F. Neese. Prediction of molecular properties and molecular spectroscopy with density functional theory: From fundamental theory to exchange-coupling. *Coord. Chem. Rev.*, 253(56):526 – 563, 2009.

[150] F. Neese and D.A. Pantazis. What is not required to make a single molecule magnet. *Faraday Discuss.*, 148:229–238, 2011.

[151] F. Neese and E.I. Solomon. Calculation of zero-field splittings, g-values, and the relativistic nephelauxetic effect in transition metal complexes. application to high-spin ferric complexes. *Inorg. Chem.*, 37(26):6568–6582, 1998.

[152] Frank Neese. Importance of direct spinspin coupling and spin-flip excitations for the zero-field splittings of transition metal complexes: A case study. *J. Am. Chem. Soc.*, 128(31):10213–10222, 2006.

[153] Z.H. Ni, H.Z. Kou, L. Zheng, Y.H. Zhao, L.F. Zhang, R.J. Wang, A.L. Cui, and O. Sato. Assembly of azido- or cyano-bridged binuclear complexes containing the bulky $[Mn(phen)_2]^{2+}$ building block: Syntheses, crystal structures, and magnetic properties. *Inorg. Chem.*, 44(13):4728–4736, 2005.

[154] M. Nishino, S. Yamanaka, Y. Yoshioka, and K. Yamaguchi. Theoretical approaches to direct exchange couplings between divalent chromium ions in naked dimers, tetramers, and clusters. *J. Phys. Chem. A*, 101(4):705–712, 1997.

[155] L. Noodleman. Valence bond description of antiferromagnetic coupling in transition metal dimers. *J. Chem. Phys.*, 74(10):5737–5743, 1981.

[156] L. Noodleman and D.A. Case. Density-functional theory of spin polarization and spin coupling in iron–sulfur clusters. volume 38 of *Advances in Inorganic Chemistry*, pages 423 – 458, 458a, 458b, 459–470. Academic Press, 1992.

[157] L. Noodleman, J. Li, X.G. Zhao, and W.H. Richardson. *Density Functional Methods: Applications in Chemistry and Materials Science*. Wiley: New Yor, 1997.

[158] L. Noodleman, C.Y. Peng, D.A. Case, and J.-M. Mouesca. Orbital interactions, electron delocalization and spin coupling in iron-sulfur clusters. *Coordin. Chem. Rev.*, 144:199 – 244, 1995.

[159] Louis Noodleman and Ernest R. Davidson. Ligand spin polarization and antiferromagnetic coupling in transition metal dimers. *Chem. Phys.*, 109(1):131–143, 1986.

[160] K. Park, M.R. Pederson, S.L. Richardson, N. Aliaga-Alcalde, and G.. Christou. Density-functional theory calculation of the intermolecular exchange interaction in the magnetic Mn_4 dimer. *Phys. Rev. B*, 68(2):020405, 2003.

[161] C. Paulsen, J.-G. Park, B. Barbara, R. Sessoli, and A. Caneschi. Novel features in the relaxation times of $mn_{12}ac$. *J. Magn. Magn. Mater.*, 140144, Part 1(0):379 – 380, 1995. ¡ce:title¿International Conference on Magnetism¡/ce:title¿.

[162] M.R. Pederson, N. Bernstein, and J. Kortus. Fourth-order magnetic anisotropy and tunnel splittings in Mn_12 from spin-orbit-vibron interactions. *Phys. Rev. Lett.*, 89(9):097202, 2002.

[163] M.R. Pederson and K.A. Jackson. Variational mesh for quantum-mechanical simulations. *Phys. Rev. B*, 41(11):7453–7461, 1990.

[164] M.R. Pederson and K.A. Jackson. Pseudoenergies for simulations on metallic systems. *Phys. Rev. B*, 43(9):7312–7315, 1991.

[165] M.R. Pederson and S.N. Khanna. Magnetic anisotropy barrier for spin tunneling in $Mn_{12}O_{12}$ molecules. *Phys. Rev. B*, 60(13):9566–9572, 1999.

[166] M.R. Pederson, D.V. Porezag, J. Kortus, and D.C. Patton. Electronic structure methods for predicting the properties of materials: Grids in space. *Phys. Status Ssolidi B*, 217(1):173–195, 2000.

[167] J.P. Perdew. Density functional theory and the band gap problem. *Int. J. Quantum Chem.*, 28(S19):497–523, 1985.

[168] J.P. Perdew, K. Burke, and M. Ernzerhof. Generalized gradient approximation made simple. *Phys. Rev. Lett.*, 77(18):3865–3868, 1996.

[169] J.P. Perdew, K. Burke, and Y. Wang. Generalized gradient approximation for the exchange-correlation hole of a many-electron system. *Phys. Rev. B*, 54(23):16533–16539, 1996.

[170] J.P. Perdew, J.A. Chevary, S.H. Vosko, K.A. Jackson, M.R. Pederson, D.J. Singh, and C. Fiolhais. Atoms, molecules, solids, and surfaces: Applications of the generalized gradient approximation for exchange and correlation. *Phys. Rev. B*, 46(11):6671–6687, 1992.

[171] J.P. Perdew, A. Ruzsinszky, J. Tao, V.N. Staroverov, G.E. Scuseria, and G.I. Csonka. Prescription for the design and selection of density functional approximations: More constraint satisfaction with fewer fits. *J. Chem. Phys.*, 123(6):062201, 2005.

[172] J.P. Perdew and Y. Wang. Accurate and simple analytic representation of the electron-gas correlation energy. *Phys. Rev. B*, 45:13244–13249, Jun 1992.

[173] J.P. Perdew and A. Zunger. Self-interaction correction to density-functional approximations for many-electron systems. *Phys. Rev. B*, 23(10):5048–5079, 1981.

[174] P.H.T. Philipsen, G. te Velde, and E.J. Baerends. The effect of density-gradient corrections for a molecule-surface potential energy surface. slab calculations on Cu(100)c(2x2)-CO. *Chem. Phys. Lett.*, 226(5-6):583 – 588, 1994.

[175] J.J. Phillips and J.E. Peralta. Towards the blackbox computation of magnetic exchange coupling parameters in polynuclear transition-metal complexes: Theory, implementation, and application. *J. Chem. Phys.*, 138(17):174115, 2013.

[176] D. Pines and D. Bohm. A collective description of electron interactions: Ii. collective vs individual particle aspects of the interactions. *Phys. Rev.*, 85:338–353, Jan 1952.

[177] M. Pinsky and D. Avnir. Continuous symmetry measures. 5. the classical polyhedra. *Inorg. Chem.*, 37(21):5575 – 5582, 1998.

[178] V. Polo, J. Gräfenstein, E. Kraka, and D. Cremer. Influence of the self-interaction error on the structure of the dft exchange hole. *Chem. Phys. Lett.*, 352(56):469 – 478, 2002.

[179] V. Polo, J. Grfenstein, E. Kraka, and D. Cremer. Long-range and short-range coulomb correlation effects as simulated by hartreefock, local density approximation, and generalized gradient approximation exchange functionals. *Theor. Chem. Acc.*, 109(1):22–35, 2003.

[180] D. Porezag and M.R. Pederson. Optimization of gaussian basis sets for density-functional calculations. *Phys. Rev. A*, 60(4):2840–2847, 1999.

[181] A.V. Postnikov, J. Kortus, and M.R. Pederson. Density functional studies of molecular magnets. *Phys. Status Solidi B*, 243(11):2533–2572, 2006.

[182] A. Prescimone, C.J. Milios, J. Sanchez-Benitez, K.V. Kamenev, C. Loose, J. Kortus, S. Moggach, M. Murrie, J.E. Warren, A.R. Lennie, S. Parsons, and E.K. Brechin. High pressure induced spin changes and magneto-structural correlations in hexametallic SMMs. *Dalton Trans.*, 0:4858–4867, 2009.

[183] E.I. Proynov, E. Ruiz, A. Vela, and D.R. Salahub. Determining and extending the domain of exchange and correlation functionals. *Int. J. Quantum Chem.*, 56(S29):61–78, 1995.

[184] J. Qian, W. Gu, S.-P. Yan, D.-Z. Liao, and P. Cheng. Di-μ-azido-κ_4 N : N-bis{(azido-κ N)[N,N-bis(2-pyridylmethyl-κ N)ethylamine]manganese(II)}. *Acta Crystallogr. E*, 63(3):687–688, 2007.

[185] A. Caneschi R. Sessoli, D. Gatteschi and M.A. Novak. Magnetic bistability in a metal-ion cluster. *Nature*, 365:141, 1993.

[186] V.V Rakitin and V.T Kalinnikov. Magnetic properties of bridged azido complexes. *Russ. Chem. Bull.*, 53(4):766–774, 2004.

[187] J. Reinhold. *Quantentheorie der Moleküle: eine Einführung*. Teubner, Wiesbaden, 2006.

[188] R. Reviakine, A.V. Arbuznikov, J.-C. Tremblay, C. Remenyi, O.L. Malkina, V.G. Malkin, and M. Kaupp. Calculation of zero-field splitting parameters: Comparison of a two-component noncolinear spin-density-functional method and a one-component perturbational approach. *J. Chem. Phys.*, 125(5):054110, 2006.

[189] J. Ribas, A. Escuer, M. Monfort, R. Vicente, R. Cortas, L. Lezama, and T. Rojo. Polynuclear NiII and MnII azido bridging complexes. structural

trends and magnetic behavior. *Coordin. Chem. Rev.*, 193-195(0):1027 – 1068, 1999.

[190] J. Ribas, M. Monfort, C. Diaz, C. Bastos, and X. Solans. Ferromagnetic nickel(II) polynuclear complexes with end-on azido as bridging ligand. the first nickel(II)-azido one-dimensional ferromagnetic systems. *Inorg. Chem.*, 33(3):484–489, 1994.

[191] J. Ribas-Arino, T. Baruah, and M.R. Pederson. Density-functional study of two Fe_4-based single-molecule magnets. *J. Chem. Phys.*, 123(4):044303, 2005.

[192] J. Ribas-Arino, T. Baruah, and M.R. Pederson. Toward the control of the magnetic anisotropy of FeII cubes: a DFT study. *J. Am. Chem. Soc.*, 128(29):9497–9505, 2006.

[193] W. Ritz. "über eine neue methode zur lösung gewisser variationsprobleme der mathematischen physik". *"Journal für die Reine und Angewandte Mathematik"*, 135:1–61, 1909.

[194] E. Ruiz. Exchange coupling constants using density functional theory: Long-range corrected functionals. *J. Comp. Chem.*, 32(9):1998–2004, 2011.

[195] E. Ruiz, P. Alemany, S. Alvarez, and J. Cano. Toward the prediction of magnetic coupling in molecular systems: Hydroxo- and alkoxo-bridged Cu(II) binuclear complexes. *J. Am. Chem. Soc.*, 119(6):1297–1303, 1997.

[196] E. Ruiz, S. Alvarez, J. Cano, and V. Polo. About the calculation of exchange coupling constants using density-functional theory: The role of the self-interaction error. *J. Chem. Phys.*, 123(16):164110, 2005.

[197] E. Ruiz, J. Cano, S. Alvarez, and P. Alemany. Magnetic coupling in end-on azido-bridged transition metal complexes: A density functional study. *J. Am. Chem. Soc.*, 120(43):11122–11129, 1998.

[198] E. Ruiz, J. Cano, S. Alvarez, and P. Alemany. Broken symmetry approach to calculation of exchange coupling constants for homobinuclear and heterobin-

uclear transition metal complexes. *J. Comp. Chem.*, 20(13):1391–1400, 1999. cited By (since 1996)457.

[199] E. Ruiz, J. Cano, S. Alvarez, and V. Polo. Reply to "comment on 'about the calculation of exchange coupling constants using density-functional theory: The role of the self-interaction error"' [j. chem. phys. [bold 123], 164110 (2005)]. *J. Chem. Phys.*, 124(10):107102, 2006.

[200] E. Ruiz, J. Cirera, J. Cano, S. Alvarez, C. Loose, and J. Kortus. Can large magnetic anisotropy and high spin really coexist? *Chem. Commun.*, (1):52–54, 2008.

[201] A. Ruzsinszky, J.P. Perdew, G.I. Csonka, O.A. Vydrov, and G.E. Scuseria. Density functionals that are one- and two- are not always many-electron self-interaction-free, as shown for H_2^+, He_2^+, LiH^+, and Ne_2^+. *J. Chem. Phys.*, 126(10):104102, 2007.

[202] S. Sarkar, A. Mondal, M.S. El Fallah, J. Ribas, D. Chopra, H. Stoeckli-Evans, and K.K. Rajak. Synthesis, structure and magnetic properties of two end-on double azido bridged nickel(II) dinuclear entities incorporating N,N,N-coordinating tridentate reduced Schiff base ligands. *Polyhedron*, 25(1):25–30, 2006.

[203] S. Sarkar, A. Mondal, J. Ribas, M.G.B. Drew, K. Pramanik, and K.K. Rajak. Synthesis, structure and properties of a mononuclear and an end-on double azido-bridged copper(II) complex incorporating an N,N,N,O-coordinating tripodal ligand. *Eur. J. Inorg. Chem.*, (23):4633–4639, 2004.

[204] A. Schäfer, H. Horn, and R. Ahlrichs. Fully optimized contracted gaussian basis sets for atoms Li to Kr. *J. Chem. Physics*, 97(4):2571–2577, 1992.

[205] S. Schmitt, P. Jost, and C. van Wüllen. Zero-field splittings from density functional calculations: Analysis and improvement of known methods. *J. Chem. Phys.*, 134(19):194113, 2011.

[206] E. Schrödinger. Quantisierung als eigenwertproblem. *Ann. Phys. (Berlin)*, 385(79):361–376, 1926.

[207] E. Schrödinger. Quantisierung als eigenwertproblem. *Ann. Phys. (Berlin)*, 385(79):489–521, 1926.

[208] A. Seidl, A. Görling, P. Vogl, J. A. Majewski, and M. Levy. Generalized kohn-sham schemes and the band-gap problem. *Phys. Rev. B*, 53:3764–3774, Feb 1996.

[209] C.D. Sherrill and H.F. Schaefer III. The configuration interaction method: Advances in highly correlated approaches. volume 34 of *Advances in Quantum Chemistry*, pages 143 – 269. Academic Press, 1999.

[210] J.C. Slater. Atomic shielding constants. *Phys. Rev.*, 36(1):57–64, 1930.

[211] T. Soda, Y. Kitagawa, T. Onishi, Y. Takano, Y. Shigeta, H. Nagao, Y. Yoshioka, and K. Yamaguchi. Ab initio computations of effective exchange integrals for HH, HHeH and Mn_2O_2 complex: comparison of broken-symmetry approaches. *Chem. Phys. Lett.*, 319(34):223 – 230, 2000.

[212] P. J. Stephens, F. J. Devlin, C. F. Chabalowski, and M. J. Frisch. Ab initio calculation of vibrational absorption and circular dichroism spectra using density functional force fields. *J. Phys. Chem.*, 98(45):11623–11627, 1994.

[213] C.C. Stoumpos, R. Inglis, O. Roubeau, H. Sartzi, A.A. Kitos, C.J. Milios, G. Aromí, A. J. Tasiopoulos, V. Nastopoulos, E.K. Brechin, and S.P. Perlepes. Rare Oxidation-State Combinations and Unusual Structural Motifs in Hexanuclear Mn Complexes Using 2-Pyridyloximate Ligands. *Inorg. Chem.*, 49(10):4388–4390, 2010.

[214] J. Tao, J.P. Perdew, V.N. Staroverov, and G. E. Scuseria. Climbing the density functional ladder: Nonempirical meta˘generalized gradient approximation designed for molecules and solids. *Phys. Rev. Lett.*, 91:146401, Sep 2003.

[215] L. Thomas, F. Lionti, R. Ballou, D. Gatteschi, R. Sessoli, and B. Barbara. Macroscopic quantum tunnelling of magnetization in a single crystal of nanomagnets. *Nature*, 383(6596):145147, 1996.

[216] L.H. Thomas. The calculation of atomic fields. *Proc. Cambridge Philos. Soc.*, (23):542–548, 1927.

[217] A.-R. Tomsa, J. Martinez-Lillo, Y. Li, L.-M. Chamoreau, K. Boubekeur, F. Farias, M.A. Novak, E. Cremades, E. Ruiz, A. Proust, M. Verdaguer, and P. Gouzerh. A new family of oxime-based hexanuclear manganese(iii) single molecule magnets with high anisotropy energy barriers. *Chem. Commun.*, 46:5106–5108, 2010.

[218] S. Triki, C.J. Gomez-Garcia, E. Ruiz, and J. Sala-Pala. Asymmetric azido-copper(II) bridges: Ferro- or antiferromagnetic? Experimental and theoretical magneto-structural studies. *Inorg. Chem.*, 44(15):5501–5508, 2005.

[219] C. Van Wüllen. Magnetic anisotropy from density functional calculations. comparison of different approaches: Mn_{12} o_{12} acetate as a test case. *J. Chem. Phys.*, 130(19), 2009. cited By (since 1996)16.

[220] C. van Wüllen. Broken symmetry approach to density functional calculation of magnetic anisotropy or zero field splittings for multinuclear complexes with antiferromagnetic coupling. *J. Phys. Chem. A*, 113(43):11535–11540, 2009. PMID: 19708660.

[221] R. Vicente, A. Escuer, J. Ribas, M.S. Elfallah, X. Solans, and M. Font-bardia. New dinuclear penta- and hexacoordinated nickel(II) complexes with μ-azido bridges. Crystal structures of ferromagnetically coupled (μ-N_3)$_2$[Ni(Me_3[12]N_3)]$_2$(ClO_4)$_2$·2H_2O and (μ-N_3)$_2$[Ni(232-N_4)]$_2$(ClO_4)$_2$. *Inorg. Chem.*, 32(10):1920–1924, 1993.

[222] S. H. Vosko, L. Wilk, and M. Nusair. Accurate spin-dependent electron liquid correlation energies for local spin density calculations: a critical analysis. *Can. J. Phys.*, 58(8):1200–1211, 1980.

[223] E. Wigner. On the interaction of electrons in metals. *Phys. Rev.*, 46:1002–1011, Dec 1934.

[224] E. Wigner. Effects of the electron interaction on the energy levels of electrons in metals. *Trans. Faraday Soc.*, 34:678–685, 1938.

[225] E. Wimmer, H. Krakauer, M. Weinert, and A.J. Freeman. Full-potential self-consistent linearized-augmented-plane-wave method for calculating the electronic structure of molecules and surfaces: O_2 molecule. *Phys. Rev. B*, 24(2):864–875, 1981.

[226] H.-Y. Wu, H.-Q. An, B.-L. Zhu, S.-R. Wang, S.-M. Zhang, S.-H. Wu, and W.-P. Huang. Synthesis, crystal structure and magnetic characterization of a dinuclear Mn(II) complex with double end-on azide ligands. *Inorg. Chem. Comm.*, 10(10):1132–1135, 2007.

[227] K. Yamaguchi, Y. Takahara, and T. Fueno. Ab-initio molecular orbital studies of structure and reactivity of transition metal-oxo compounds. In *Applied Quantum Chemistry*, pages 155–184. Springer Netherlands, 1986.

[228] M.-M. Yu, Z.-H. Ni, C.-C. Zhao, A.-L. Cui, and H.-Z. Kou. Synthesis and magnetic study of $\mu_{1,1}$-azido-bridged dinuclear manganese(II) complexes based on tripyridyl ligands. *Eur. J. Inorg. Chem.*, (36):5670–5676, 2007.

[229] S. Zein, C. Duboc, W. Lubitz, and F. Neese. A systematic density functional study of the zero-field splitting in Mn(II) coordination compounds. *Inorg. Chem.*, 47(1):134–142, 2008.

[230] C. Zener. Interaction between the *d* shells in the transition metals. *Phys. Rev.*, 81(3):440–444, 1951.

[231] T. Ziegler, A. Rauk, and E.J. Baerends. On the calculation of multiplet energies by the hartree-fock-slater method. *Theor. Chim. Acta*, 43(3):261–271, 1977. cited By (since 1996)407.

[232] A. Zupan, J.P. Perdew, K. Burke, and M. Caus. On-top pair-density interpretation of spin density functional theory, with applications to magnetism. *Int. J. Quantum Chem.*, 61(2):197–205, 1997.

8 List of Publications

[1] T. Birnbaum, T. Hahn, C. Martin, J. Kortus, M. Fronk, F. Lungwitz, D.R.T. Zahn, and G. Salvan. Optical and magneto-optical properties of metal phthalocyanine and metal porphyrin thin films. *Journal of Physics: Condensed Matter*, submitted, 2013.

[2] J. Kortus C. Loose. Systematic study of the influence of different equations of state on the calculation of elastic properties. *High pressure Research*, in print, 2013.

[3] R. Friedrich, S. Lindner, T. Hahn, C. Loose, S. Liebing, M. Knupfer, and J. Kortus. Systematic theoretical investigation of the phthalocyanine based dimer: $MnPc^{+}/F_{16}CoPc^{-}$. *Physical Review B - Condensed Matter and Materials Physics*, 87(11), 2013.

[4] U. Lehmann, J. Lach, C. Loose, T. Hahn, B. Kersting, and J. Kortus. Binuclear nickel complexes with an edge sharing bis(square-pyramidal) $N_3Ni(\mu\text{-}S_2)NiN_3$ core: Synthesis, characterization, crystal structure and magnetic properties. *Dalton Transactions*, 42(4):987–996, 2013. Cited By (since 1996):2.

[5] E. Rose, C. Loose, J. Kortus, A. Pashkin, C. A. Kuntscher, S. G. Ebbinghaus, M. Hanfland, F. Lissner, T. Schleid, and M. Dressel. Pressure-dependent structural and electronic properties of quasi-one-dimensional $(TMTTF)_2PF_6$. *Journal of Physics Condensed Matter*, 25(1), 2013. Cited By (since 1996):1.

[6] J. Lach, A. Jeremies, V. Lozan, C. Loose, T. Hahn, J. Kortus, and B. Kersting. Stabilization of hypophosphite in the binding pocket of a dinuclear macrocyclic complex: Synthesis, structure, and properties of $[Ni_2L(\mu\text{-}O_2PH_2)]BPh_4$ (L = N_6S_2 Donor Ligand). *Inorganic chemistry*, 51(22):12380–12388, 2012. Cited By (since 1996):1.

[7] S. Förster, T. Hahn, C. Loose, C. Röder, S. Liebing, W. Seichter, F. Eiss mann, J. Kortus, and E. Weber. Synthesis and characterization of new derivatives of azulene, including experimental and theoretical studies of electronic and

spectroscopic behavior. *Journal of Physical Organic Chemistry*, 25(10):856–863, 2012. Cited By (since 1996):2.

[8] M. Grobosch, B. Mahns, C. Loose, R. Friedrich, C. Schmidt, J. Kortus, and M. Knupfer. Identification of the electronic states of manganese phthalocyanine close to the Fermi level. *Chemical Physics Letters*, 505(4-6):122–125, 2011. Cited By (since 1996):9.

[9] N. Clement, C. Toussaint, G. Rogez, C. Loose, J. Kortus, L. Brelot, S. Choua, S. Dagorne, P. Turek, and R. Welter. Novel CrIII dinuclear complexes supported by salicyloylhydrazono dithiolane and dithiane ligands: Synthesis, stability, crystal structures and magnetic properties. *Dalton Transactions*, 39(19):4579–4585, 2010. Cited By (since 1996):5.

[10] V. Lozan, C. Loose, J. Kortus, and B. Kersting. Coordination chemistry of Robson-type polyamine-dithiophenolate macrocycles: Syntheses, structures and magnetic properties of dinuclear complexes of first-row transition metals. *Coordination Chemistry Reviews*, 253(19-20):2244–2260, 2009. Cited By (since 1996):35.

[11] A. Prescimone, C. J. Milios, J. Sanchez-Benitez, K. V. Kamenev, C. Loose, J. Kortus, S. Moggach, M. Murrie, J. E. Warren, A. R. Lennie, S. Parsons, and E. K. Brechin. High pressure induced spin changes and magneto-structural correlations in hexametallic SMMs. *Dalton Transactions*, (25):4858–4867, 2009. Cited By (since 1996):17.

[12] S. Jie, R. Pattacini, G. Rogez, C. Loose, J. Kortus, and P. Braunstein. Synthesis, structure, magnetic and catalytic properties of new dinuclear chromium(iii) complexes with oxazoline alcoholate ligands. *Dalton Transactions*, (1):97–105, 2009. Cited By (since 1996):5.

[13] C. Loose, E. Ruiz, B. Kersting, and J. Kortus. Magnetic exchange interaction in triply bridged dinickel(II) complexes. *Chemical Physics Letters*, 452(1-3):38–43, 2008. Cited By (since 1996):13.

[14] E. Ruiz, J. Cirera, J. Cano, S. Alvarez, C. Loose, and J. Kortus. Can large magnetic anisotropy and high spin really coexist? *Chemical Communications*, (1):52–54, 2008. Cited By (since 1996):19.

9 Acknowledgements

Are you still reading? Well done. I hope you will keep reading as this is the most important part of my thesis. I want to say "Thank you" to a couple of people without whom I would most likely never have finished this work.

- First of all I want to thank my supervisor Prof. Dr. Jens Kortus for all the patience he had with me and my "never-ending" thesis. Thank you for not giving up on me also it took me quite a while to finish. Thank you for trusting me. Thank you for all the things that you taught me. Thank you for being a supervisor that takes care of his students. I could add much more here, but I think "Thank you!" pretty much sums it up.

- Furthermore, I want to thank Prof. Eliseo Ruiz for undertaking the task of being the coreferee of this thesis. We have known each other for quite a while now and I am always amazed about you knowledge in Chemistry.

- I also want to thank Prof. Dr. Berthold Kersting for many fruitful collaborations over the years. I think I good part of my thesis was only possible due to your work.

- This thesis was started within the priority program of the DFG: SPP 1137 "limits and performance of the calculation of magnetic anisotropy energies from first -principles DFT calculations" which ended in 2008. Continuative funding was provided by the Konrad-Adenauer-Stiftung within a PhD grant. After my parental leave I was able to finish my thesis under the ESF grant 080945373. I am very grateful for all this funding.

- I am very grateful that I could do my PhD in the group of Prof. Dr. Jens Kortus. I really enjoyed the friendly atmosphere here and I will miss you all dearly.

- I promised myself not to make "special thanks" to people from my working group but I am bound to thank Gabriela Naumann for keeping nearly all the administrative chaos away from me. I will be forever grateful that you took

care of so many printed forms that would have surely driven me crazy in the end.

- Since I started I might as will go on with special thanks to people belonging to my group. Thank you Silvia, Andreas and Christian. You never failed to cheer me up, to help me or simply to listen whenever I run into trouble. Our Afternoon Tea was always a pleasure and source of many a good idea. You are amazing!

- Furthermore, I want to thank Ronald for the enlightening discussions on the topic of electronic structure theory. You have an impressive understanding of these things.

- I think I also have to thank "my" bachelor students. You taught me nearly as much as I taught you.

- A huge thanks goes to the the center for information services and high performance computing Dresden for the constant support. Whenever I had trouble on one of your machines you solved my problem immediately. I have rarely seen such a good support!

- Many thanks also to all the official and unofficial network administrators in the group. You know I can break every given hardware, software, operating system, ..., you name it... Thank you for taking the time to help me fix whatever I messed up whenever I messed it up.

- Special thanks go to Karolin. I could add much more here but I will settle for "Thank you for being the way you are!"

- Last but not least I have to thank my family. Thank you for sharing and caring, for backing me in hard times, for taking my mind away from work whenever I needed it and for letting me work without any complaints when there were urgent matters.

And with that I am truly done. All that is left is to say "Thank you" to you dear reader for braving this thesis.